Electronic Thesis and Dissertation Repository

11-29-2012 12:00 AM

Studies on Molecular Sieve Crystallization and Heteroatomic Substitution

Adam R. MacIntosh
The University of Western Ontario

Supervisor
Yining Huang
The University of Western Ontario

Graduate Program in Chemistry

A thesis submitted in partial fulfillment of the requirements for the degree in Master of Science

© Adam R. MacIntosh 2012

Follow this and additional works at: https://ir.lib.uwo.ca/etd

Part of the Inorganic Chemistry Commons, and the Materials Chemistry Commons

Recommended Citation

STUDIES ON MOLECULAR SIEVE CRYSTALLIZATION AND HETEROATOMIC SUBSTITUTION

(Spine title: Molecular Sieve Crystallization and Heteroatomic Substitution)

An Integrated-Article Thesis

by

Adam Robert <u>MacIntosh</u>

Graduate Program in
the Department of Chemistry

A thesis submitted in partial fulfillment
of the requirements for the degree of
Master of Science

The School of Graduate and Postdoctoral Studies
The University of Western Ontario
London, Ontario, Canada

THE UNIVERSITY OF WESTERN ONTARIO
School of Graduate and Postdoctoral Studies

CERTIFICATE OF EXAMINATION

Supervisor   Examiners

_____   _____

Dr. Yining Huang   Dr. François Lagugné-Labarthet

Supervisory Committee

                                                    _____

_____   Dr. T.K. Sham

Dr. David Shoesmith

                                                    _____

                                                    Dr. José Herrera

The thesis by

Adam Robert <u>MacIntosh</u>

entitled:

Studies on Molecular Sieve Crystallization and Heteroatomic Substitution

is accepted in partial fulfillment of the
requirements for the degree of
Master of Science

_____   _____
        Date   Chair of the Thesis Examination Board

ii

"To suffer woes which Hope thinks infinite;
To forgive wrongs darker than Death or Night;
To defy Power, which seems Omnipotent;
To love, and bear; to hope, till Hope creates
From its own wreck the thing it contemplates;
Neither to change nor falter nor repent;
This, like thy glory, Titan! is to be
Good, great and joyous, beautiful and free;
This is alone Life; Joy, Empire, and Victory!"

-Percy Bysshe Shelley, from
Prometheus Unbound, 1818

Dedicated to my heroes; the people who believed in me,

and who showed me how to believe in myself.

ABSTRACT

Molecular sieves have been scientifically and industrially important materials since their inception. These porous, crystalline networks of tetrahedrally coordinated atoms bridged by oxygen are known for their extremely high surface area and low density, making them excellent systems for catalysis. The framework of the $AlPO_4$ family of molecular sieves is itself non-catalytic, but through heteroatomic substitution these materials can diversify into the catalytically active silicoaluminophosphate (SAPO) and metalloaluminophosphate (MAPO) families of heterogeneous acid and redox catalysts. Research into the methods by which these substitutions occur, and the effects therein on the crystallization of the sieves, is of great importance, as discoveries can lead to refined control over material property and function.

To that end, this thesis is concerned with heteroatomic substitution in $AlPO_4$ molecular sieves. SAPO-5 and MAPO-5 were chosen as model systems. Both the dry-gel conversion and hydrothermal synthesis methods were used to produce crystallization intermediates for study. Solid state NMR spectroscopy was used as the primary method of investigation. The SAPO-5 study determined that the dry-gel conversion methods of steam assisted conversion and vapour phase transport follow similar reaction pathways. After an initial divergence caused by the lack of organic structure directing agent in the gel in the VPT method, crystallization is similar between methods, and silicon incorporation results in two populations of silicon sites. One is well incorporated into the framework, while the other either represents reagent silica or dense silicon islands within the framework. The vapour phase silicon uptake method provides a contrast to this data, producing a uniquely well-incorporated silicon population (albeit with significantly less substitution). The MAPO-5 study, looking at manganese and iron substitution, showed that metal centers coordinate with

phosphorous very early in the reaction, and are incorporated into the developing sieve before any channels or framework structure are formed. It showed that the use of the hydrothermal synthesis can be effective in capturing crystallization intermediates, and that the presence of paramagnetic materials does not exclude NMR from being a vital source of information.

KEYWORDS: Molecular sieve, $AlPO_4$, SAPO, MAPO, AFI, dry-gel conversion (DGC), hydrothermal synthesis (HTS), heteroatomic substitution, crystallization.

CO-AUTHORSHIP STATEMENT

This thesis contains materials from manuscripts co-authored by Adam R. MacIntosh and Yining Huang. For copyright information, see the appendix. Yining Huang is the co-author of any published manuscripts and was responsible for the supervision of Adam R. MacIntosh during his M.Sc. study. Adam R. MacIntosh was responsible for writing these manuscripts.

ACKNOWLEDGEMENTS

Above all I have to thank my thesis supervisor, Dr. Yining Huang. Over the past years, first as a professor, then as a supervisor, he has provided guidance, council and encouragement through one of the most challenging undertakings of my life. It goes without saying that absent his influence this work could not have been done.

Special thanks go out to my past and present group members. They are Dr. Andre Sutrisno, Lu Zhang, Jun Xu, Margaret Hanson, Tanya Levchenko, Sonia Lin, Donghan Chen, Yue Hu, Jennifer Bates, Nick Battram, Kamila Bladek, Le Xu, Peng He, Maxwell Goldman, Regina Sinelnikov, Balsam Ibrahim and Dr. David Wang. Their informative discussion and friendship have been extremely supportive over the past years. I wish them all the best in their future endeavors.

My thanks go out to the staff at UWO Chemistry, who cheerfully worked at making my life easier. Specifically my thanks go out to Ms. Grace Yau and Ms. Kim Law (XRD), Dr. Mathew Willans (NMR), Mr. John Vanstone, Mr. Barakat Misk, Ms. Darlene McDonald, Ms. Sandy McCaw, Ms. Clara Fernandes and Ms. Anna Vandendreis-Barr. Additional thanks to Dr. Felix Lee, Ms. Kay Calvin, Ms. Jan Mathers and Ms. Sandra Zakaria-Holtslag, my superiors as a graduate teaching assistant.

Thanks also to Dr. Viktor Staroverov and Dr. Nicholas Payne for their relevant, interesting and provocative courses in group theory and crystallography, respectively. Their patient instruction showed me that even seemingly complicated problems can be overcome with rigorous analysis and hard work. Additionally my thanks go out to my thesis examiners; Drs. François Lagugné-Labarthet, T.K. Sham and José Herrera and my thesis advisor Dr. David Shoesmith.

Finally, my heartfelt thanks go to my family and friends. This experience has been rewarding and demanding in ways that I did not predict. As has always been the case, it was the love and support of the people close to me that made the experience worthwhile.

TABLE OF CONTENTS

LIST OF TABLES

LIST OF FIGURES

LIST OF ABBREVIATIONS

AEL: Aluminophosphate type **el**even

AFI : Aluminophosphate type **fi**ve

AlPO$_4$: Aluminophosphate

Calx.: Calcination

CP: Cross-polarization

CSA: Chemical shift anisotropy

d4R: Double 4-ring

DGC: Dry-gel conversion

DPA: Di-n-propylamine

EDX: Energy-dispersive X-ray spectroscopy

FID: Free induction decay

γ: Gyromagnetic ratio

HTS: Hydrothermal synthesis

IZA: International Zeolite Association

LTA: Linde type A

MAPO: Metalloaluminophosphate

MAS: Magic-angle spinning

Q^n: Inorganic oxide silicon signal (n= number of 2nd neighbour silicon nuclei)

SAC: Steam-assisted conversion

SAPO: Silicoaluminophosphate

SBU: Structural building unit

SDA: Structure directing agent

SEM: Scanning electron microscopy

SM(X): Substitution mechanism (X=1-3)

SSNMR: Solid state nuclear magnetic resonance

T_1: Spin-lattice relaxation time

τ: Inversion/saturation recovery sequence delay time

TEA: Triethylamine

TEOS: Tetraethyl orthosilicate

T^n: Organic oxide silicon signal (n= number of 2nd neighbour carbon nuclei)

VPI: Virginia polytechnic institute

VPSU: Vapour phase silicon uptake

VPT: Vapour phase transport

XRD: X-ray diffraction

ZK: Zones-Kerr

ZSM: Zeolite Socony Mobil

CHAPTER ONE
Thesis Introduction

1.1 Overview

Microporous materials are crystalline systems which possess a regular network of channels or pores. Figure 1.1 describes some common microporous materials. They typically have very low densities and high surface areas as a result of their porous or channeled nature. This also explains their usage in the physisorption of gasses and other small molecules, as these can fit and travel within microporous channel networks.[4-6] The shapes of the openings which define these pores can restrict certain molecular shapes, sizes or configurations from entering the system in a form of shape selectivity. These features make molecular sieves widely useful in the fields of separation and heterogeneous catalysis.[7-9]

Only valences of elements which are stable in a tetrahedral coordination can be located in a microporous framework due to the geometric constraints of their bond lengths and angles. The largest and currently most well-studied group of microporous materials are the aluminosilicate zeolites.[10-12] Types of these materials are found at small abundance naturally in the earth's crust and many have been made synthetically, as have some novel zeolitic structures.

Zeolites, being made of a network of tetrahedrally co-ordinated aluminum and silicon nuclei bridged by oxygen atoms, carry overall negative charges, and so can be loaded with protons to perform acid catalysis. Depending on the type of elemental substitution, molecular sieves with variable, predictable and tunable catalytic sites are achievable. Efforts have been made to produce sieves able to participate in acid/base and

redox catalysis.[13, 14] A working knowledge of the methods of elemental substitution that take place during a sieve crystallization is required for the production of shape selective, heterogeneous catalysts that have tunable catalytic properties, and that endeavour is the focus of this thesis.
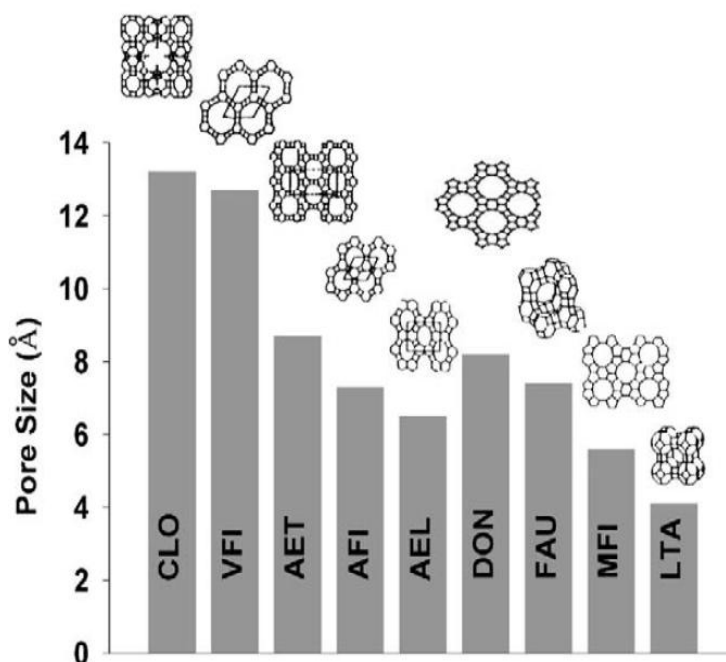
Figure 1.1: A comparison of the pore opening sizes of some common frameworks, labeled with the standard three-letter code.[2]

1.2 Primer on the Field of Zeolitic Materials

1.2.1 Natural Zeolites: Discovery and Prevalence

Axel Frederik Cronstedt, a Swedish mineralogist, is credited as the discoverer of the aluminosilicate zeolites.[15] Further proof of these remarkable structures came with the advent of X-ray diffraction techniques, with the first zeolite structure being solved in the 1930's.[16] At that time, the world knew that microporous materials could be used as molecular sieves in applications of ion exchange and molecular storage, and that their synthesis was poorly reproducible and they were difficult to find in abundance in the

earth's crust. Zeolite minerals can be found in great abundance in sedimentary rock.[17] Large zeolite deposits have been discovered in the United States of America, Japan, Italy, the Indian subcontinent, and many other locations around the world. The most commonly mined zeolite minerals are clinoptilolite, mordenite and chabazite. In 2010, 2.75 million metric tonnes of zeolite minerals were mined from the earth and processed for sale. At prices ranging from $70 to $120 per metric tonne depending on the grade and type of zeolite in question, the global market for naturally occurring zeolites represents between 192 and 330 million dollars annually.[18]

1.2.2 Richard Barrer: The Father of Modern Zeolite Science

The contributions Richard Barrer made to the field of microporous material synthesis and development have gone unmatched in its entire history. Barrer first recognized that zeolites could be used for gas storage, one of their most important and definitional uses.[19] His early work pioneered the classification of zeolitic materials on the basis of their pore size. He was the first person to report a reliable synthesis of a natural zeolite. He published frequently throughout his career on a wide range of subjects pertaining to the microporous sciences; synthesis gel chemistry, diffusion in solid systems, molecular sieve adsorption, etc. Most importantly he managed to determine and characterize how alkylamines and alkylammonium salts can be used as space filling agents, structure directing agents and templating agents in the laboratory synthesis of zeolites.[20] This finding made it possible to create new zeolite frameworks that did not exist in nature. The benefits of this discovery extended beyond aluminosilicates. Nitrogen-containing organic complexes are used commonly today in a far broader

collection of microporous material syntheses. Furthermore, his discovery of facile synthetic routes to materials with industrially important abilities changed molecular sieves from a field of niche interest to one of significant academic and industrial importance.

1.2.3 Structural Building Units, Topology Codes, and the IZA

Without a standard method of classification, porous material scientists would have had a hard time keeping up with the expansion and development of zeolites that has occurred over the past ca. 70 years. Definitions and designations for new materials were beginning to become splintered. For instance, it became common in the Union Carbide laboratories to assign names to their materials that reflect their compositions (e.g. SAPO = Silico-Alumino-Phosphate, MAPO = Metal Alumino-Phosphate) along with a number to differentiate between structure types (SAPO-5, SAPO-11, SAPO-34, etc.). Elsewhere, novel materials were named based on the laboratories or individuals responsible for their discovery (VPI-5 = Virginia Polytechnical Institute, ZSM-11 = Zeolite Socony Mobil, ZK-4 = Zones-Kerr). To avoid confusion in future publication, a common language was needed when referring to these materials. To begin describing such complicated structures, first they must be broken down to their least complicated common structural building units (SBUs).

Connecting simple SBUs together and arranging them in certain fashions can result in the creation of more complicated SBUs, and further to complete topological motifs. For example, Figure 1.2 shows a primitive cubic arrangement of sodalite (β) cages (truncated octahedra) separated at their square windows by double-4 rings (d4R, cubes) produces the LTA (α) cage, the descriptive constituent of the LTA topology,

which many zeolites and other molecular sieves adopt. SBUs differ from crystallographic unit cells in that repeating an SBU along with a translation in any crystallographic direction will not commonly reproduce the desired structure. It is the orientation and connectivity of multiple SBUs that produce a unit cell. When one of these is discovered and proven to be unique, it is given a three-letter designation, or topology code. Multiple different materials can have the same topology, differing in the constitution or proportion of the framework elements. These topologies are recognized, documented and officially assigned by the current reigning body in zeolitic science; the International Zeolite Association (IZA)[21], which has held that position for the past ca. 50 years.
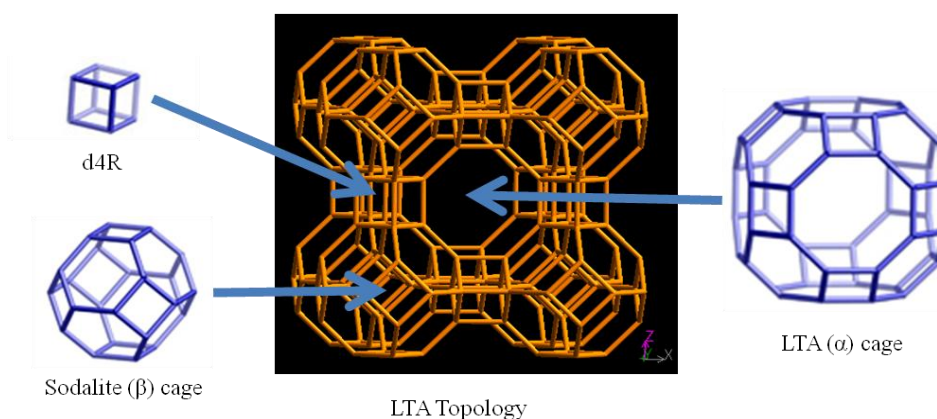
Figure 1.2: An LTA cage formed by the cubic arrangement of sodalite cages separated by d4R rings.

1.2.4 Novel Methods of Zeolite Synthesis

The first zeolitic syntheses, attempting to produce natural materials, were done using a large volume of water as a solvent. It was found that a nutrient gel containing oxides of desired framework constituents and water, given enough time, heat and pressure, would form relatively simple zeolitic structures. The complexities of potential

synthetic zeotypes were expanded with the introduction of organic structure directing agents (SDAs).

The addition of organic species to the nutrient gel provides a template over which the framework can grow. Without actually joining into the framework, these species have a marked effect on structure, regardless of their involvement in direction. It is believed there are three methods by which an organic species can direct zeotypical structure.[22] The first has the SDA acting as a space-filling agent. It serves to prevent water from filling the framework voids in a developing sieve. An important feature is that one space-filler can direct for multiple different structures, and there is no direct connection between the species and the formed framework. A "true" SDA is similar to a space-filling agent in every way except that one SDA will only direct for one structure. This exception is also true for "true" templates, with the added condition that there must be some shape similarity between the template and the eventual shape of the framework. The terms space-filling agent, structure directing agent, and template are often used interchangeably in the literature. With Barrer's innovation of using quaternary amines as SDAs, the began to serve a second purpose: altering the pH of the starting gel.

It has been demonstrated that water is essential to sieve synthesis. However, progress has been made using non-aqueous solvents in similar conditions. These solvents, typically alcohols or ionic liquids, provide interesting systemic properties. For instance, using ethylene glycol as a solvent instead of water, Venkatathri was able to synthesize SAPO-35 with a higher level of silicon substitution than had been previously reported.[23] Using imidazolium-based ionic liquids, Recham et al. were able to synthesize lithium and

iron-substituted aluminophosphates crystals in record sizes, sought after for their potential usage in lithium-ion battery technology.[24]

The addition of fluoride ions to zeolitic syntheses has many effects. It can assist in the breaking of starting material T-O-T bonds through acid hydrolysis (being that a common source of fluoride is hydrofluoric acid), mineralizing the desired framework elements and preparing them for reaction. Fluoride has also been used successfully in a structure directing role. It can corral charged organic SDAs into their proper location within the framework. It can also serve more directly in structure direction. Most specifically, the fluoride ion is known to direct for d4R SBUs in many different systems ($AlPO_4$, $GaPO_4$, etc.).[25, 26]

By a wide margin, the most popular and well-documented methods of sieve synthesis are hydrothermal synthesis (HTS) and dry-gel conversion (DGC). These methods will be discussed in detail in a following section.

1.3 Aluminophosphate ($AlPO_4$) Molecular Sieves

Elemental substitution of silicon for phosphorus is, ignoring topology, what distinguishes a zeolite from an $AlPO_4$. Further substitution led to the development of SAPO and MAPO sieves, the focus of this thesis. To provide a simpler background of the synthesis, development and chemical bonding nature in these materials, they will be explained in terms of the $AlPO_4$ systems in this section, and special details about elemental substitution and application of the materials made in this thesis will be provided in the next section.

1.3.1 Comparison of Zeolite and AlPO$_4$ Systems

There are a number of consequences to using aluminophosphate instead of silica or aluminoilicate in framework systems which are very important to note. In synthesis, zeolites tend to form from more basic pHs (8-12), while mild acidity or basicity more often lead to successful AlPO$_4$ syntheses (6-8). Low-pH syntheses tend to form dense AlPO$_4$ phases. The source of aluminum for both systems tend to be hydroxides (e.g. pseudoboehmite), and in AlPO$_4$ systems the overwhelming majority of syntheses use orthophosphoric acid as a source of phosphorus. This combination tends to keep the pH around neutral. In zeolites, the use of various forms of silica instead (fumed, colloidal, etc.) means that the reaction gel becomes more basic than would be good for an AlPO$_4$ synthesis.[27] Another factor in determining the reaction pH is the use of a template, which tends to be a tertiary alkylamine or quaternary alkylammonium species for both cases.

Zeolites have a negative framework charge, and so are readily useful as acid catalysts, while AlPO$_4$ sieves are neutrally charged and must be further modified to display framework catalytic ability. Directly after workup, however, both material types will tend to have their channels filled with organic structure directing agents from the synthesis. The SDA serves a multi-pronged purpose in both cases. They fill pore voids, adding to the stability of the crystallite, balance framework charge, as well as manage the pH of the solution, as was previously mentioned. AlPO$_4$s, being one of the first modifications on naturally-inspired zeolites, serve as an excellent base when attempting to model and study elemental substitution in frameworks. Over 25 elements have been successfully substituted into AlPO$_4$s[27], representing a large number of publications and a diverse family of materials with varied abilities over the past ca. 30 years.

1.3.2 Restrictions on Connectivity in AlPO₄s

Crystalline AlPO₄s will have a strictly alternating network of aluminum and phosphorus oxide tetrahedra. This protects the charge neutrality, as well as prevents the incidence of Al(III)-O-Al(III) bridges, which are unstable arrangements due to charge repulsion (a restriction known as Loewenstein's rule).[5] P(V)-O-P(V) bridges are also not present, this arrangement is energetically unfavourable, and does not exist in a crystalline AlPO₄.[28] As such, the Al/P atomic ratio of any pure AlPO₄ will be fixed at 1. This fact can be used to determine the degree and type of elemental substitution that takes place when trying to create SAPO or MAPO systems, as will be shown below. Another consequence of these rules is that AlPO₄ sieves will only possess even-numbered rings and pore openings.

1.3.3 Crystallization of AlPO₄ Molecular Sieves

Studying HTS reactions, a great deal of information has already been obtained about the crystallization of AlPO₄ molecular sieves. Many aspects of the crystallization procedure are shared between different porous materials such as zeolites and AlPO₄s. There appear to exist three different stages of crystallization in a zeolite system: induction, nucleation and propagation.[29] Materials progress through these steps from amorphous gels to crystalline structures as can be observed via powder XRD.

The induction period of molecular sieve crystallization is defined as the time between the start of the reaction and the first moment at which crystalline material can be detected using XRD. Materials collected during this time will appear to be amorphous using XRD by definition. During this time, the oxide form of desired framework elements are hydrolyzed and made available for eventual transition into the crystalline

framework. Equilibria are established between solutions of framework constituents and semi-organized phases of different degrees of order that will become the framework. These phases form under the influence of the organic structure directing agents or cations. When enough highly ordered framework pieces join together, small seeds for the framework are formed that can be detected by XRD, and the crystallization enters the nucleation phase.

Nucleation is a more difficult phase to define, in that during this phase there is a constantly shifting equilibrium between semi-ordered and ordered crystal structure. Oxygen bridges between framework tetrahedra in the proper crystal structure and improper, disordered structures are constantly being made and broken. The difference is that in this phase, the reaction equilibrium begins to shift toward crystal nuclei that have sufficient 3-D ordering in order to propagate into the eventual framework structure. Once this occurs, the rapid phase of crystal propagation begins. By this stage, the crystal unit cell has been laid out, and crystals grow very quickly in three dimensions for as long as sufficient reactive framework nuclei exist inside the reaction solution.

Propagation is the final stage in sieve crystal growth. In this stage, new framework tetrahedra are attracted to sites on crystal nuclei to which multiple attachments can be made. The bulk of the change in crystallinity can occur in a surprisingly short window of time, which is the reason it can be difficult to collect crystallization intermediates for study. As more nuclei aggregate and the nuclei themselves grow, the crystalline sieves become larger. Crystallinity will cease to increase once the concentration of precursor has dropped.
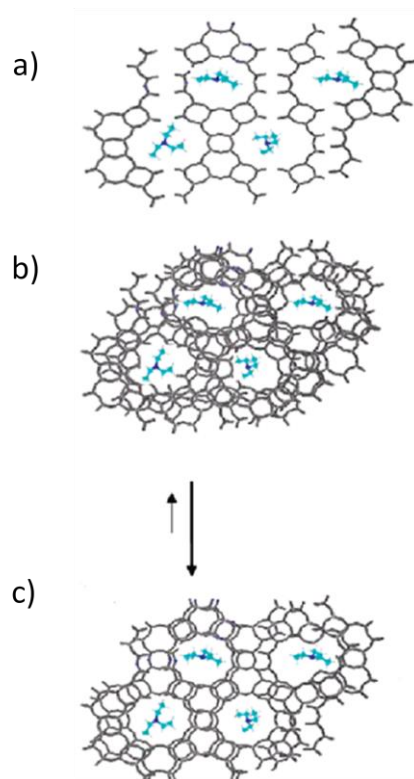
Figure 1.3: A proposed model for the DGC crystallization of an AFI framework. a) An amorphous collection of pre-framework molecules organize around the organic SDA. b) Layers of these precursors form atop one another, condensation reactions link them together. c) The sieve pore systems become apparent, further condensation finalizes the sieve[3].

The actual method of transport of framework tetrahedra to their spots in the crystal lattice on a crystal nucleus is a matter of some debate.[30] It is thought that this could occur via the diffusion of tetrahedral species in solution, or that a dense gel could reorganize itself into a low-density phase without the use of solution phase diffusion. A combination of these two pathways is a third possibility.

AlPO$_4$ family sieves have a few subtle differences in crystallization from zeolites, and are not studied nearly as well.[30, 31] The aluminum oxide in the reaction gel appears to react with phosphoric acid to form an amorphous or layered aluminophosphate phase. The possibilities are similar to those in zeolites, either the solid phase rearranges as the

crystallization proceeds or framework components dissolve and reorganize in that manner. Organized by the SDAs, building units or chains can be brought into close enough proximity to condense into sieve systems as well.

1.3.4 The Dry-gel Conversion Process

Another method of synthesis used in this thesis was dry-gel conversion.[32] In this method, a solid precursor gel is subjected to heat and autogeneous pressure inside an autoclave. A small amount of water is also in the autoclave, physically separated from the dry-gel. The water vaporizes and saturates the reactor, including the gel itself, throughout the reaction. This simplifies the reaction when compared to a similar HTS, as the reagents are in very close contact and need not find each other in solution in order to begin to react. DGC reactions require less solvent than HTS, and the products of a DGC reaction require far less workup than those for a HTS, making DGC a research-friendly method of sieve synthesis. In reality, the term "dry-gel" is a misnomer: the gel is usually at least half water by mass.

Three distinct methods of DGC were used in combination in this thesis. The first, steam assisted conversion (SAC), has all reagents for the desired sieve inside the dry-gel. The second, vapour phase transport (VPT), changes the position of the organic SDA from the dry-gel to the water in the autoclave. Upon heating, the SDA vaporizes along with the water and condenses on the sieve. The third method, called vapour phase silicon uptake (VPSU), removes the source of the desired substitution element (silicon, in this case) from the dry-gel. Instead, TEOS is added to the water in the autoclave, and it condenses on the dry-gel through the course of the reaction. Studying the incorporation of silicon from a different source provides the ability to compare and contrast multiple points of

entry for a desired framework element. All three methods possess the common benefit over HTS in that a reaction can be reliably halted by quenching the reactor in cold water. There is no reason, however, to assume that the crystallization mechanisms at play in a HTS reaction would be different from a DGC, as both require oxide species to be solubilised before reaction occurs. The only difference, essentially, is that the reagents would be at a much higher concentration within that solvent in a DGC reaction. An explanation of crystallization that works for DGC would likely apply to HTS, keeping in mind this difference in concentration. A proposed dry-gel crystallization is shown in Figure 1.3.

1.4 Si- and Transition Metal-Substituted AlPO$_4$ Sieves

1.4.1 Substitution of Silicon and Transition Metals into AlPO$_4$ Sieves

There has been a considerable amount of work done to look into heteroatomic substitution into AlPO$_4$s. The nature of the atoms and the method of substitution that occurs have a direct effect on the catalytic activity of the sieve, and so this process is one of the main focuses of this thesis. Acknowledging the fact that a pure AlPO$_4$ would have a 1 : 1 ratio of Al : P, elemental analyses can be easily interpreted into information about what kind of substitution has occurred over the course of a crystallization.
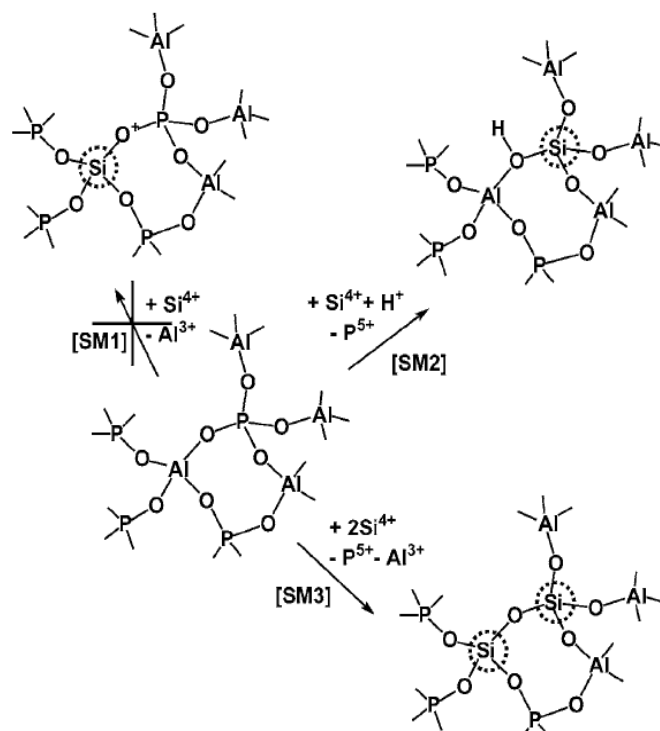
Figure 1.4: An AlPO$_4$ framework undergoes three different methods of heteroatomic substitution[1].

Silicon substitution in AlPO$_4$ sieves has been found to follow any combination of three distinct mechanisms, labeled SM1, SM2 and SM3, shown in Figure 1.4.[33, 34] In SM1, one silicon atom will take the place of one aluminum atom in the tetrahedral framework. In SM2, silicon replaces phosphorus. In SM3, two silicon atoms will take the place of an adjacent aluminum and phosphorus pair in the framework. These mechanisms are observant of the final state of the sieve, i.e. they do not describe how the substituting atom got to its place in the framework. That is not to say that they are not helpful descriptions. For instance, SM1 substitution produces energetically unfavourable Si-O-P bridging units. As such, this substitution mechanism is unlikely in SAPO systems. SM2 is the preferred method of silicon substitution. This method leads to the presence of Q^0 silicon nuclei (Q^n, a notation where n = the number of silicon atoms in the second

coordination sphere from the silicon nucleus in question. These nuclei are distinguishable via NMR). This substitution will upset the charge neutrality of the AlPO$_4$ framework, producing bridging hydroxyl groups that act as Brönsted acid sites. SM3 substitution causes the development of silica islands within a framework.

Transition metal substitution in AlPO$_4$s, forming the MAPO family, is less well studied than silicon, but the number of publications regarding it has increased in recent years.[35-40] Interest has peaked due to the fact that MAPO sieves can be used as shape selective heterogeneous redox catalysts. Transition metals with a 3+ oxidation state will tend to take the place of aluminum atoms in the developing framework. When in the +3 state, the MAPO framework is charge neutral. Reducing the metal center produces a site with an overall negative charge that can support a Brönsted acid site, much in the same fashion as in similar SAPO sieves. This potential dual catalytic activity is currently the subject of much study.

1.4.2 Applied SAPOs – Heterogeneous Acid Catalysis

Four different methods of catalytic selectivity are available to sieve catalysts.[41] First, the pore openings may have such a shape or size that prohibits the entrance of one reagent while allowing another via sterics. Second, the openings or channels may be of such a shape that does not allow certain reaction products to exit the sieve. In this way, the reaction will convert products between isomers until the one that has proper geometry to exit is able to do so. Third, the geometry in the pore system may disallow certain transition states in a reaction, and so direction of that reaction can be controlled in that fashion. Fourth, unique from the first three, is the idea of molecular traffic control. A sieve with a two-dimensional channel system may allow reagents to enter through one

channel and exit through the other, with catalysis occurring at the channel intersections. This feature keeps the catalytic sites inside the sieve accessible, and increases the turnover rate of the catalyst.

The acidic sites in SAPO sieves resemble those which exist in zeolite syntheses. Si-O-Al bridging units present in the sieve will attract positively charged guest molecules in order to balance the framework charge. These cations (commonly alkylammonium SDAs or alkaline/alkali earth metal cations) can be ion-exchanged for protons, producing the acid catalyst form of the sieve. This form of site creation produces Brönsted acid sites. The deprotonation of this site or the loss of the bridging hydroxyl group can produce a Lewis acid site.

1.4.3 Applied MAPOs – Heterogeneous Redox Catalysis

Redox catalysis using sieve systems is a goal that the field has been reaching toward for some time. Particularly the laboratory of Robert Raja has been paying special attention to molecular sieves applied as redox catalysts.[42-44] Transition metals substituted into $AlPO_4$ sieves are well studied because of the potential for redox chemistry to occur without destruction of the framework, resulting in a shape selective, heterogeneous redox catalyst. It has been shown, in addition, that an observable colour change in the samples can be used as an indicator of oxidation and reduction of the tetrahedrally coordinated framework transition metals.[44-46] As a direct result, MAPO systems of various topologies and substituted using a wide variety of transition metals have been studied for their potential as redox and acid catalysts.[47-54] The development of this class of materials has opened the door to a new application, and this serves as an example of the potential that

investigation of crystallization and substitution in molecular sieves has to expand the utility of these special materials.

Molecular sieve catalytic oxidation, by way of an instructive example, can be carried out via a free-radical pathway.[55] A metal center in a MAPO sieve can be oxidized and accept a hydroxyl group from an oxygen donor species (alkylperoxy species in this example, also hydrogen peroxide) producing an alkoxy radical intermediate. Reaction with a second oxygen donor species reduces the metal center back to its original oxidation state, producing H_2O and an alkylperoxy radical. These radical species can then go on to oxidize targeted reagents into desired products. The process is summarized in the equations below:

$$RO_2H + M^{II} \rightarrow RO\bullet + M^{III}OH$$

$$RO_2H + M^{III}OH \rightarrow RO_2\bullet + M^{II} + H_2O$$

$$RO\bullet + R'H \rightarrow R'\bullet + ROH$$

$$RO_2\bullet + R'H \rightarrow R'\bullet + RO_2H$$
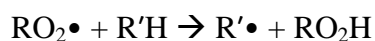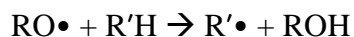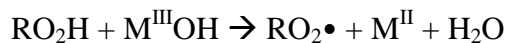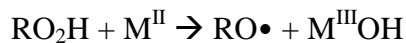
The use of the tetrahedrally-coordinated framework metal center M facilitates this process and increases the turnover rate of the catalyst. This, combined with the aforementioned shape selectivity of the molecular sieve, makes for an extremely efficient heterogeneous catalyst system.

1.4.4 Accomplishments to Date in Substituted $AlPO_4$ Sieves

Owing to their promising abilities and relatively simple synthesis, a good deal of research has been done to study substituted $AlPO_4$ sieves of various kinds. For instance, low or poor silicon incorporation has shown to produce acid catalysts with only slightly acidic character**.** As such, efforts have been made to increase the overall concentration of acid sites in the sieve, i.e., the number of incorporated silicon nuclei, without producing large silica islands. It has been shown that methods which slowly make available silicon nuclei for incorporation can achieve this goal.[56]

The maximum heteroatom substitution possible into an $AlPO_4$ framework is constantly being improved upon. All-silica systems, isostructural with certain $AlPO_4$s not inspired by zeolites, have even been synthesized (these species are useless as acid catalysts, but are an interesting point of research nonetheless).[57] Increasing the amount of silicon substituted into an $AlPO_4$ framework without creating dense silica phases is a persistent goal in the porous material sciences, and the record varies between materials.

1.4.5 Deficits in Substituted $AlPO_4$ Research

For all the work that has gone into studying $AlPO_4$ sieves and their substituted counterparts, there still remain several questions to be answered. A great deal of publications have been put forth that study sieves crystallized hydrothermally to completion, paying special attention to their thermal stability, decomposition and/or catalytic activity. Even when synthesized using the DGC method, studies on sieves focus on finished crystals and their properties, and comparing these results to similar sieves synthesized via HTS. This information is valuable for the application of these materials in

industry, but does not offer insight into how the sieves came to be in the first place, and a comprehensive knowledge of this process is quite valuable.

Using the dry-gel conversion method, crystallization intermediates for study are easy to synthesize reliably. This means that snapshots of a crystallizing sieve can be taken, and using various characterization techniques (most notably solid state NMR spectroscopy) data can be obtained that paint a picture about how these complicated crystallizations occur. This information could be used to develop methods of control over very precise sieve characteristics: their size, shape, and the amount and type of catalytic sites that exist within them. These types of studies are underrepresented in the literature, despite their evident value as research tools.

1.5 Thesis Motivation and Outline

The goal behind this thesis was to develop a method of studying the crystallization of molecular sieve systems. A fully realized, standard method of investigation would lead to a clearer picture of the crystallization process; the role and contribution of every variable within the reaction. Familiarity with the origins and development of such complicated structures will lead to the future ability to control the shapes, sizes and catalytic properties (in other words, the functions) of microporous materials.

While the performance of molecular sieves of many kinds are well studied and detailed in literature, the happenings during the crystallization of these materials are under-represented. Specifically, in the field of aluminophosphates and their substituted forms, information within the scientific community about exactly what goes on while these materials form is spotty at best. The dry-gel conversion method provides a unique

opportunity while studying molecular sieve crystallization: the same mechanisms are likely at play as during a HTS reaction, however it can be reliably halted to obtain crystallization intermediates for study. In this way, through multiple characterization techniques but spearheaded by solid-state NMR, snapshots of the reactions at different times can be used to show how sieve formation occurs, and this information can be used to develop control over these complicated systems.

To that end, the works behind this Master's thesis will be presented as follows. After an overview of the experimental methods commonly used in the projects is described in chapter two, studies on three different heteroatomlically substituted molecular sieve systems will be presented. Chapter three details the results of attempts to study the crystallization and silicon substitution into the aluminophosphate AFI framework synthesized via three variations of the dry-gel conversion method. Chapter four reports on the results of the hydrothermal synthesis of two transition-metal substituted aluminophosphate AFI, again paying attention to sieve substitution. Chapter five summarizes the thesis and makes suggestions for future work.

1.6 References

1.   Pastore, H.O.; Coluccia, S.; Marchese, L. *Ann. Rev. Mater. Res.* **2005**, *35*, 351-395.

2.   Payra, P.; Dutta, P.K. *Handbook of Zeolite Science and Technology*. **2003**, New York, USA: Marcel Dekker.

3.   Chen, B.; Kirby, C.W.; Huang, Y. *J. Phys. Chem. C.* **2009**, *113*(36), 15868-15876.

4.   Davis, M.E. *Nature* **2002**, *417*(6891), 813-821.

5.   Dyer, A. *An Introduction to Zeolite Molecular Sieves*. **1988**, Avon, GB: John Wiley & Sons, Ltd.

6.   Szostak, R. *Molecular Sieves: Principles of Synthesis and Identification*. **1998**, Suffolk, GB: Thomson Science.

7.   Michiels, P., *Molecular Sieve Catalysts*. **1987**, Virginia, USA:Pergamon Infoline Inc.

8.   Menon, V.C.; Komarneni, S. *J. Porous Mater.* **1998**, *5*(1), 43-58.

9.   Dincǎ, M.; Dailly, A.; Liu, Y.; Brown, C.M.; Neumann, D.A.; Long, J.R. *J. Am. Chem. Soc.* **2006**, *128*(51), 16876-16883.

10.   Cundy, C.S.; Cox, P.A. *Chem. Inform.* **2003**, *34*(19), 663-701.

11.   Barrer, R.M. *Zeolites* **1981**, *1*(3), 130-140.

12.   Flanigen, E.M., in *Studies in Surface Science and Catalysis*, E.M.F. H. van Bekkum and J.C. Jansen, Editors. **1991**, Elsevier, 13-34.

13.   Čejka, J.; Wichterlová, B. *Cat. Rev.* **2002**, *44*(3), 375-421.

14.   Sayari, A. *Chem. Mater.* **1996**, *8*(8), 1840-1852.

15.   Cronstedt, A.F. *Kongl Vetenskaps Academiens Handlingar Stockholm.* **1756**, *17*, 120.

16.   Pauling, L. *Proc. N.A.S.* **1930**, *16*(7), 453 - 459.

17.   Deffeyes, K.S. *J. Sediment. Res.* **1959**, *29*(4), 602-609.

18.   Virta, R., *U.S. Geologic Survey*. 2011, Mineral Commodity Summary.

19.   Barrer, R.M. *Proc. Roy. Soc. A.* **1938**, *167*, 392-406.

20. Barrer, R.M.; Denny, P.J. *J. Chem. Soc.* **1961**, 983-1000.

21. *Images & figures from IZA Database of Zeolite Structures.* [cited 2011 Aug. 6th]; Available from: http://www.iza-structure.org/databases/.

22. Davis, M.E.; Lobo, R.F. *Chem. Mater.* **1992**, *4*(4), 756-768.

23. Venkatathri, N. *Cat. Comm.* **2006**, *7*(10), 773-777.

24. Recham, N.; Dupont, L.; Courty, M.; Djellab, K.; Larcher, D.; Armand, M.; Tarascon, J.M. *Chem. Mater.* **2009**, *21*(6), 1096-1107.

25. Guth, J.L.; Kessler, H.; Higel, J.M.; Lamblin, J.M.; Patarin, J.; Seive, A.; Chezeau, J.M.; Wey, R. in *Zeolite Synthesis.* **1989**, American Chemical Society, 176-195.

26. Matijasic, A.; Paillaud, J.-L.; Patarin, J. *J. Mater. Chem.* **2000**, *10*(6), 1345-1351

27. Van Bekkum, H., ed. *Introduction to Zeolite Science and Practice.* **1991**, New York, USA: Elsevier.

28. Pauling, L.J. *J. Am. Chem. Soc.* **1929**, *106*, 1010-1016.

29. Cundy, C.S.; Cox, P.A. *Micropor. Mesopor. Mater.* **2005**, *82*(1–2), 1-78.

30. Francis, R. *J. Chem. Soc. Dalton* **1998**, 3133-3148.

31. He, H.; Klinowski, J. *J. Phys. Chem.* **1994**, *98*(4), 1192-1197.

32. Bandyopadhyay, R.; Bandyopadhyay, M.; Kubota, Y.; Sugi, Y. *J. Porous Mater.* **2002**, *9*, 83-95.

33. Yu, J.; Xu, R. *Chem. Soc. Rev.* **2006**, *35*(7), 593-604.

34. Flanigen, E.M.; Patton, R.L.; Wilson, S.T. *Stud. Surf. Sci. Catal.* **1988**, *37*, 13-27.

35. Chen, J.; Sankar, G.; Thomas, J.M.; Xu, R.; Greaves, G.N.; Waller, D. *Chem. Mater.* **1992**, *4*(6), 1373-1380.

36. Barrett, P.A.; Sankar, G.; Catlow, C.R.A.; Thomas, J.M. *J. Phys. Chem.* **1996**, *100*(21), 8977-8985.

37. Karthik, M.; Vinu, A.; Tripathi, A.K.; Gupta, N.M.; Palanichamy, M.; Murugesan, V. *Micropor. Mesopor. Mater.* **2004**, *70*(1–3), 15-25.

38. Balkus, K.J.; Ball, L.J.; Gnade, B.E.; Anthony, J.M. *Chem. Mater.* **1997**, *9*(1), 380-386.

39. Lohse, U.; Brückner, A.; Schreier, E.; Bertram, R.; Jänchen, J.; Fricke, R. *Micropor. Mater.* **1996**, *7*(2–3), 139-149.

40. Bruckner, A.; Lohse, U.; Mehner, H. *Micropor. Mesopor. Mater.* **1998**, *20*(1–3), 207-215.

41. Davis, M.E. *Ind. Eng. Chem. Res.* **1991**, *30*(8), 1675-1683.

42. Thomas, J.M.; Raja, R.; Sankar, G.; Bell, R.G. *Acc. Chem. Res.* **2001**, *34*(3), 191-200.

43. Thomas, J.M.; Raja, R.; Sankar, G.; Bell, R.G. in *Studies in Surface Science and Catalysis*, Avelino Corma and G.F. José Luis, Editors. **2000**, Elsevier, 887-892.

44. Raja, R.; Sankar, G.; Thomas, J.M. *J. Am. Chem. Soc.* **1999**, *121*(50), 11926-11927.

45. Thomas, J.M.; Raja, R.; Sankar, G.; Bell, R.G. *Nature* **1999**, *398*(6724), 227-230.

46. Dugal, M.; Sankar, G.; Raja, R.; Thomas, J.M. *Angew. Chem. Int. Edit.* **2000**, *39*(13), 2310-2313.

47. Luna, F.J.; Ukawa, S.E.; Wallau, M.; Schuchardt, U. *J. Mol. Catal. A-Chem.* **1997**, *117*(1–3), 405-411.

48. Machado, M.d.S.; Pérez-Pariente, J.; Sastre, E.; Cardoso, D.; Giotto, M.V.; García-Fierro, J.L.; Fornés, V. *J. Catal.* **2002**, *205*(2), 299-308.

49. Akolekar, D.B.; Kaliaguine, S. *J. Chem. Soc. Faraday T.* **1993**, *89*(22), 4141-4147.

50. Akolekar, D.B. *J. Catal.* **1993**, *143*(1), 227-238.

51. Akolekar, D.B. *J. Mol. Catal. A-Chem.* **1995**, *104*(1), 95-102.

52. Venuto, P.B. *Micropor.Mater.* **1994**, *2*(5), 297-411.

53. Raj, K.J.A.; Vijayaraghavan, V.R. *Cat. Lett.* **2004**, *96*(1), 67-70.

54. Wan, B.-Z.; Huang, K. *App. Catal.* **1991**, *73*(1), 113-124.

55. Arends, I.W.C.E.; Sheldon, R.A.; Wallau, M.; Schuchardt, U. *Angew. Chem. Int. Edit.* **1997**, *36*(11), 1144-1163 and references therein.

56. Han, X.S. *Chem. Comm.* **2002**, *5*(16), 166 - 167.

57. Van Nordstrand R., A.; Santilli Don, S.; Zones Stacey, I., in *Perspectives in Molecular Sieve Science*. **1988**, American Chemical Society. 236-245.

CHAPTER TWO
Experimental Details

2.1 Overview

The goals of the projects described by this thesis required an adaptable but well-outlined system of synthesis and characterization. This chapter provides information on some common experimental details. It provides background information on the hydrothermal synthesis (HTS) and dry-gel conversion (DGC) methods of molecular sieve synthesis as well as some common methods of sieve characterization: powder X-ray diffraction (XRD) and solid state nuclear magnetic resonance spectroscopy (SS-NMR). Project-specific details on sample and data collection can be found at the outset of each chapter.

2.2 Molecular Sieve Synthesis

Hydrothermal synthesis[1-3] (HTS) is a common method of molecular sieve synthesis. In this method, sources of all desired framework elements (Al, P, Si, transition metals, etc.) are added together with water and homogenized into a gel. Also present in the gel is an organic structure directing agent. Aluminophosphate-based sieves tend to form more effectively from gels that are mildly acidic. When the gel is well homogenized it is added to a TEFLON lined autoclave and heated to the required temperature for the required time. After the reaction, the gel must be washed and the product isolated from the solution before it can be characterized or used.

Dry-gel conversion[4-6] (DGC) was also used for some synthetic work done in this thesis. Three variations of DGC were used. First, steam-assisted conversion (SAC), where the dry-gel contains all precursor species and the steam source is only water. Second, vapour-phase transport[7] (VPT), where the SDA is in the lower cup and only contacts the dry-gel during crystallization. Lastly, a third configuration, less well-studied, where the silicon, in the form of tetraethyl orthosilicate (TEOS), is found in the lower cup, and the dry-gel is devoid of silicon.[8] Over the course of the crystallization, the TEOS boils and travels to the developing framework in the dry-gel by the fashion of vapour-phase silicon uptake (VPSU).
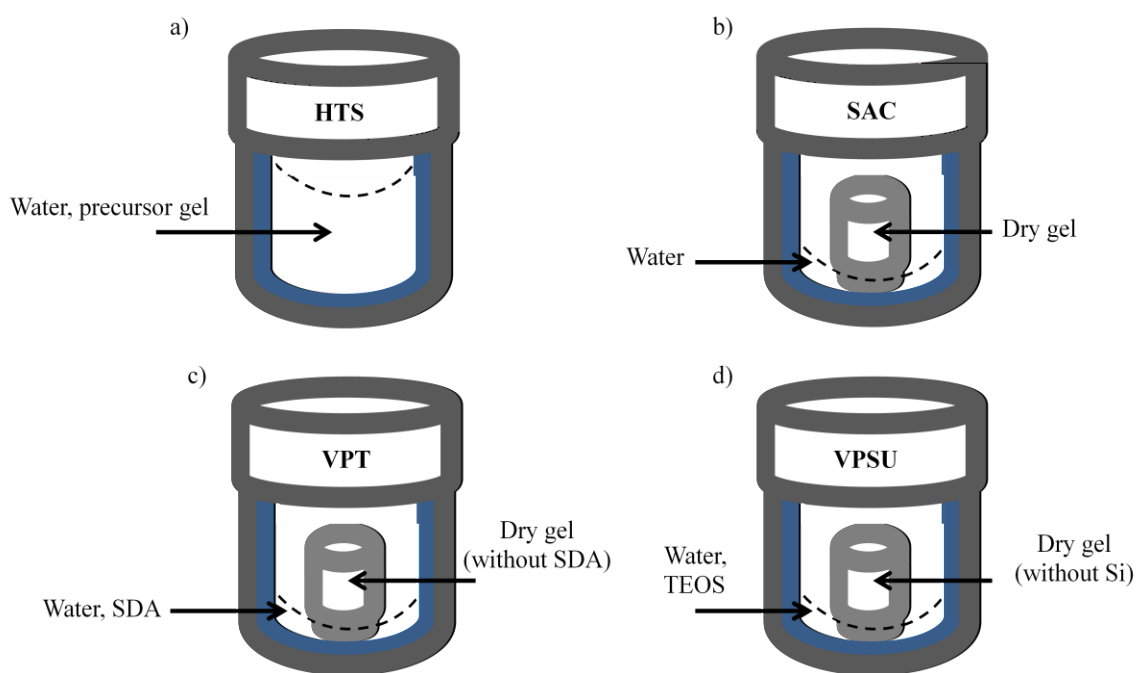
Figure 2.1: Drawings of autoclave reactors set to perform a) HTS, as well as three variations on the DGC method, b) SAC, c) VPT and d) VPSU.

A typical dry-gel synthesis and sieve crystallization proceeds as follows.[9, 10] An appropriate amount of aluminum source (typically alumina or aluminum hydroxide) is stirred in water to obtain a homogenous suspension. Phosphorus, usually in the form of orthophosphoric acid, is then slowly added to the mix and stirred vigorously (at this stage

the syntheses of different DGC dry-gels (SAC, VPT or VPSU) differs, the description will continue assuming SAC conditions). Colloidal silica is then added drop-wise as the mix continues to stir. The organic SDA is then added and the mix is placed in an oil bath. Gentle heating (ca. 120˚C) is employed to remove excess water, and the mix is manually stirred and heated in an 80˚C oven until a white solid is obtained. The solid is ground to a powder and used as the precursor gel in crystallization reactions inside of stainless-steel autoclaves, described in Figure 2.1 (in the case of VPT or VPSU, the sources of SDA or silicon, respectively, are not added to the dry-gel mix, and are instead added to the lower-cup steam source later on).

Typically, 1.00 g of precursor gel is placed in the TEFLON inside cup of the autoclave assembly. The noted amount of water (along with SDA or TEOS, as is necessary) is added to the TEFLON outside cup of the same assembly. The autoclaves are sealed and heated at various temperatures for various times. When removed from the oven, the autoclaves are quenched in cold water to stop the reaction. When necessary (e.g. for SEM characterization) the sieves are washed multiple times with deionised water.

2.3 Powder X-ray Diffraction (XRD)

The nature of many solid-phase syntheses is such that the reactions occur over relatively long time spans. With a large volume of samples, a rapid, reliable method of characterization and quality assurance was desirable. This method would also have to be useful for powdered, solid samples. This was done using powder X-ray diffraction.[11-14]

X-rays can be diffracted in the same way that visible light is diffracted by a physical grating. Being of a shorter wavelength, X-rays require a finer grating than visible light in order to be diffracted, and the periodic nature of electron density in a crystalline sample fills this requirement perfectly. Powdered samples can be thought of as a population of micro-crystals in an infinite number of orientations. When bombarded with X-rays, at appropriate angles constructive interference will occur between waves reflecting off of layers of atoms in the sample. The specific angles are dependent on the crystal structure and reveal some important structural information, specifically, the spacing between defined lattice planes (known as Miller indices) as described by Bragg diffraction[15] illustrated in Figure 2.2.

$$n\lambda = 2d\sin\theta$$
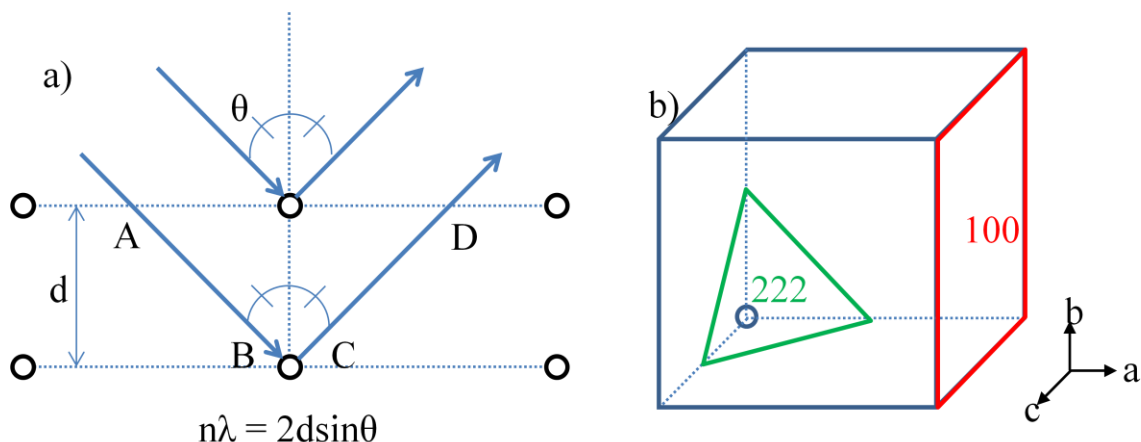
Figure 2.2: a) Bragg's Law. Constructive interference will occur at angles θ where AB + CD = nλ. b) Miller indices displayed on a hypothetical cubic unit cell.

Single crystal X-ray diffractograms can be interpreted into precise spatial information about the unit cell and atomic movement within solids. XRD information can be used for structural determination. However it is much more common in microporous materials to use XRD as a fingerprinting tool.[16] The heights and positions of reflections are indicative of particular framework topologies. These fingerprints have been verified and indexed with a high degree of discrimination, and so a sample whose diffractogram

matches that of one from an index (e.g., the ones provided by the International Zeolite Association[17] synthesis commission) will possess the same framework. For the purposes of this study, XRD was also used as it has been in the past to monitor and roughly quantify the progress of crystallization reactions from amorphous dry-gel powder to highly order molecular sieve, and through any layered intermediates that may exist in between.

It is crucial at this point to clarify that although XRD is one of the most frequently used methods of characterization in this work, its usefulness ends at verifying the framework of a given sample. Central to the experiments described here is the concept of heteroatomic substitution into these frameworks. A fully-crystallized SAPO-5 molecular sieve would have an identical X-ray diffractogram to its $AlPO_4$-5 cousin, and so XRD is less effective for monitoring incorporation.

2.4 Solid State Nuclear Magnetic Resonance Spectroscopy (SS-NMR)

2.4.1 Overview

Table 2.1: Relevant NMR parameters.

Isotope	^{27}Al	^{29}Si	^{31}P
Spin, I	5/2	1/2	1/2
Abundance (%)	100	4.7	100
Gyromagnetic Ratio, γ (10^7 rad/s•T)	6.976	-5.319	10.839
Larmor Frequency @ 9.4 T, v_L (MHz)	104.308	79.468	161.924
Quadrupole Moment (Barns)	0.15	0	0
Reference Material	$Al(NO_3)_{3(aq)}$	$C_{12}H_{36}Si_5$ (TTMSS)	$H_2PO_4NH_4$ (ADP)

The phenomenon of nuclear magnetic resonance (NMR) has been exploited in the fields of chemistry, particle physics, and medicine for roughly 75 years, and in that time

NMR has made large contributions to modern science.[18-23] Central to the concept is the fact that NMR active nuclei possess spin and charge, therefore also possessing magnetization vectors. The Z components of these vectors will align with or against a stronger, external magnetic field, B_0, such as the ones produced by the electromagnets inside NMR spectrometers. This has the effect of splitting the energy levels of these once-degenerate magnetizations into $2I + 1$ non-degenerate states, as seen in Figure 2.3, where I is the spin of the isotope in question. NMR parameters relevant to this study are summarized by Table 2.1.[24]

$B_0 = 0$ $B_0 \neq 0$

$-1/2$

$\Delta E = \gamma \hbar B_0$

B_0

$1/2$

Bulk Magnetic
Procession
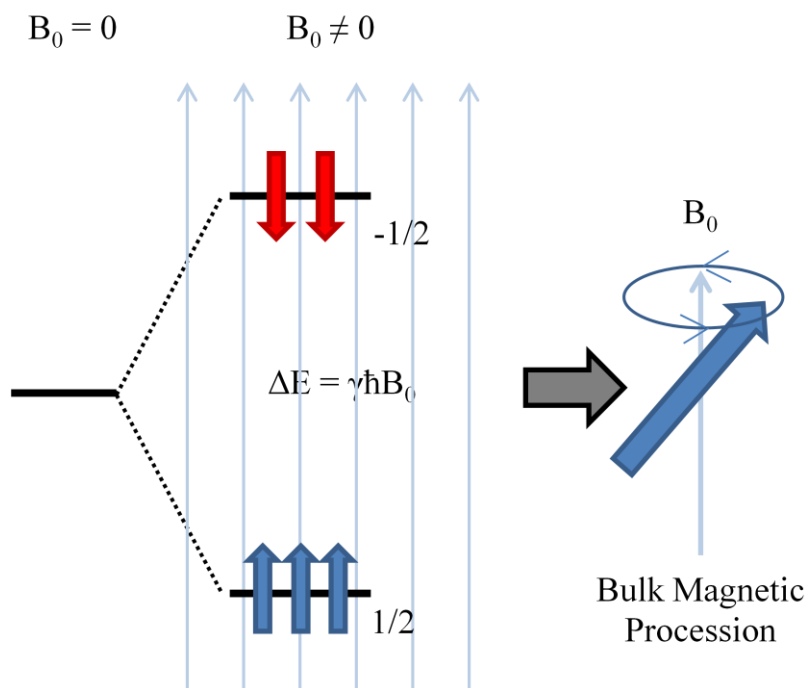
Figure 2.3: A small population difference in nuclear spin states, described by a Boltzmann distribution, is the cause of the precessing bulk magnetization with which the applied B_1 pulse interacts.

The basic principle of NMR is explained as follows:[25, 26] a small population difference exists between nuclei whose magnetization z-components are aligned with and against the external field, resulting in a net or bulk magnetization, as seen in Figure 2.3. This magnetization vector will precess around the applied field at a given frequency, ν_0,

the Larmor frequency, and electromagnetic radiation of the same frequency can be used as a probe for this magnetic environment through nuclear magnetic resonance. This frequency depends on the strength of the external magnetic field as well as a property of the nucleus known as the magnetogyric ratio, γ. Subjecting a population of spins in the sample to a source of radiation of the same frequency ("pulsing the sample", typically the frequency is in the MHz range) can exert torque on the bulk magnetization vector of the sample. When the pulse ends and the vector relaxes to its equilibrium state, its motion can be characterized and interpreted into important information about the magnetic and structural environment of the nuclei under study. This is because the nuclei are under the influence of spin interactions, described in Table 2.2.[27-31]

Table 2.2: Descriptions of Nuclear Spin Interactions.

Interaction	Strength (Hz)	Description
Zeeman	$10^6 - 10^9$	Interaction between the external magnetic field and the bulk magnetization.
Dipole coupling	$10^3 - 10^5$	Interaction between two nuclei through space.
Quadrupole coupling	$10^3 - 10^9$	Effect of the electric field gradient for non-spin-1/2 nuclei.
Spin coupling	$1 - 10^3$	Interaction between two nuclei through bonds.
Chemical shift	$10^2 - 10^5$	Nuclei are shielded or deshielded from the external field by circulating electrons.

2.4.2 Solid-State Versus Solution Phase NMR

The molecules in solids are far less mobile than those in solution, and so the directional nuclear interactions that make solids so difficult to characterize in solution conditions are averaged out to zero or to their isotropic values via molecular tumbling over the timescale of the NMR experiment. In solids, high signal resolution is difficult to

achieve, even in the best cases, but the situation can be improved by a number of different means, for instance by employing stronger and stronger external magnetic fields, using signal-boosting pulse sequences, or by subjecting the sample to magic-angle spinning (MAS)[32].
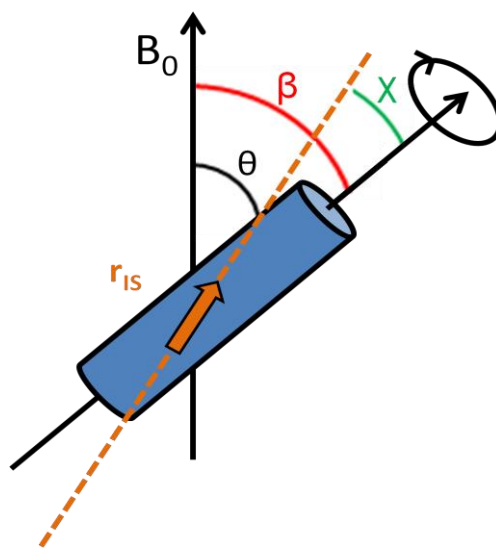
Figure 2.4: NMR rotor with internuclear vector r_{IS} defining angles θ,β and χ. B_0 coincides with the laboratory z-axis.

The mathematical treatments of many of the aforementioned nuclear interactions, most significantly dipolar and chemical shift interactions, all possess a common directional dependence. For instance, in the case of the dipole-dipole interaction, the internuclear axis forms the angle θ with the laboratory z axis. To employ MAS, the sample is packed into a ceramic NMR rotor. This rotor sits in the NMR probe inside a stator at a specific angle, β, with respect to the lab-frame z-axis, called the spinning angle. A third angle, χ, is defined between the spinning axis and the internuclear axis. Over the course of a rotation, the value of θ will oscillate between β – χ and β – χ. The now time-dependant value of θ becomes directly reliant on a modifiable experimental variable, the angle β. This treatment is illustrated in Figure 2.4. When set to 54.74˚, the

magic angle, the directional components of most internuclear interactions become 0, and so the dipole and (1st order) quadrupole interactions are eliminated and chemical shift and spin-coupling are reduced to their isotropic values, as shown below:

Heteronuclear Dipolar Broadening:

$$\nu = \nu_L \pm \frac{1}{2}D(\mathbf{1 - 3cos^2\theta})$$

Chemical Shift (axial symmetry):

$$\sigma_{zz} = \sigma_{iso} + (\sigma_{//} - \sigma_{iso})\frac{(\mathbf{3cos^2\theta - 1})}{2}$$

1st Order Quadrupole Broadening (axial symmetry):

$$\omega_m^{1st} = \left(\frac{\omega_Q}{2}\right)\left(m - \frac{1}{2}\right)(\mathbf{3cos^2\theta - 1})$$

Under Fast MAS:

$$\mathbf{3cos^2\theta - 1} = \frac{1}{2}(3cos^2\beta - 1)(3cos^2\chi - 1)$$

When β = 54.74:

$$\mathbf{3cos^2\theta - 1} = 0$$

...where ν is the experimental frequency, ν_L is the resonance frequency absent dipolar coupling, D is the dipolar coupling constant, σ_{zz} and $\sigma_{//}$ are components of the CSA tensor and σ_{iso} is the isotropic CS constant, ω_m^{1st} is the 1st order quadrupolar frequency for an mth-energy level transition and ω_Q is the quadrupole frequency.

2.4.3 NMR experiments

2.4.3.1 The One Pulse MAS Experiment with Decoupling and the Spin Echo

The one pulse or simple MAS experiment[33] with decoupling is a two-channel pulse sequence illustrated in Figure 2.5. On the observed channel, a pulse is applied to the sample. This exerts torque on the bulk magnetization aligned with the laboratory z-axis, tipping it into the x-y plane, and so is called a 90˚ or a $\pi/2$ pulse. As soon as the pulse ends, the bulk magnetization begins to relax back to its equilibrium value, recorded in a free induction decay (FID) graph, which is Fourier-transformed into a NMR spectrum. The mechanics of this relaxation are sensitive to the type of nucleus under study and its environment in the sample.
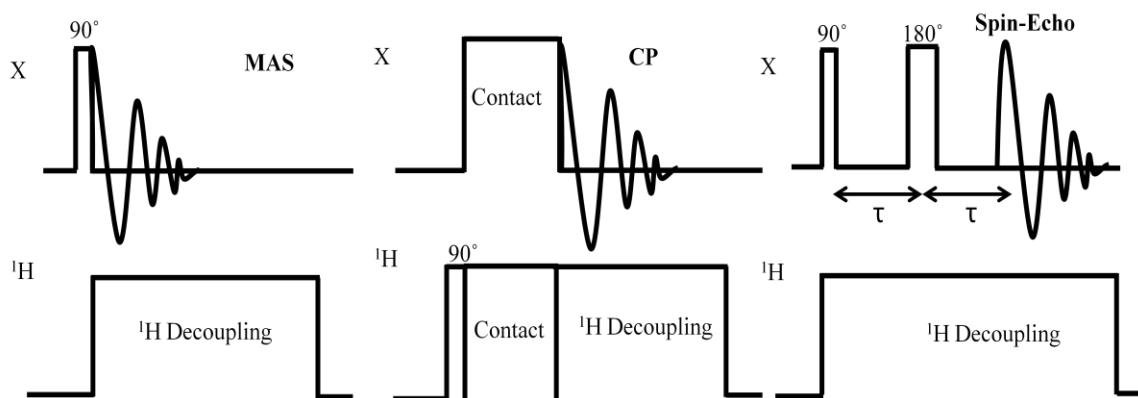
Figure 2.5: Schematic diagrams of NMR pulse sequences used in this thesis.

The strength of the dipolar coupling between ^{1}H and the observed nucleus is often too strong to be averaged out by MAS. Proton decoupling is thus employed during signal acquisition. A long pulse is applied to the sample at the proton Larmor frequency. This decoupling pulse occupies the proton spin-system, applying constant torque and stopping it from interacting with the observed spin system. Effectively, this removes the dipolar coupling that exists between the abundant ^{1}H and the less abundant observed nucleus,

simplifying spectral interpretation and increasing resolution. The MAS experiment can provide quantitative information about nuclear environments, and is used in this thesis as the main source of NMR information, identifying the presence and prevalence of different nuclear sites within developing molecular sieve samples.

Application of the radiofrequency pulse and acquisition of the FID from the nuclei are both done through the same cable within the physical NMR setup. In order to prevent pulse breakthrough, which would result in distortion of the signal, a short time passes before signal acquisition begins, called the dead time. For some samples, particularly ones with severe CSA or dipole interactions, a large portion of the FID can be lost in this dead time, resulting in broadening and distortion of the signal. To avoid this, a modification can be made to the pulse sequence in order to acquire the full FID. This is the aim of the spin-echo experiment seen in Figure 2.5.

After a 90˚ pulse, the spin magnetization is allowed to dephase under the effects of CSA and dipolar coupling for a given time, τ. At this point, a 180˚ pulse is applied so that the magnetization components refocus in the x-y plane over another τ period. At the end of the second τ period, the FID can be collected in its entirety from the top of the echo, undistorted by the required dead time.

2.4.3.2 The Cross Polarization Experiment

The collection of spectra for dilute spin systems can be difficult due to low isotopic abundance, low magnetogyric ratios and long relaxation times. For these reasons, the cross-polarization (CP) technique[34], which can significantly enhance the

apparent receptivity of a spin system, is a widely used pulse sequence. The CP pulse sequence is shown in Figure 2.5.

Cross polarization between a non-receptive nucleus, S, and a receptive one, I (very commonly ^{1}H), is mediated by the dipolar interaction, and is strongly dependent on internuclear distance. After an initial 90˚ pulse on the I channel, a contact pulse is applied to both channels for a given amount of time, the contact time. The powers of these two contact pulses must be chosen to satisfy the Hartmann-Hahn[35] matching condition:

$$\nu_I B_{1I} = \nu_S B_{1S} \pm \nu_r$$

Where B_1 is the strength of the radiofrequency pulse, $\nu_{I,S}$ are the Larmor frequencies of spin system I and S, and ν_r is the rotor spinning speed.. When this condition is met, in a rotating frame of reference, the differences in energy between spin states of both spin systems become close enough that magnetization can be transferred from the I system to the S system. This phenomenon has multiple effects on the observation of dilute system S:

1) The signal strength of any resonances is enhanced by a maximum factor of γ_I / γ_S .

2) In the case of ^{1}H, the pulse delay now depends only on the relaxation of the ^{1}H system, leading to shorter waiting periods between scans and more scans over the same amount of time.

3) Due to dependence on internuclear distance, CP can be used to edit the spectra of S nuclei based on their proximity in the sample to I nuclei, leading to structural information.

During the collection of the observed nucleus FID, decoupling must be applied to the I channel to avoid the effects of severe dipolar coupling between systems I and S. The selective amplification of certain signals means that a CP spectrum cannot give quantitative data. In this thesis, CP was used as a signal enhancment technique and as a way to monitor which nuclear sites (S systems) were in close proximity to protons (I systems) during the crystallization of molecular sieves.

2.4.3.3 T_1 Measurement: The Inversion and Saturation Recovery Experiments
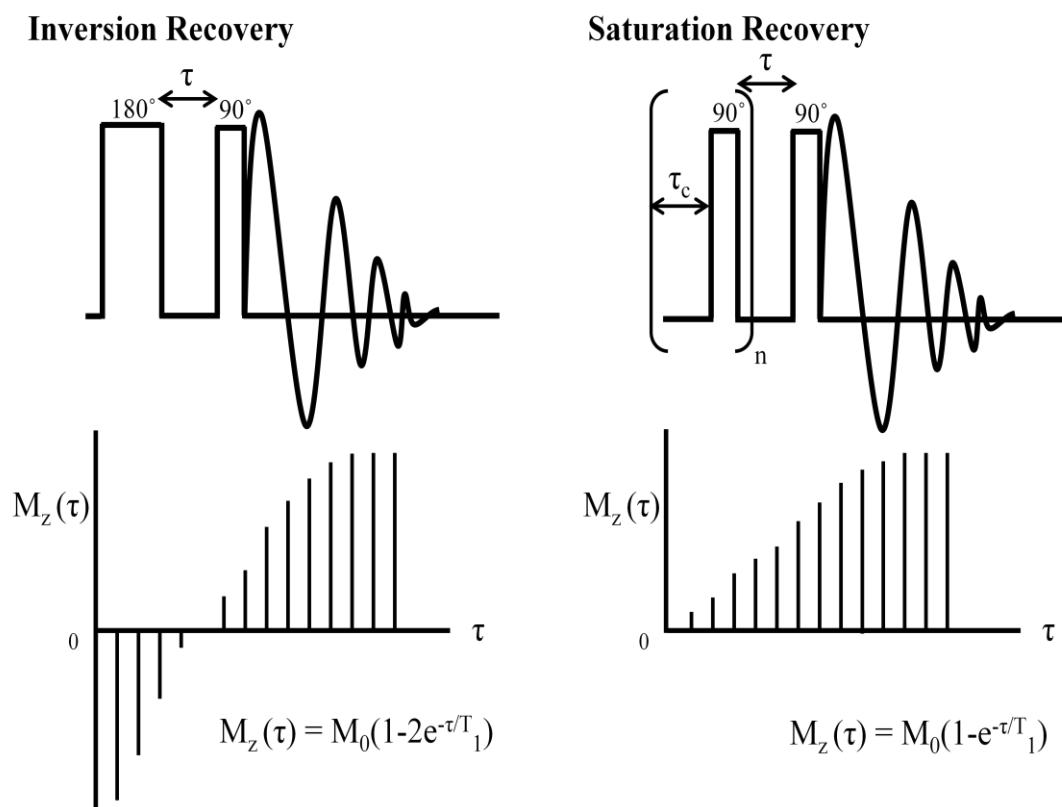
Figure 2.6: Pulse diagrams and simulated data for the inversion and saturation recovery T_1 measurement experiments. The equations used to fit the data and extract the parameter T_1 are included.

The spin-lattice relaxation time (T_1) of a nucleus is defined as the time it takes for the z-component of the magnetization vector of a nucleus to return to its equilibrium position after being subjected to a radiofrequency pulse. The amount of time between

scans in an NMR experiment is dictated by the T_1, a property of a given nucleus in a sample. Measurement of the T_1 through inversion or saturation recovery[33, 36] can reveal how long to wait between scans for efficient relaxation, and can also reveal information about the efficiency of the exchange of energy between a spin and its surroundings i.e. the magnetic relaxation pathways available to a spin system.

For nuclei with relatively short T_1s, measurement can be done using the inversion recovery experiment shown in Figure 2.6. A 180˚ pulse is first applied to flip the full magnetization, M_0, upside-down on the z axis. A period of time, τ, is then waited for the magnetization to relax along the z-axis before a 90˚ pulse is applied, pushing the vector onto the x-y plane. Acquisition of the FID begins at this point, and the experiment is repeated increasing the τ value. Plotting the intensity of the NMR signal against the τ value produces a graph simulated in Figure 2.6. The values are initially negative, but pass through a null point and become positive as longer τ values are applied, eventually reaching a plateau when τ is long enough to allow total relaxation along the z-axis. Fitting of this curve to the equation shown in Figure 2.6 provides the T_1 for a specific nucleus in a specific sample.

The inversion recovery experiment provides a very accurate measurement of T_1, but for nuclei which relax slowly, where T_1 is long (e.g. >30 seconds), inversion recovery can require an unreasonable amount of time to perform, as $5T_1$ needs to pass between scans. The saturation recovery experiment, also detailed in Figure 2.6, solves this problem at the cost of accuracy. A series of 90˚ pulses, separated by a very short $τ_c$ time, are applied to saturate the system and push all magnetization into the x-y plane. After this comb pulse, a length of time, τ, is then waited while the magnetization relaxes along the

z-axis before another 90˚ pulse pushes it back into the x-y plane and the FID is collected. Increasing the τ value and plotting it against the signal intensity produces a graph simulated in Figure 2.6, which when fitted to the adjacent equation, produces a reasonable approximation of the T_1 of the system. The wait time in between multiple scans becomes irrelevant with the use of the combing pulse, and so the saturation recovery is more experimentally efficient when dealing with systems which have long T_1s.

The exponential equations in Figure 2.6 were developed for and are most accurate when dealing with systems which relax under the effects of the magnetic internuclear interactions listed previously. When additional relaxation pathways are available (i.e. paramagnetism, conductivity), the optimized values of T_1 which arise from a fit of the data from an inversion or saturation recovery become less reliable. In the case of a paramagnetic system, it has been noted that the use of a stretched exponential equation models the relaxation more accurately.[37]

$$M_z(\tau) = M_0(1\text{-}2e^{-\tau/T_1})^n$$

The stretching factor, n, allows this equation to more closely model the relaxation of a nucleus in a hypothetical system with evenly-spaced paramagnetic sites throughout the sample. This model closely resembles a MAPO molecular sieve in which the metal centers are paramagnetic (MnAPO-5, FeAPO-5, etc.) and was used to that effect in this thesis.

2.5 References

1.   Cundy, C.S.; Cox, P.A. *Chem. Rev.* **2003**, *103*(3), 663-701.

2.   Cundy, C.S.; Cox, P.A. *Micropor. Mesopor. Mater.* **2005**, *82*(1–2), 1-78.

3.   Feng, S.; Xu, R. *Acc. Chem. Res.* **2000**, *34*(3), 239-247.

4.   Bandyopadhyay, R.; Bandyopadhyay, M.; Kubota, Y.; Sugi, Y. *J. Porous Mater.* **2002**, *9*(2), 83-95.

5.   Matsukata, M.; Osaki, T.; Ogura, M.; Kikuchi, E. *Micropor. Mesopor. Mater.* **2002**, *56*(1), 1-10.

6.   Matsukata, M.; Ogura, M.; Osaki, T.; Hari Prasad Rao, P.; Nomura, M.; Kikuchi, E. *Top. Catal.* **1999**, *9*(1), 77-92.

7.   Kim, M.-H.; Li, H.-X.; Davis, M.E. *Microporous Mater.* **1993**, *1*(3), 191-200.

8.   Chen, B.; Huang, Y. *Micropor. Mesopor. Mater.* **2009**, *123*(1–3), 71-77.

9.   Chen, B.; Kirby, C.W.; Huang, Y. *J. Phys. Chem. C.* **2009**, *113*(36), 15868-15876.

10.   Chen, B.; Huang, Y. *J. Phys. Chem. C.* **2007**, *111*(42), 15236-15243.

11.   Niemantsverdriet, J.W. *Spectroscopy in Catalysis*. **2007**, Weinheim, GE: Wiley-VCH.

12.   O'Hare, D.; Evans, J.S.O.; Francis, R.J.; Shiv Halasyamani, P.; Norby, P.; Hanson, J. *Micropor. Mesopor. Mater.* **1998**, *21*(4–6), 253-262.

13.   Liu, G.; Tian, P.; Zhang, Y.; Li, J.; Xu, L.; Meng, S.; Liu, Z. *Micropor. Mesopor. Mater.* **2008**, *114*(1–3), 416-423.

14.   Longstaffe, J.G.; Chen, B.; Huang, Y. *Micropor. Mesopor. Mater.* **2007**, *98*(1–3), 21-28.

15.   Bragg, W.L. *Proc. Royal Soc.* **1913**, *89*, 428 - 438.

16.   Szostak, R. *Molecular Sieves*. **1998**, London, GB: Thomson Science.

17.   Dyer, A. *An Introduction to Zeolite Molecular Sieves*. **1988**, Avon, GB: John Wiley & Sons, Ltd.

18.   Lauterbur, P.C. *Nature* **1973**, *242*, 190-191.

19.   Bloch, F.; Siegert, A. *Phys. Rev.* **1940**, *57*(6), 522-527.

20.   Bax, A.; Grzesiek, S. *Acc. Chem. Res.* **1993**, *26*(4), 131-138.

21.   Glaser, S.J. *Angew. Chem. Int. Ed.* **2001**, *40*(1), 147-149.

22.   Sutrisno, A.; Lu, C.; Lipson, R.H.; Huang, Y. *J. Phys. Chem. C.* **2009**, *113*(50), 21196-21201.

23.   McBrierty, V.J.; Douglass, D.C. *J. Polym. Macro.* **1981**, *16*(1), 295-366.

24.   Van Bekkum, H., ed. *Introduction to Zeolite Science and Practice*. **1991**, New York, USA: Elsevier.

25.   Akitt, J.W. *NMR and Chemistry: An Introduction to Modern NMR Spectroscopy*. **1992**, London, GB: Chapman & Hall.

26.   Harris, R.K., *NMR of the Solid State: Basic Principles*, in *Multinuclear Magnetic Resonance in Liquids and Solids*. **1990**, Netherlands: Kluwer Academic Publishers.

27.   Klinowski, J., *New Techniques in Solid-State NMR*. **2004**, Heidelberg, GE: Springer-Verlag.

28.   Vaughan, R.W. *Ann. Rev. Phys. Chem.* **1978**, *29*, 397-419.

29.   Andrew, E.R. *Philos. Trans. R. Soc. London, Ser. A.* **1981**, *299*(1452), 505-520.

30.   Frydman, L. *Ann. Rev. Phys. Chem.* **2001**, *52*(1), 463-498.

31.   Friebolin, H. *Basic One- and Two-dimensional NMR Spectroscopy*. **2011**, Weinheim, GE: Wiley VCH.

32.   Fyfe, C.A., *Magic-Angle Spining*, in *Multinuclear Magnetic Resonance in liquids and Solids*, P. Granger, Editor. **1990**, Netherlands: Kluwer Academic Publishers.

33.   Duer, M.J. *Introduction to Solid-State NMR Spectroscopy*. **2004**, Oxford, GB: Blackwell Science.

34.   Pines, A.; Gibby, M.G.; Waugh, J.S. *J. Chem. Phys.* **1972**, *56*(4), 1776-1777.

35.   Hartmann, S.R.; Hahn, E.L. *Phys. Rev.* **1962**, *128*(5), 2042-2053.

36.   Bakhmutov, V. *Practical NMR Relaxation for Chemists*. **2004**, West Sussex, G.B.: John Wiley and Sons, Ltd.

37.   Narayanan, A.; Hartman, J.S.; Bain, A.D. *J. Magn. Reson. Ser. A* **1995**, *112*(1), 58-65

CHAPTER THREE

Studying the Crystallization of SAPO-5 Molecular Sieves Synthesized via Dry-gel Conversion

3.1 Introduction

The field of molecular sieves has been a closely studied branch of material science since their discovery. These crystal structures are unique in that they feature networks of pores and channels as a feature of their unit cells, producing low density and high surface area. The sizes of these pore systems range from the microporous (< 2 nm pore opening) to the macroporous (> 50 nm pore opening). The openings can be circular, ellipsoidal or have a pronounced shape, meaning the materials can be shape and size selective when it comes to their guests.[1-4] Applications for these materials exist in the fields of molecular storage, gas separation/purification and heterogenous catalysis.[6-9] The most well known family of molecular sieves are the aluminosilicate zeolites. Since the 1980's, however, a new class of materials has garnered significant attention: the aluminophosphates ($AlPO_4$s).[10]

$AlPO_4$ sieves are frameworks of tetrahedrally coordinated aluminum and phosphorus atoms linked together by oxygen. Due to charge repulsion and bond instability, the ordering of these frameworks strictly alternates between aluminum and phosphorus, and the framework is therefore charge-neutral.[11, 12] While $AlPO_4$ systems have applications in molecular storage and as catalyst supports, they lack inherent chemical activity. Their true value comes in their receptivity to framework atomic substitution. By exchanging atoms in the $AlPO_4$ framework with atoms of different valency, catalytic sites can be produced that act as Brønsted or Lewis acid sites. Such is

the case when silicon is added to the framework, producing the heterogeneous, shape selective acid catalyst family of the SAPOs.[13]

Typically SAPOs are made via a hydrothermal synthesis (HTS) method.[14, 15] The volumes of solvent (water, in the case of HTS) are easily manageable and products easy to retrieve on a laboratory scale but quickly become unmanageable with scale-up, and so from an industrial point of view a hydrothermal synthesis is non-ideal. Furthermore, the precise mechanisms of atomic substitution are difficult to study within a hydrothermal system, as reliable collection of reaction intermediates can be difficult. An alternative approach was employed in this study: dry-gel conversion (DGC).[16]

In DGC, the starting material is an amorphous gel containing desired framework elements that is physically separated from a small quantity of water in an autoclave reactor. This method of synthesis produces several benefits. A reduction in the necessary amount of solvent means that DGC can be run at a lower cost and with easier clean-up than HTS. Product retrieval is also facilitated in DGC, precluding the need for post-reaction filtration and treatment. Perhaps most importantly to this work, temperature and reaction progress control are much more closely correlated in DGC than in HTS. This means that by quenching the reactions with cold water at fixed times, a reliable method of obtaining reaction intermediates emerges. In the past, DGC has been performed in two slightly different ways: steam-assisted conversion (SAC), where the SDA resides with the starting dry-gel, and vapour-phase transport (VPT), where the SDA resides with the steam source.[16-19]

Despite all the work that has gone into the field, understanding of the crystallization or substitution mechanisms are still underdeveloped. As such, the

predictable design of a molecular sieve based on experience is still not feasible. Understanding how the materials crystallize becomes easier when using the DGC method of synthesis and when collecting crystallization intermediates. The use of DGC instead of HTS does not significantly change the crystallization mechanism, i.e. conclusions drawn from a DGC synthesis would apply to similar sieves crystallized hydrothermally due to the fact that crystallization only occurs after the condensation of liquid water onto the dry-gel, indicating that the reaction conditions are similar in a microscopic sense.

This chapter details the DGC synthesis of SAPO-5 (AFI topology, large-pore sieve), a well-known, highly stable silico-aluminophosphate. The synthesis of SAPO-5 is well studied and robust, and crystallization is rapid in comparison with other SAPO systems, making it a desirable research target. Studies based on SAPO-5 already in publication tend to be interested in crystalline sieves investigating their catalytic or adsorption properties, or with novel methods of synthesizing SAPO-5.[9, 20-31] Studies on the structural properties of SAPO-5 as they relate to function have also been published. Sastre et al. were able to use energy calculations to probe the connections between silicon concentration, framework silica island formation and acid catalyst strength in SAPO-5 and SAPO-34.[32] Zibrowius et al. used ^{29}Si and ^{1}H MAS NMR to look at silicon incorporated into crystalline aluminophosphate sieves synthesized via HTS.[33] They were able to clearly identify the presence of two distinct hydroxyl groups within frameworks, also apparent using IR spectroscopy. Most recently, Li et al. were able to synthesize SAPO-5 hydrothermally in novel crystal morphologies by adding acetic or hydrochloric acid to the developing gel.[34] In addition, SAPO-5 sieves have proven useful in various

hydrocracking and hydroisomerization reactions (especially if loaded with catalytic Pt) and so are industrially important materials.[35-37]

Figure 3.1 shows the hexagonal unit cell of AFI as part of the full pore opening on the left, and illustrates the channel system from two different perspectives on the right. Lines in the illustration represent a T-O-T linkage, where T represents a tetrahedrally coordinated Al, Si or P atom, in contrast to the common chemical bond notation. The synthesis of reaction intermediates which could be used to determine the order of events during the DGC synthesis of these molecular sieves was a main goal. Specific attention would be paid to the incorporation of silicon into the framework. It is hoped that a similar method of study can be used on other aluminophosphate or zeolitic sieve systems as well as other heteroatomic substitutions. Characterization and analysis of the products were carried out by powder X-ray diffraction (XRD), multi-nuclear solid state magic-angle spinning nuclear magnetic resonance spectroscopy (SS-MAS-NMR), energy-dispersive X-ray spectroscopy (EDX) and scanning electron microscopy (SEM).
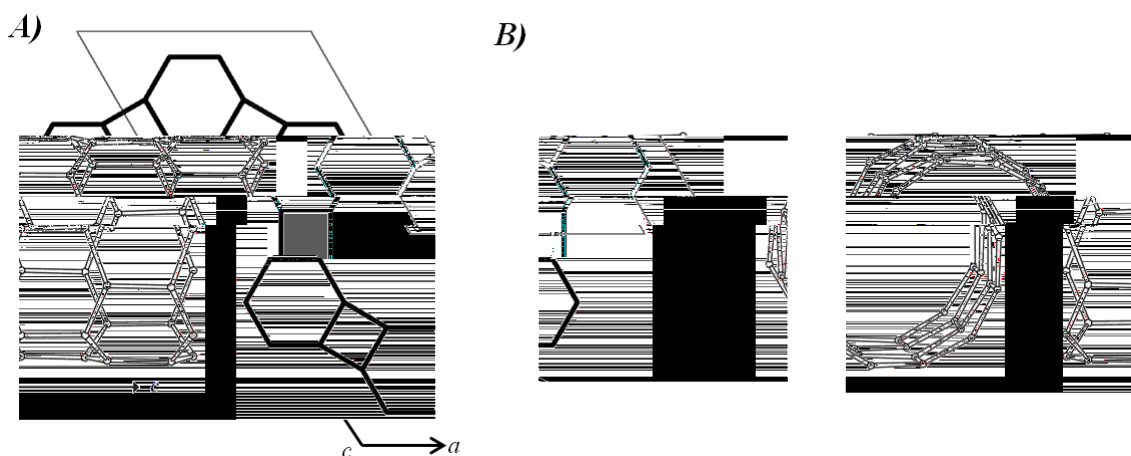
Figure 3.1: a) Schematic drawing of the AFI pore opening showing the crystal unit cell. One line represents a T-O-T bridge. b) Skeletal drawings of the AFI channel system. The channel is open along the c-axis.[5]

3.2 Experimental Details

3.2.1 Synthesis

The synthesis methods used to obtain crystallization intermediates for study were based on literature procedures.[17, 38, 39] Three different variations of the DGC procedure described below were used to investigate the effects of different reaction participants on the crystallizing sieve. The same reagents and molar ratios would be used commonly between all three lines, including the organic structure directing agent, triethylamine (TEA). The molar ratio was set at 1.0 Al_2O_3 : 1.0 P_2O_5 : 0.6 SiO_2 : 1.0 TEA : 40 H_2O for the beginning dry-gel synthesis, where possible. The method below describes the SAC method of synthesis.

Aluminum hydroxide ($Al(OH)_3$, Sigma-Aldrich) was stirred vigorously in deionized water. Phosphoric acid (85%, Caledon) was added slowly after which the beaker was covered with Parafilm and left to stir for 1 hour. Colloidal silica (LUDOX-HS40, 40% wt suspension in water, Aldrich) was added to the beaker, which was left to stir for a further 30 minutes. Triethylamine (TEA) (99.5%, Aldrich) was then added drop-wise, and the complete dry-gel precursor was left to homogenize once more for 30 minutes. Afterwards, the majority of the water was gently boiled off in an oil bath, and once the dry-gel became too thick for a magnetic bar to stir, manual homogenization was performed until the gel solidified. The beaker was then placed in an oven at 80 ˚C overnight to complete drying. The newly solid product was then ground into a fine powder and placed in the autoclave for reaction.

Typically, 1.00 g of dry-gel precursor was added to the inside cup of a stainless steel Teflon-lined double cup autoclave assembly. To the bottom of the outside cup a fixed mass of deionized water was added. The seams of the assembly were sealed off

with Teflon tape before the assembly was closed. The autoclave reactors then were placed into ovens at various temperatures (170-180°C) for various amounts of time (1 hour – several days). When removed from the oven, the autoclaves were quenched with cold water to cease the reactions occurring within. The products were then retrieved and washed with deionized water (if necessary).

Other syntheses of SAPO-5 involve a relocation of some reagents. For the VPT method, rather than adding TEA to the starting dry-gel, it was added to the outside cup of the autoclave assembly mixed with water. The amount used in this study was 0.40 g. In another method, here called vapour-phase silicon uptake (VPSU), the silicon source is added to water in the outside cup of the autoclave. The volatile silicon source used here was tetraethyl orthosilicate (TEOS, 98%, Aldrich). 0.20 g of TEOS were used for this study. Details of the DGC reaction are shown in Table 3.1.

Table 3.1: Summary of relevant synthesis details for the three DGC methods used to synthesize SAPO-5.

Parameter	SAC	VPT	VPSU
Dry-gel formula	$Al_2O_3 : P_2O_5 : 0.6\ SiO_2$ $: TEA : 40\ H_2O$	$Al_2O_3 : P_2O_5 : 0.6\ SiO_2$ $: 40\ H_2O$	$Al_2O_3 : P_2O_5 :$ $TEA : 40\ H_2O$
Silicon source	Colloidal silica	Colloidal silica	Tetraethyl orthosilicate
Water added (g/g of dry-gel)	1.20	1.20	0.80
Temp. (°C)	170	170	180

3.2.2 Characterization

Product identification and determination of relative crystallinity was done through XRD using a Rigaku diffractometer using Co Kα radiation (λ = 1.7902 Å). MAS, Hahn

echo and cross-polarization NMR experiments, investigating ^{27}Al, ^{29}Si and ^{31}P nuclei, were performed using a Varian/Chemagnetics Infinityplus 400 WB NMR spectrometer operating at 9.4 T. The Larmor frequencies of ^{27}Al, ^{29}Si and ^{31}P nuclei were set at 104.1, 79.6 and 161.7 MHz, respectively. The spectra taken were standardized against 1M Al(NO$_3$)$_3$ solution (0 ppm), tetrakis(trimethylsilyl) silane (major peak -9.8 ppm from TMS at 0 ppm) and ammonium dihydrogen phosphate (0.81 ppm from 85% H$_3$PO$_4$ at 0 ppm) for ^{27}Al, ^{29}Si and ^{31}P, respectively.[40, 41] SEM and EDX measurements were done using a Hitachi S-4500 field emission scanning electron microscope equipped for EDX with an EDAXTM system.

3.3 Results and Discussion

3.3.1 Added Water Optimization

The first step towards obtaining crystallization intermediates was to determine the correct amount of water to be added to the bottom cup of the autoclave for the three synthesis methods under study. As the incorporation of silicon into an AFI framework was the main topic of study in this work, the crystallinity of samples was important to optimize. Literature reports have variously used low and high relative amounts of water[17, 42] to varying degrees of success in synthesizing AFI sieves, and so ranges of added water were used. The products of these experiments were studied using XRD and ^{29}Si NMR to investigate the effect water content made on the crystallinity and silicon content in the SAPO-5 sieve.

The results of the SAC optimization based on added volume of water are shown in Figure 3.2. According to previously reported studies, the resonances centered around -90, -95, -100, -105, and -110 ppm have been assigned to Si(OAl)$_4$, Si(OAl)$_3$(OSi),

$Si(OAl)_2(OSi)_2$, $Si(OAl)_1(OSi)_3$ and $Si(OSi)_4$ respectively.[33, 43, 44] This work will refer to these silicon sites in the common notation: Q^0 for $Si(OAl)_4$, Q^4 for $Si(OSi)_4$, etc. A range of added amounts of water from 0.3 g to 1.8 g per gram of dry-gel were tested. The spectra clearly indicate the amount of water added has a marked effect on the degree of silicon incorporation for this synthesis method. Simultaneously, it is clear that the amount of added water had little to no effect on the crystallinity of the sieves as observed by XRD.
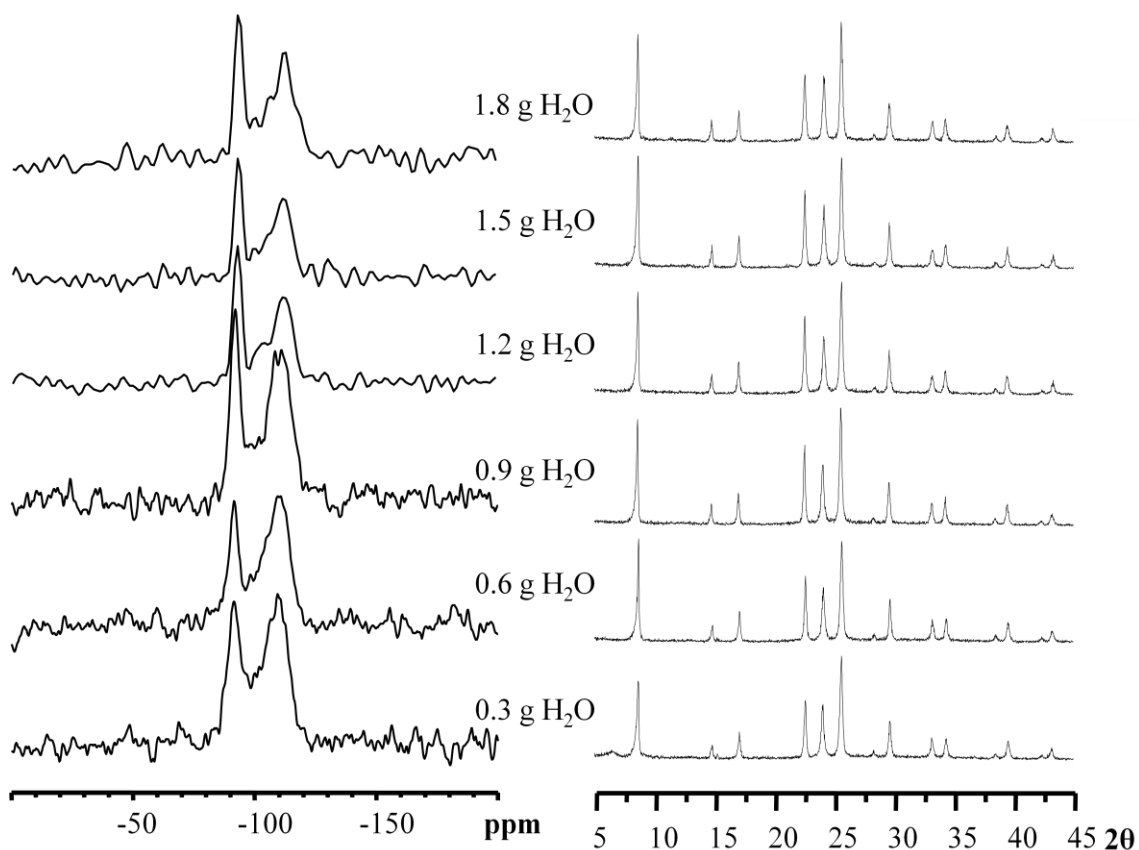
Figure 3.2: ^{29}Si MAS spectra and X-ray diffractograms for the added water optimization of the SAC synthesis of SAPO-5.

After three days reaction under SAC conditions, in all cases a peak centered around -91.5 ppm is present. This peak can be assigned to Q^0 nuclei, i.e. silicon atoms with only aluminum in their second coordination spheres, $Si-(OAl)_4$. Increasing the

relative amount of these kinds of silicon nuclei in the sieve is desirable, as they represent homogeneously incorporated silicon nuclei that act as acid sites. The other main feature of the spectra is a broader, asymmetric peak centered around -110 ppm (Q^4) but with significant intensity between -100 and -115 ppm. This resonance represents Q^{2-4} nuclei, which could either be unreacted silica left over from the added reagents or may represent silica islands within the sieve. The relative size of the Q^0 peak compared with dense silica phase peaks of any kind (specifically Q^4, though not exclusively) was used to determine which amount of water was able to yield the highest amount of silicon incorporation. A clear difference can be seen between the 0.3 g and 1.2 g samples: more silicon is incorporated as Q^0 nuclei when using more added water. From 1.2 g to 1.8 g of added water, the relative sizes of the incorporated Q^0 silicon peak at -90 ppm versus the dense phase peaks do not change significantly,. Based on these data, the optimized amount of added water at this temperature was set at 1.2 g per gram of dry-gel, and this amount was used to obtain crystalline intermediates with significant silicon incorporation.

An optimization of the added amount of water in the VPT synthesis method based on XRD results can be seen in Figure 3.3. The crystallinity of all samples, ranging from 0.4 g to 2.0 g added water per gram of added dry-gel precursor are comparable. The minor amorphous halo seen in the 1.6 g of water added sample excluded it from usage. The other samples would have to be compared based on their silicon uptake, as studied using ^{29}Si NMR. For the water optimization of the VPT syntheses the same NMR parameters were used as for the SAC samples. Figure 3.3 shows the results of these experiments, with accompanying X-ray diffractograms. The diffractograms all show highly crystalline AFI frameworks developed after the three-day reaction time. Only a
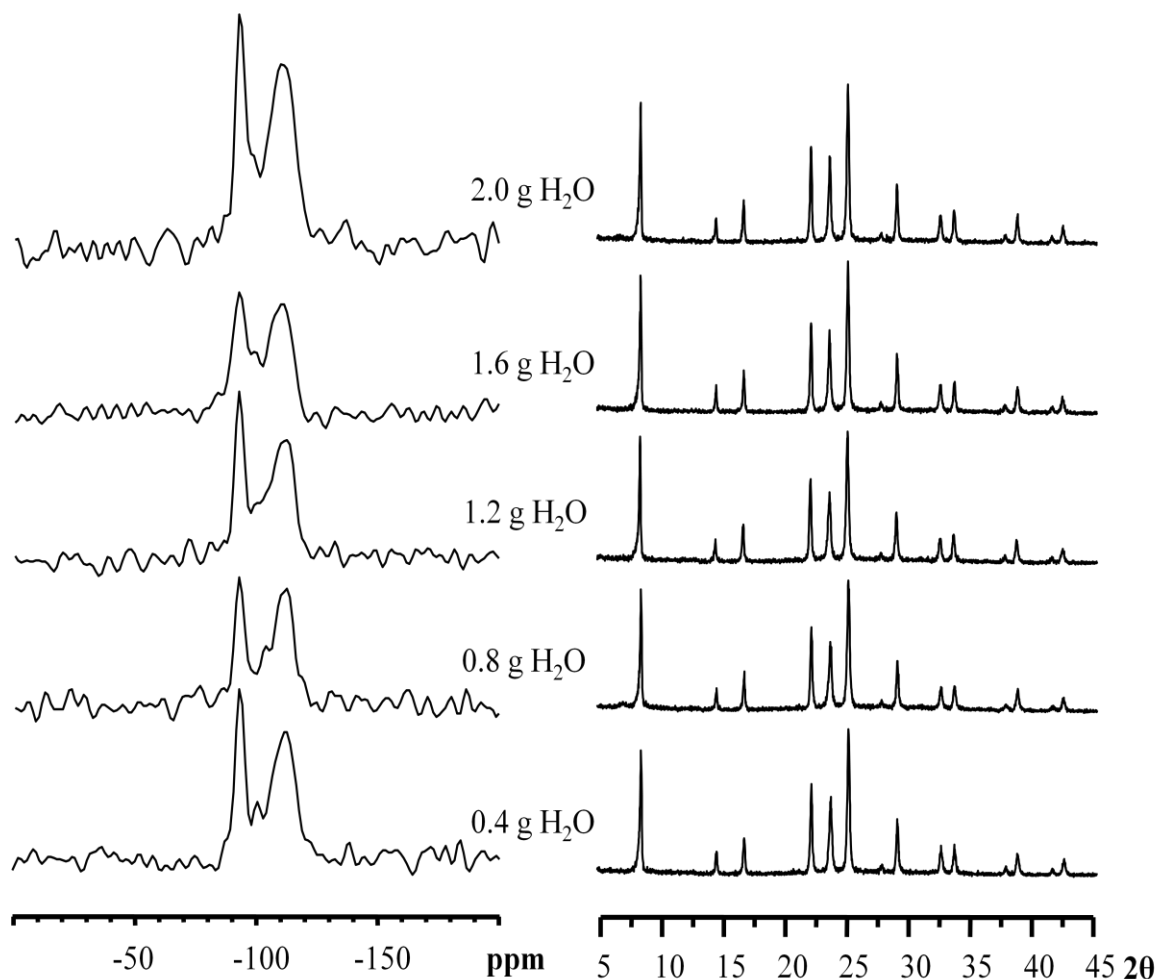
Figure 3.3: ^{29}Si MAS spectra and X-ray diffractograms for the added water optimization of the VPT synthesis of SAPO-5.

very slight difference in crystallinity can be observed between the samples. The ^{29}Si NMR results are also similar to the SAC results, with the finished crystals showing well-resolved Q^0 nuclei peaks at ca. -90 ppm and the presence of leftover dense silica starting material present as signified by the peak centered ca. -110 ppm. There is no pattern noted for better silicon incorporation with increasing or decreasing water added, as was the case in the SAC method. Incorporation does change depending on how much water was used, but not in a predictable fashion. Based on the relative sizes of the incorporated and non-incorporated silicon sites, as well as the aforementioned slight differences in crystallinity
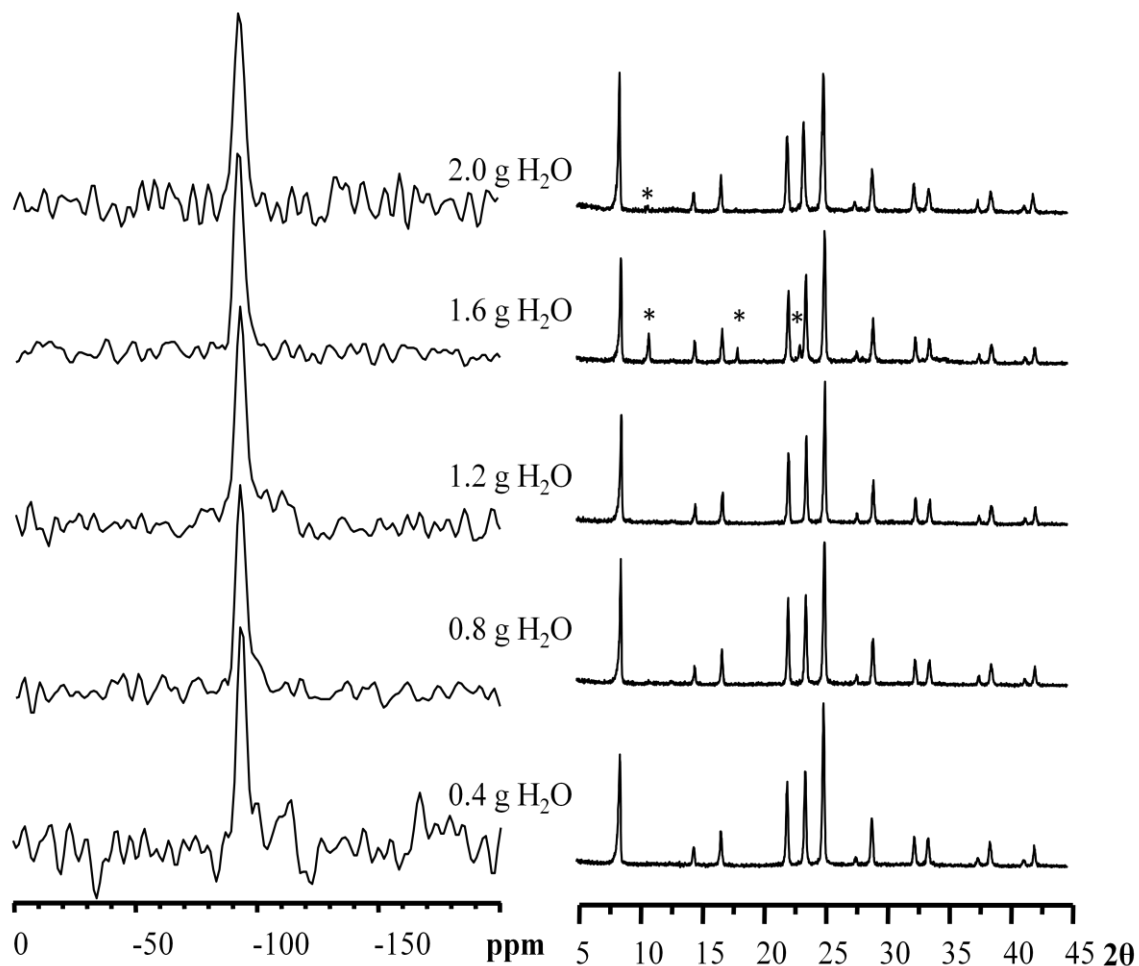
Figure 3.4: ^{29}Si MAS spectra and X-ray diffractograms for the added water optimization of the VPSU synthesis of SAPO-5. Impurities are marked with an asterisk.

notable via XRD, the added amount to be used in the crystallization runs was set at 1.2 g of water per 1.00 g dry-gel.

The results of water volume optimization in the VPSU method looking at XRD and ^{29}Si NMR are shown in Figure 3.4. Aside from the 1.6 g added water sample, which shows a significant presence of co-crystalline SAPO-18[45], all the samples are well crystalline AFI frameworks when looking at XRD after the three-day reaction time. The ^{29}Si one pulse MAS NMR spectra of the crystallized samples show only one sharp peak at ca. -90 ppm. This peak can be assigned to Q^0 well incorporated framework silicon nuclei. No other peaks were visible, indicating little, if any, silicon was present that had

other silicon atoms as its next closest neighbours, i.e. no silica was present in the finished product. Without another peak for comparison, this made selection of the optimized synthesis parameters difficult. Based on crystallinity and the symmetry and resolution of the Q^0 peak, the 0.8 g of water sample was chosen for the crystallization run.

3.3.2 Steam Assisted Conversion

X-ray diffractograms for the synthesis intermediates of SAPO-5 under SAC conditions are shown in Figure 3.5. After three days reaction time, highly crystalline AFI-framework crystals seem to be the dominant species in the powder, with no discernible co-crystalline phase or impurity. The peaks in these diffractograms match literature patterns for the AFI framework[17]. On closer inspection, the bulk of the crystal structure forms in a very short time early on in the reaction. The onset of crystallization occurs between 2.5 and 3 hours, after which well-crystallized AFI framework crystals are present. The crystallinity improves over the next ca. three hours up to six, and then remains stable up to three days and beyond.

The dry-gel diffractogram shows that the material is amorphous in nature prior to any autoclave heating. Very weak and/or broad reflections can be seen in the low-angle region for the samples collected at $1 - 2.5$ hours reaction time, but the dominant character of these diffractograms remaining amorphous. The amorphous phase is present and dominant up until the onset of crystallization. No crystalline intermediate phase forms between the amorphous phase and the final crystal structure. This is in agreement with previous work from this group when studying the crystallization of $AlPO_4$-5 sieves made via SAC.
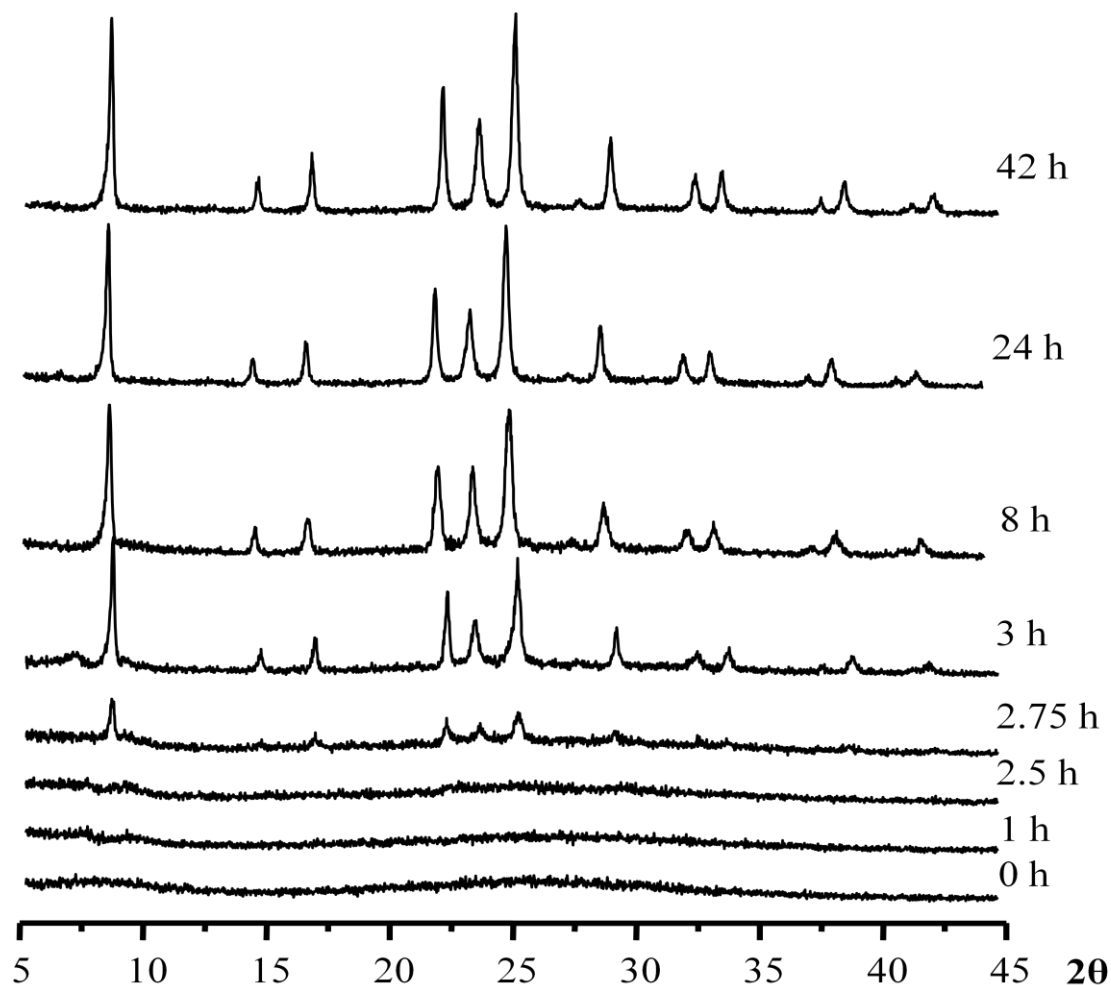
Figure 3.5: X-ray diffractograms for the crystallization of SAPO-5 under SAC conditions.

The lack of any layered intermediate indicates that the AFI crystal grows in three dimensions without the need of stacking or layering framework components first. The rapid completion of crystallization indicates that the induction and nucleation periods of crystal growth are short. It is likely that, under the influence of the SDA, small AFI framework crystallites form early on in the reaction. Being that the crystallization occurs so rapidly, these simultaneously forming crystal nuclei are able to aggregate and grow into large crystals very efficiently.

XRD does not provide any data on elemental composition. This fact is particularly important to keep in mind for these data, as both SAPO-5 and $AlPO_4$-5 crystallize in an AFI framework, and look identical when analyzed by XRD. These measurements were taken to monitor bulk crystallinity and to ensure the correct products were made, but NMR was used to investigate heteroatomic substitution.

Figure 3.6 shows the ^{27}Al and ^{31}P Hahn echo and MAS spectra, respectively, for selected crystallization intermediates in the SAC synthesis of SAPO-5. Samples were selected based on their progress in the reaction according to XRD in order to get an idea of the aluminum and phosphorus environments in a sample which is amorphous, mid-reaction and fully crystallized. The assignments given to the resonances found here match previously published data on the NMR spectroscopy of $AlPO_4$-5 or SAPO-5 molecular sieves.[39, 46] The ^{27}Al spectra for the SAC method show that the aluminum in the dry-gel can be described by three distinct sites. Two broad peaks centered around 5 and -13 ppm can be assigned to unreacted alumina and octahedrally coordinated $(Al(OP)_4(H_2O)_2)$ respectively. A sharper peak centered around 40 ppm has been assigned to tetrahedrally coordinated aluminum $(Al(OP)_4)$ as it exists in the $AlPO_4$ framework. As the reaction progresses to completion, the signal at 40 ppm sharpens and becomes more intense, at the expense of the other two signals. The final product is dominated by this product peak, indicating a high degree of crystal purity, as supported by XRD. The ^{31}P MAS dry-gel spectrum also possesses three signals centered around -18 ppm, -5 ppm, and -20 ppm. The broad peak at -18 ppm represents the wide array of phosphorous environments present in
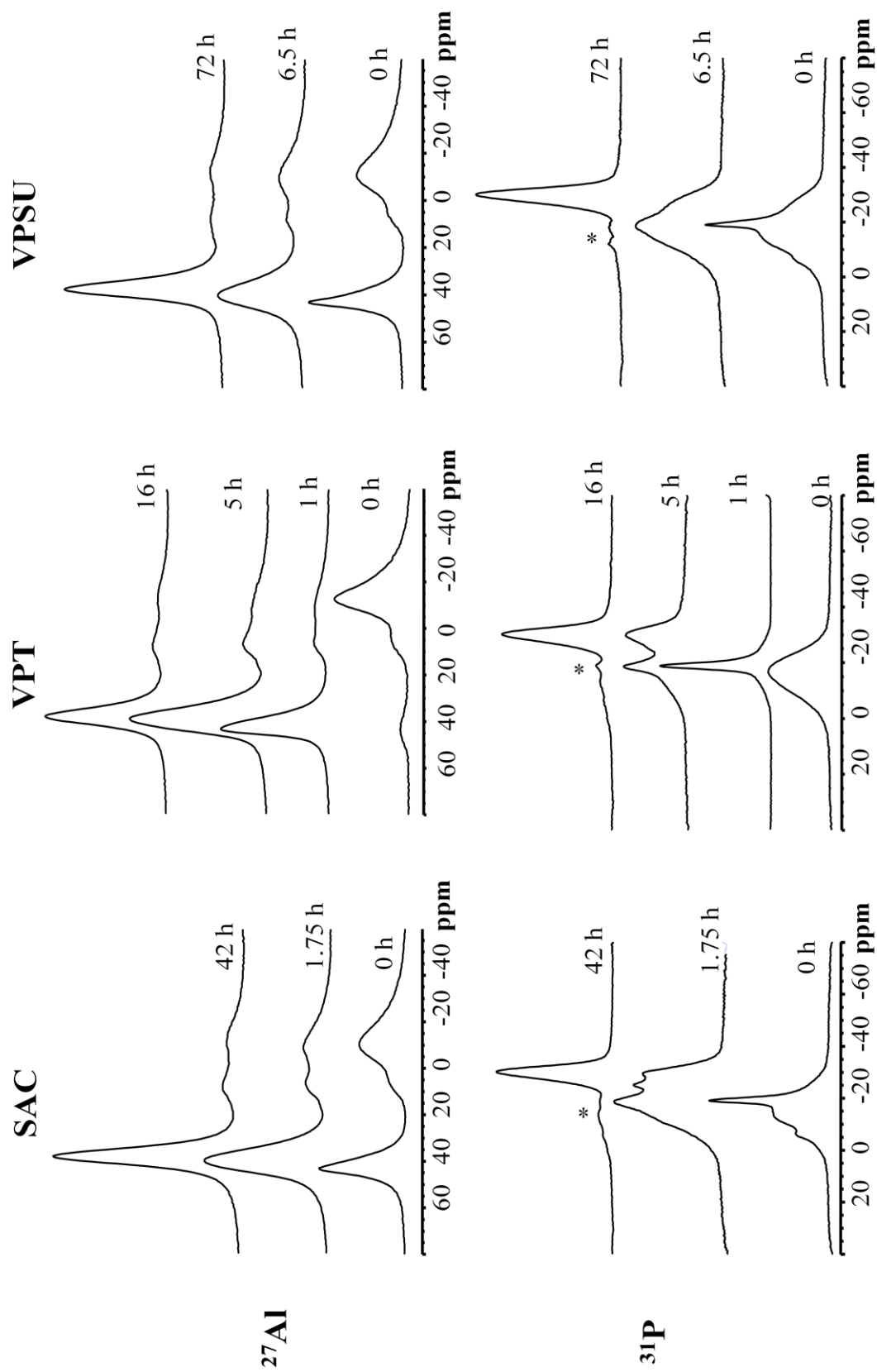
Figure 3.6: ^{27}Al Hahn echo and ^{31}P MAS spectra for selected crystallization intermediates in the synthesis of SAPO-5 (impurities are marked with an asterisk).

the amorphous precursor. The most intense, sharp peak at -20 ppm has been attributed to not fully condensed, framework phosphorous ($P(OAl_3)(OH)$), i.e. some local phosphorous ordering is present. The shoulder at -5 ppm has been assigned to impurities which are invisible to XRD in these samples. As the reaction progresses, a sharper, asymmetric peak centered around -28 ppm emerges from the initial pattern which begins as two signals at ca. -26 and -29 ppm. These can be assigned to SAPO-5 precursor phosphorus environments. As the reaction reaches completion the sole peak visible is located at -29 ppm, and as such the final product spectrum is dominated by phosphorus in the SAPO-5 framework. These results agree with previous work from this group studying the crystallization of the structurally-related $AlPO_4$-5 system in a similar manner.[38]

Scanning electron micrographs of crystalline samples of SAPO-5 are shown in Figure 3.7, and the results of the EDX analysis are listed in Table 3.2. The SEM image for the SAC synthesis shows an aggregation of small crystallites covered in circular nodes which could be amorphous starting material or crystal nuclei. The EDX results show that the SAC crystals are 4.77 % (atomic) silicon. Flat crystal surfaces were used as the targets for EDX elemental analysis in order to get a more reliable reading on the atomic ratios of the sieves. In the case of the SAC method, the P/Al and (Si+P)/(Si+Al) ratios are both very close to unity. This indicates that SM3 was the method of silicon incorporation for this synthesis, as two silicon atoms tend to take the place of an Al-P pair and therefore do not disturb the Al:P ratio of an $AlPO_4$ crystal.
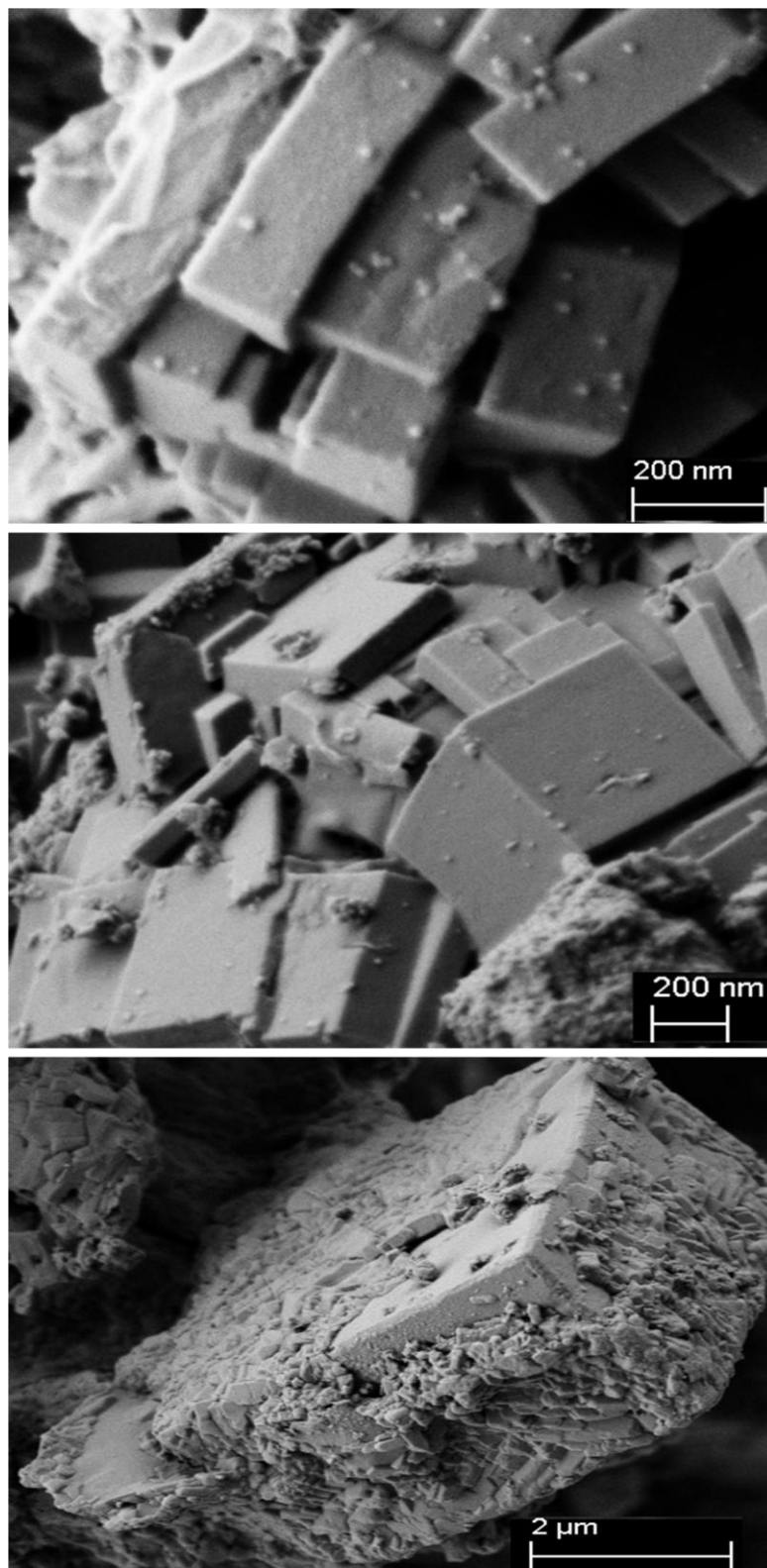
SAC

VPT

VPSU

Figure 3.7: Selected scanning electron micrographs of SAPO-5 crystals synthesized via dry-gel conversion.

Table 3.2: Elemental compositions (atomic %) of crystalline samples of SAPO-5 synthesized via dry-gel conversion.

Synthesis	Al	Si	P	P/Al	Si/P	Si/Al	(Si+P)/Al	(Si+P)/(Si/Al)	SM
SAC	8.18	4.77	8.13	0.99	0.59	0.58	1.6	1.0	3
VPT	5.10	1.58	5.02	0.99	0.31	0.31	1.3	0.99	3
VPSU	7.41	0.56	7.03	0.95	0.08	0.08	1.0	0.95	2

Figure 3.8 shows the ^{29}Si single pulse and CPMAS NMR spectra for selected crystallization intermediates in the SAC synthesis of SAPO-5. The intermediates were chosen based on the X-ray diffractograms seen in Figure 3.5 in order to get an idea of the silicon environments that were present during different stages of crystallization. The one
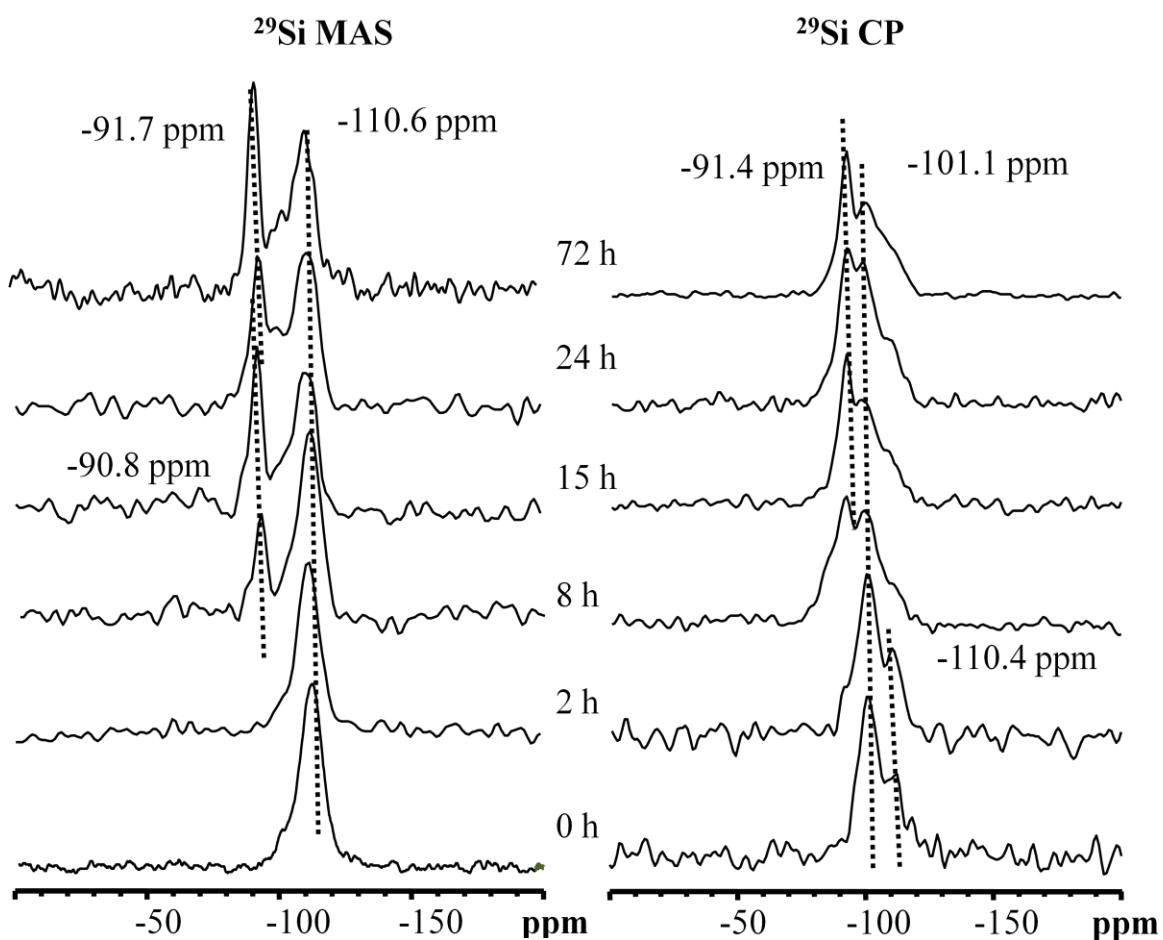
Figure 3.8: [29]Si MAS and CP spectra for selected crystallization intermediates in the SAC synthesis of SAPO-5.

pulse spectrum collected for the dry-gel shows a broad, single peak centered around -110 ppm, meaning that the starting form for silicon is a Q^4, dense phase silica, $Si(OSi)_4$. This indicates that no silicon insertion occurs into an aluminophosphate precursor phase, supported by the fact that no such phase is observable via XRD. The peak is not symmetrical, showing shoulders on the left side. These represent small quantities of Q^3 and Q^2 silicon nuclei, likely existing at surface sites within the dense silica phase(e.g. $Si(OSi)_2(OH)_2$, $Si(OSi)_3OH$).

A signal emerges at the 8 hours reaction time mark, this time centered ca. -90 ppm, which can be attributed to Q^0, well incorporated silicon sites within the growing sieve. This peak grows with time, while the dense silica peak shrinks; this indicates that the silicon is gradually activating from the silica starting material phase and being incorporated homogeneously into the developing sieve. No significant intermediate spectra where Q^3, Q^2 or Q^1 nuclei dominate were collected, which would have indicated the incorporation of large silica-like chunks into the developing sieve (e.g. Al-O-Si-O-Si-O-Al). This slow dissolution of silicon leads to well-incorporated, dispersed silicon nuclei. The spectra of the finished product show a significant peak centered ca. -110 ppm. This is potentially unused starting material, but could be indicative of large silica islands. The silicon does not begin to incorporate until after the AFI framework peaks are seen via XRD.

The CP spectra shown in Figure 3.8 complement the single pulse spectra. A short contact time of 0.8 ms was used for these experiments in order to selectively enhance silicon centers which were in close proximity to protons. A peak at ca. -110 ppm can be seen in the dry-gel, which gradually gives way to a peak at ca. -90 ppm in the finished

sieve. Present in all of these spectra as the dominant peak, however, is a broad resonance centered around -100 ppm, indicative of Q^2 nuclei. This signal decreases in intensity as reaction progress continues, meaning that at least some of these silicon atoms are from the starting material and are being slowly, evenly incorporated into the developing SAPO-5 sieve. A small shoulder at ca. -90 ppm in the two hours reaction time sample can be seen in the CP spectra. This indicates that at least a small amount of silicon exists as Q^0 nuclei, although the amount of this kind of silicon nucleus is extremely low, and may not be bridged to aluminum. This signal gets larger consistently as the reaction progresses. A minute amount of silicon may find its way into the developing sieve early on, but as evidenced by the one pulse spectra, significant silicon incorporation does not begin until the crystal is already well-formed.

3.3.3 Vapour Phase Transport

Figure 3.9 shows the XRD data taken for intermediates collected for SAPO-5 samples synthesized using the VPT method. The end products show highly crystalline, pure AFI frameworks with little, if any, amorphous halo or other co-crystalline phases. The starting materials, conversely, are amorphous in nature, indicating a completely amorphous precursor gel. In these respects, the data mirror those collected for the SAC synthesis, indicating both methods can be used to grow pure crystals from amorphous precursors. However, this is where the similarities between the methods end.
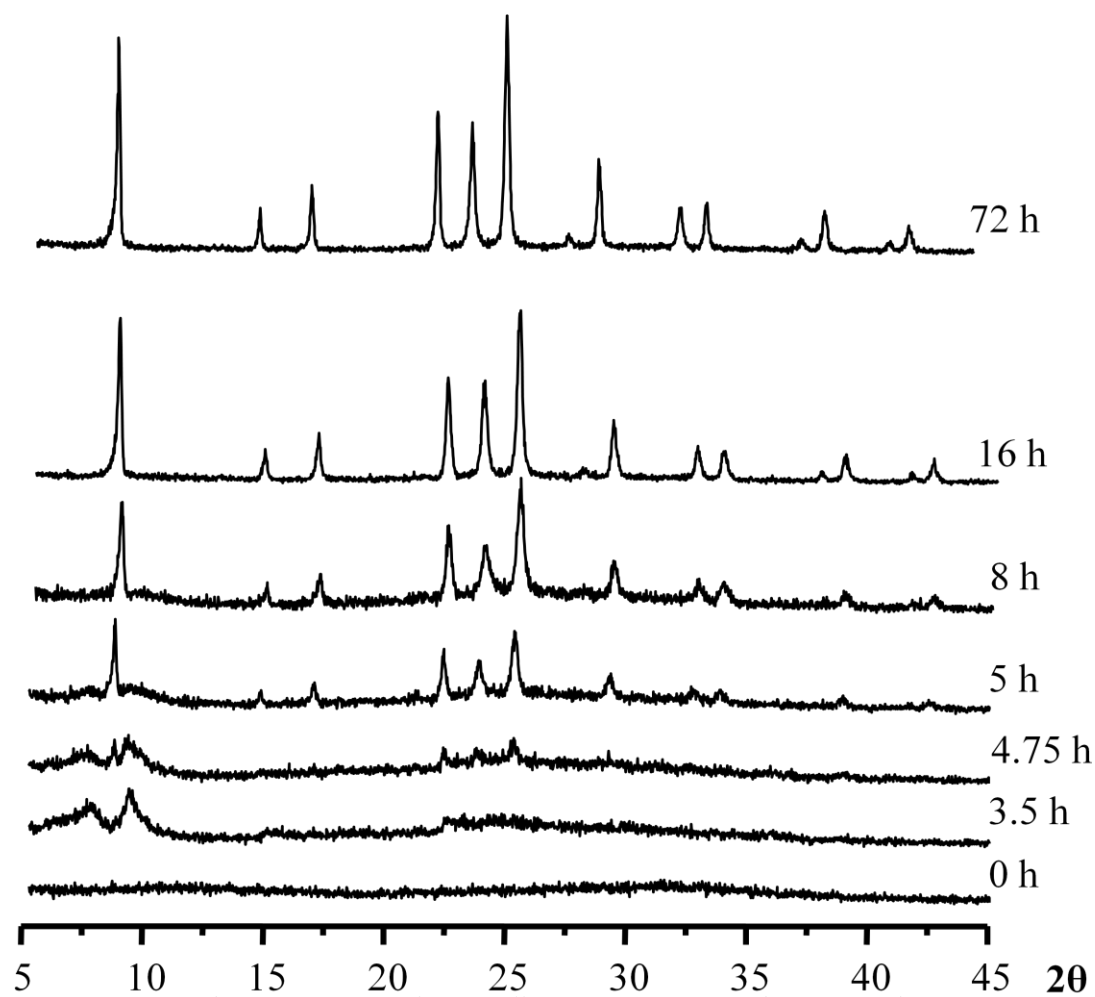
Figure 3.9: X-ray diffractograms for the crystallization of SAPO-5 under VPT conditions. Impurity peaks are marked with an asterisk.

Firstly, it is evident that the onset of crystallization occurs later in VPT, around the 4.5 hour mark. This indicates that the nucleation phase of crystallization is taking much longer to begin. This is easily rationalized: as the crystals require the influence of a SDA to form, and considering that the SDA is no longer readily available from the start of the reaction in the dry-gel, the crystallization takes significantly longer to begin. Once SDA can condense on the gel surface and the reaction does begin, however, the full crystal structure is apparent via XRD in very short time. The crystal structure is relatively stable, with the appearance of some co-crystalline SAPO-18-like materials over longer timescales (not shown). Due to the fact that TEA is a structure directing agent, not a true

template, it can direct for multiple different crystal structures based on sensitive reaction parameters. The presence of impurity peaks or co-crystalline phases is likely a result of an anomaly in that particular reaction (contaminated autoclave, improper added amount of water, SDA, etc.) and not indicative of the crystallization of the target sieve.

An interesting contrast is the presence of two low-angle diffractions, easily visible in the diffractograms for the one to four hour reaction time samples. These two broad reflections are accompanied by a number of similarly broad reflections in the mid range. This indicates that before structure direction can begin under the influence of triethylamine, another phase is being formed. Similar studies into the crystallization of $AlPO_4$-5 have described this phase as a "12-membered ring-like" AFI precursor developed under the influence of the SDA and held in place by relatively weak hydrogen bonding.[38] The pseudo-pores are larger than true AFI pores and ellipsoidal in shape. As can be seen in the diffractogram for the 4 hours 45 minutes reaction time sample, the lowest angle diffraction for the AFI framework is almost coincident with the lowest angle reflection for this intermediate. This indicates that the d-spacing is similar between the two materials, and so they could conceivably be related. Also from the 4 hours 45 minutes sample, it can be seen that the AFI framework is developing directly from this intermediate. This shows that there are no other intermediates, and further supports that the structures are indeed related. This differs from the SAC synthesis, where the AFI framework develops directly from the amorphous precursor. when the silicon incorporation begins to take place, and the effect these new synthesis parameters have on it, remain to be seen using NMR.

The VPT [27]Al and ^{31}P spectra shown in Figure 3.6 display a slightly different pattern than the SAC, particularly in the dry-gel. The dominant peaks in these spectra are octahedral aluminum for the [27]Al spectrum and amorphous material for the ^{31}P spectrum. The introduction of SDA to the dry-gel via VPT causes rapid change in the Al and P environments, and after as little as one hour of reaction time, the spectra change drastically, now being dominated by signals for tetrahedral aluminum at ca. 40 ppm and not fully condensed phosphorus at ca. -19 ppm. As crystallinity becomes apparent at around the 5 hours reaction time mark, the aluminum peak shifts slightly to 37 ppm and intensifies, and the characteristic fully condensed tetrahedral phosphorus peak appears at ca. -30 ppm, which then intensifies and dominates the spectrum as crystallinity is established. These results indicate that a dry-gel which does not contain the precursors to a molecular sieve can be rapidly converted into an AFI precursor gel under VPT conditions, as has been previously reported and exploited. The inclusion of silicon sites into the frameworks does not seem to have any significant bearing on the condensation of aluminum or phosphorus sources into an AFI sieve. This supports the assertion that during SAPO-5 crystallization, an $AlPO_4$ core forms which then expands as crystallinity increases, incorporating silicon into the outer coordination spheres only. While the SAC and VPT methods seem to produce different initial crystallization environments, after a very brief period of reaction the systems begin to converge. The SDA seems to produce ordered phosphorous framework sites and tetrahedral framework aluminum sites very efficiently, and so after only a hour of reaction time, the VPT spectra closely resemble the SAC dry-gel spectra, coming from very different beginnings.

The SEM images in Figure 3.7 of crystals of SAPO-5 synthesized via VPT resemble those made via SAC. Similarly sized crystallites are readily apparent alongside a significant amount of amorphous material or crystal nuclei. EDX results in Table 3.2 indicate that the SM3 substitution pathway is observed for this synthesis method as well. The amount of silicon which makes it into the sieve from the reactant dry-gel is different between these two synthesis methods. Nearly twice as much silicon is incorporated in the SAC method when compared with the VPT method, as shown in the Si/P and Si/Al ratios. Reconsidering the ^{27}Al and ^{31}P NMR spectra above, it would appear that a starting dry-gel with a significant presence of tetrahedrally coordinated aluminum centers and not fully condensed phosphorous is more amenable to silicon incorporation than one with amorphous sources of Al and P. This difference is likely based on the pH change involved in the presence or absence of the basic tetraalkylammonium SDA in the dry-gel. The amounts of silicon being incorporated in either case are comparable with previously published work.[31, 47, 48]

Figure 3.10 shows the ^{29}Si one pulse and CP MAS spectra for the samples of the VPT crystallization run taken at the noted reaction times. The MAS spectrum of the dry-gel as well as the early reaction time samples all show a single, broad peak centered around -110 ppm, indicating the presence of Q^4 silicon nuclei like those that exist in the dense silica starting material. The asymmetry of this peak is less pronounced than in the SAC method, indicating fewer surface sites or defect sites where silanol groups are present, which would weigh the peak more heavily on the deshielded side. The Q^4 signal at ca. -110 ppm in the CP spectra is actually enhanced from the dry-gel to the three hour sample. This is likely due to the activation of silicon source or the introduction of the
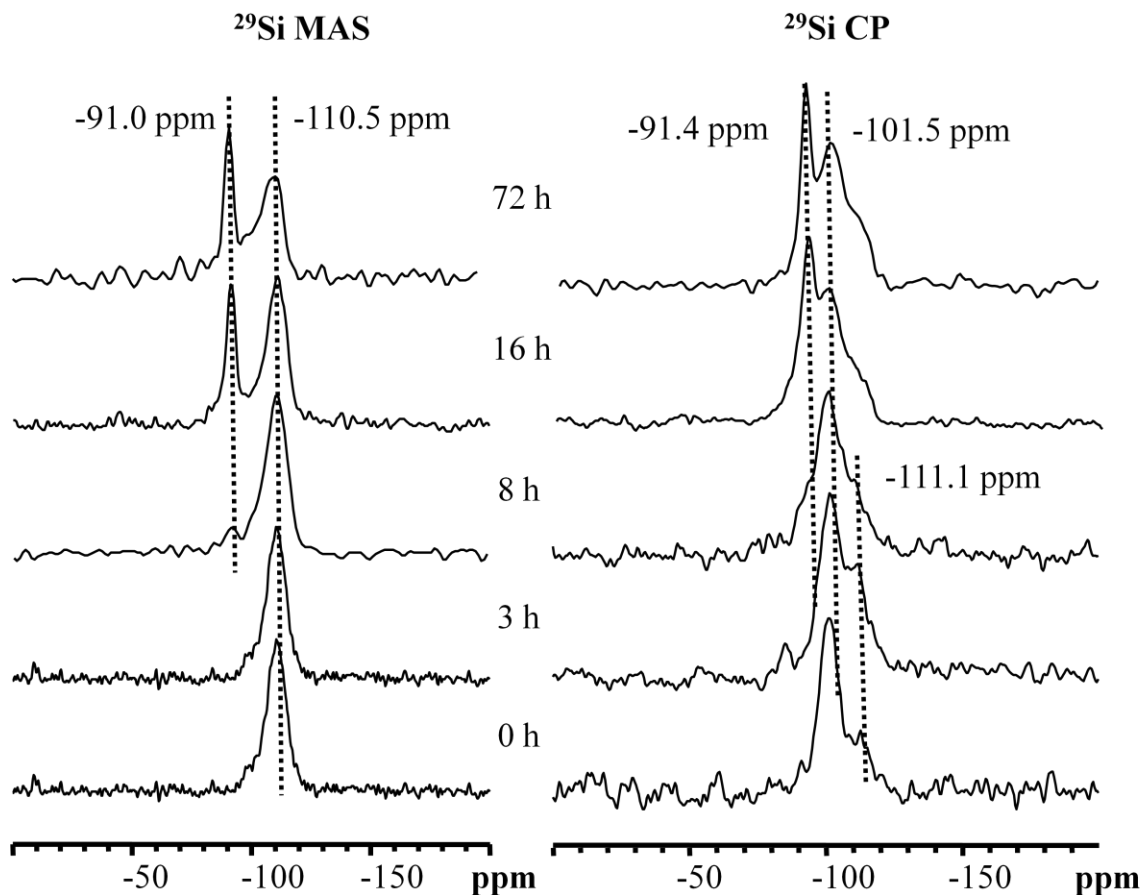
Figure 3.10: ^{29}Si MAS and CP spectra for selected crystallization intermediates in the VPT synthesis of SAPO-5.

SDA to the dry-gel, both of which would result in the enhancement of Q^4 silicon nuclei due to increasing proximity to cross-polarising protons.

The first instance of incorporated Q^0 silicon nuclei can be seen in the spectrum of the 8 hours reaction time sample, in the presence of a very small peak visible at the -90 ppm position. This signal is enhanced to an even greater degree in the corresponding CP spectrum, likely due in one part to the activation of the dense silica starting material causing hydrolysis of the Si-O-Si bridges, and in part to the introduction of gas-phase SDA protons to the gel. Both these effects would cause amplification of the Q_0 signal in the 8 hour CP spectrum. This peak does not grow significantly over the next two hours (spectrum not shown), but is clearly visible in the spectrum of the 16 hours reaction time

sample. As the reaction progresses, this peak continues to grow, while the starting material peak diminishes at a comparable rate, indicating that the new Q^0 silicon species are being incorporated into the framework homogeneously, as was the case with the SAC crystallization. The first instance of incorporated silicon does not appear until the eight hour sample, while crystal structure is observable via XRD as early as 5 hours. This indicates that an $AlPO_4$-5 sieve is first formed and then gradually incorporates silicon as it becomes available. The three-day sample shows a well-resolved major peak centered at -91.0 ppm, signifying Q^0 silicon nuclei, as well as an asymmetric peak centered ca. -110 ppm indicating either silica islands within the sieve or leftover reagent silica.

CP spectra, also shown in Figure 3.10, show a dry-gel sample with Q^2 silicon nuclei being the dominant peak. After a short reaction time, a shoulder at ca. -110 begins to intensify. This is likely due to the introduction of the SDA via the VPT method. As the SDA permeates the dry-gel, the cross-polarization between SDA protons and Q^4 silica becomes stronger, and so the peak becomes more evident. This can also signify the hydrolysis of Si-O-Si bridges to form silanol sites within the starting material silica $(Si(OSi)_3OH)$. As the reaction progresses this peak diminishes and the Q^0 peak around -90 ppm becomes the dominant peak as the sieves develop. Starting material silicon nuclei, represented by a peak centers around -101.5 ppm are now under the influence of proton CP, and are also still visible, supporting the MAS spectrum data. This shows that the gas-phase SDA is able to permeate the dry-gel and direct for the structure of the sieve, as well as find its way into the silicon starting material.

The relatively low level of silicon uptake seen in the VPT method when compared with SAC can be explained as a result of this crystallization study. From the beginning of

the VPT synthesis, without the initial structure direction of the SDA, the phosphorous and aluminum begin to form an intermediate which is not AFI, and which may not be amenable to silicon incorporation. As the SDA is introduced to the dry-gel and structure direction begins, this phase begins to give way to the AFI sieve and silicon incorporation can begin. This delay in the ability of the dry-gel to incorporate silicon into sieve precursors explains the significant drop in silicon atomic % in the VPT final products.

3.3.4 Vapour Phase Silicon Uptake

The X-ray diffractograms for samples synthesized under VPSU conditions are shown in Figure 3.11. Crystalline AFI framework sieves are detectable as early as 6 hours and 15 minutes. This makes VPSU the slowest method of synthesis out of the three detailed here (with a spread of ca. 2 hours). The material goes from largely amorphous to crystalline inside of an hour, indicating that the nucleation phase is as quick as the other two DGC methods in this study. Broad, low-angle reflections are present in the dry-gel, similar to those seen in the VPT-synthesized intermediate samples. This semi-crystalline phase is quickly degraded back to a fully amorphous phase after only one hour of heating.

Highly crystalline AFI framework sieves are detectable after seven hours reaction time, and are stable up to three days reaction time. Indeed, longer crystallization times seem to improve the crystallinity. This indicates that the by-products of TEOS hydrolysis, if present in the dry-gel (ethanol, ethane, ethene, acetaldehyde), are not interfering with the crystallization mechanism. No side reaction seems stop TEA from performing structure direction, or framework atoms from quickly forming into the desired sieve. This would be evident in the presence of a large amorphous halo or co-crystalline phase, yet

all the peaks for diffractograms taken of samples synthesized for seven hours and up can be assigned to AFI. A significant amount of white powder, amorphous by
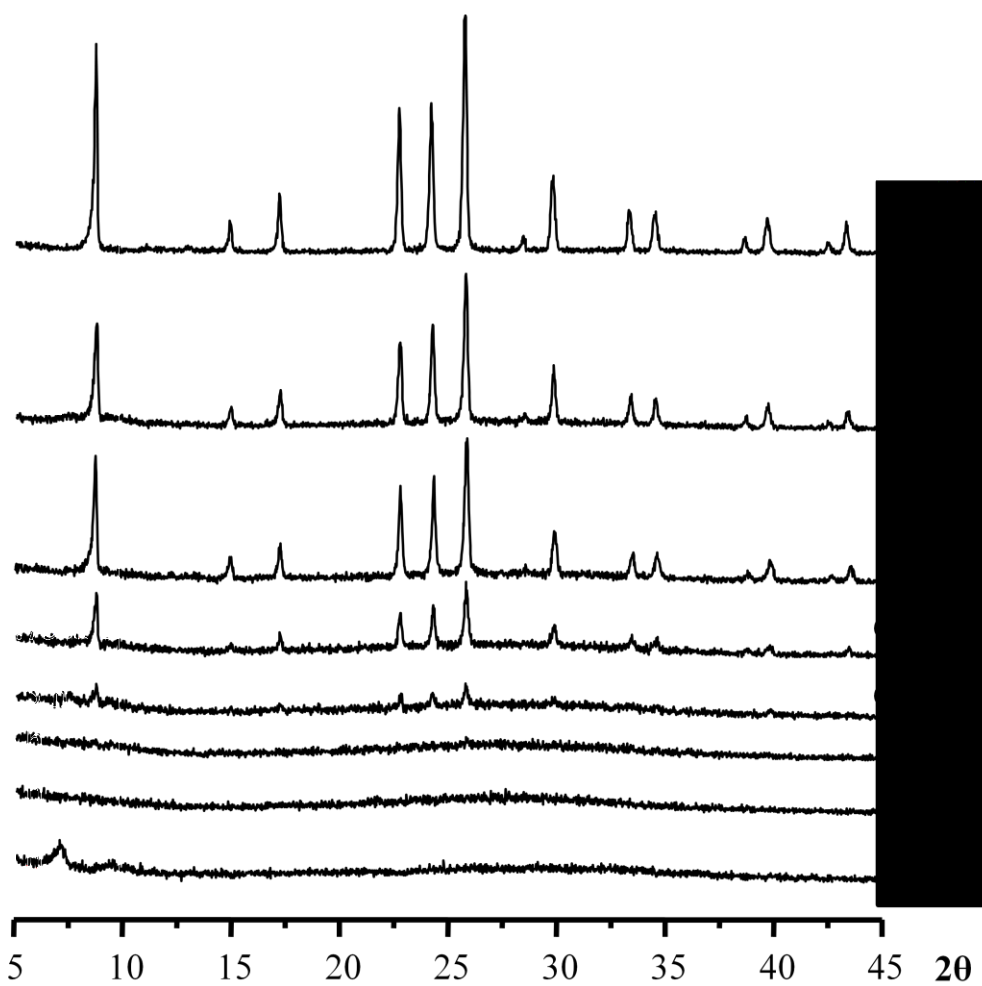
Figure 3.11: X-ray diffractograms for the crystallization of SAPO-5 under VPSU conditions.

XRD (pattern not shown), was sometimes found in the lower cup of the autoclave after reaction. This is likely to be silica that was produced as a hydrolysis product of TEOS when the reaction started, but before the TEOS could boil and condense on the dry-gel. This result indicates that not all the silica added to the lower cup will be found in the finished sieve, and a lower than usual amount of silicon in the crystal products can be expected.

Assuming that silicon is in fact being added to the developing framework (confirmed using ^{29}Si NMR, shown below), the completed sieves indicate that this method of silicon incorporation is effective, as has been shown in past reports. The marked increase in crystallinity and total absence of co-crystalline or amorphous phase, coupled with the slower onset of crystallization, indicate that the incorporation of silicon using the VPSU method causes a more gradual, reliable method of synthesis, leading to purer crystal samples over longer reaction times.

The ^{27}Al and ^{31}P spectra for the VPSU crystallizations seen in Figure 3.6 follow nearly the same progression as those for the SAC syntheses. This is evidence that the presence of TEA in the dry-gel is the cause of the conversion of reagent aluminum and phosphorus sources partially into tetrahedrally coordinated aluminum and not fully condensed phosphorus which can condense into the amorphous precursors to the desired framework. The VPSU reaction is, however, notably slower than the SAC reaction.

The SEM images in Figure 3.7 of the SAPO-5 crystals made using the VPSU method show a relatively large crystallite covered again in either starting materials or crystal nuclei. The VPSU method EDX results in Table 3.2 show a divergence from the first two syntheses as well. As seen in the (Si+P)/Al ratio, the primary method of substitution appears to be SM2. This result agrees with the ^{29}Si NMR and CP spectra above, which indicate only the presence of Q^4 silicon centers. The amount of silicon within the sieves is far lower than in the previous methods. This result is unsurprising, as there would be a lower effective molar ratio of silicon within the dry-gel when compared with the other two synthesis methods because of the aforementioned premature TEOS

hydrolysis. The lower presence of silicon is also supported by the relatively low amount of signal acquired during the NMR analysis.
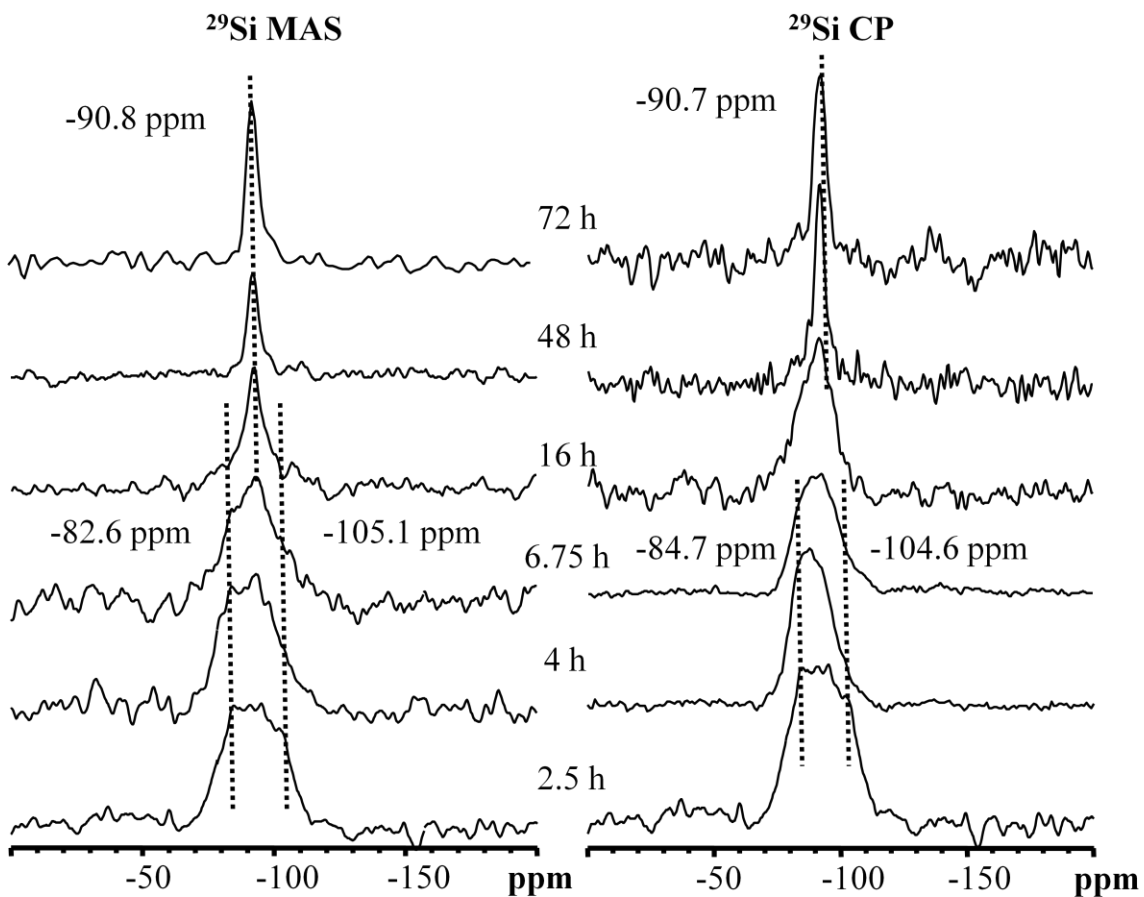
Figure 3.12: ^{29}Si MAS and CP spectra for selected crystallization intermediates in the VPSU synthesis of SAPO-5.

^{29}Si MAS and CP NMR are shown in Figure 3.12. No spectra for the 0 reaction time sample were collected as this sample contained no silicon. The MAS results raise a stark contrast to the prior two DGC methods. The spectra for the short reaction times shows a broad resonance, centred around -90 ppm but spanning from -70 to -105 ppm. This peak is evidence for a few important pieces of information. The majority of the signal in these samples is centered around -95 ppm, which indicate well incorporated silicon nuclei. While peaks for SAPO sieves indicating Q^0 to Q^4 nuclei are commonly assigned between -90 and -110 ppm, peaks around -60 to -90 ppm are more commonly

assigned to alkoxy- or hydroxyl-bound silicon nuclei. These types of silicon centers are found in the decomposition products of the silicon source used in the VPSU method, TEOS.[49, 50] Unique silicon centers can be seen in the ^{29}Si NMR spectra of these samples as a result of the incorporation of these organosilicon moieties. It has been noted in the past that organosilicon moeities can be incorporated into mesoporous silicon systems, and the presence of signal in the range of -75 to -85 ppm indicates that T^n silica species (organically linked siloxanes with attached hydroxyl groups) are prevalent in the early samples for this method. These are decomposition products of TEOS being incorporated into the dry-gel. Being that the signal does not become appreciably higher than ca. -75 ppm, only T^3 and T^2 sites are prevalent in the sample, and so (EtO)-Si-$(OAl)_3$ and $(EtO)_2$-Si-$(OAl)_2$ groups are present. Oddly, there is little intensity in any collected spectrum for T^1 silicon nuclei, indicating there is little presence in the samples of a silicon center bound to three alkoxy groups. This hydrolysis can occur in TEOS in the gas phase or after condensation via α or β elimination or through a free-radical pathway.[50] The free radical pathway results in T^1 silicon nuclei, and so it is more likely that α or β elimination was the main method of TEOS decomposition under these synthesis conditions. In fact there is no T^n signal present in samples which are crystalline by XRD, and so these organic groups do not seem to exist in the actual framework, but organosilicon species are present in the developing sieve when made using VPSU. This indicates that under VPSU synthesis conditions, the silicon is able to travel from the lower cup of the autoclave into the dry-gel in the upper cup and begin condensing and decomposing on the dry-gel itself homogeneously.

The decomposition seems to cause some degree of Si-O-Si bridge building, as indicated by the minor presence of Q^{1-3} silicon nuclei signified by the shoulders noticed at -105 ppm in the early reaction time spectra. The lack of intensity of a signal at ca. -110 ppm, even in the CP spectra, indicates that a comparably low number of Q^4 silicon nuclei are being generated by TEOS decomposition. This means that any silica-like phase that is generated as a result of TEOS decomposition (SiO_2 is a common product) is only able to produce small silica crystallites with few Q^4 silicon nuclei in the dry-gel. An illustration of this procedure is given in Figure 3.13.
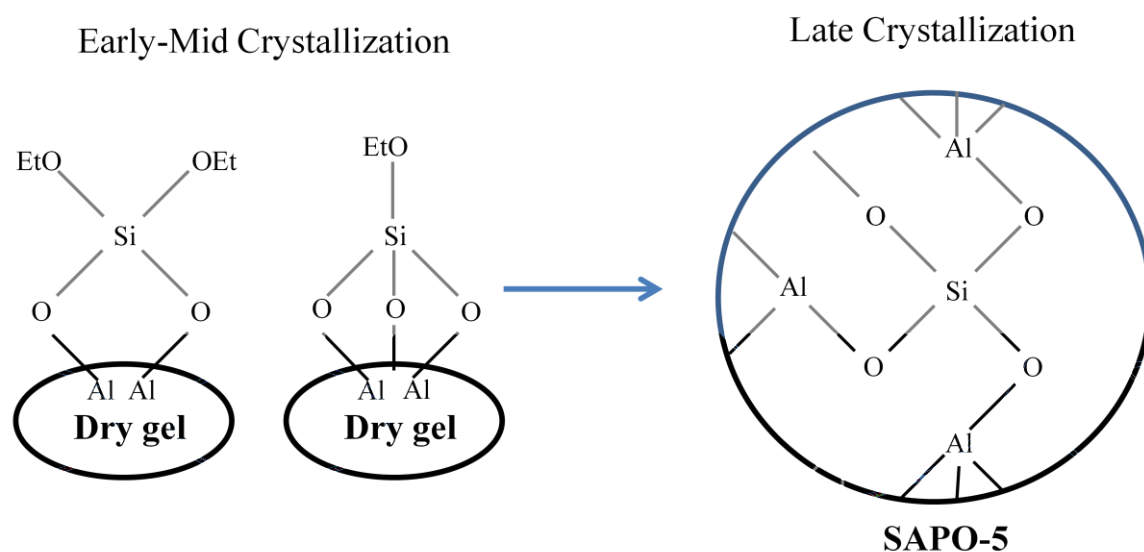
Figure 3.13: Illustrations of unique Si nuclear environments during the VPSU synthesis of SAPO-5. In the early to middle stage of the synthesis, T^n alkoxysilicon sites are present in the dry gel in addition to Q^n sites. As the reaction proceeds and the sieve develops, further hydrolysis of the ethoxy groups by the dry-gel leads to well-incorporated Si sites in the finished SAPO-5 sieve.

As the reaction progresses, the broad peak begins to narrow after approximately seven hours; exactly the same point in the reaction where AFI frameworks begin to crystallize as shown by XRD. The peak narrows over the duration of the reaction until it is well-resolved and centered around -90 ppm, representing Q^0 incorporated silicon sites

in a SAPO-5 sieve. This pattern is confirmed when examining CP MAS spectra of the same samples; no new information is revealed by these spectra.

The change in spectra over the course of the reaction and the timing of this change show that the VPSU method is able to incorporate silicon more thoroughly than SAC and VPT. The silicon incorporation starts at the same time as the crystallization, meaning that the sieve will be a SAPO all the way through, instead of having an $AlPO_4$ core. The sharpness of the finished product peak indicate that the overwhelming majority of silicon in the sample is in the Q^0 state: little or no silica islands or unreacted precursor silicon remain at the end of the reaction. The VPSU method of synthesis is evidently able to homogeneously deliver TEOS to the developing gel surface and graft on alkoxysilicon sites through TEOS decomposition and hydrolysis. Further condensation provides well-incorporated silicon centers within the finished sieve. While the same experimental parameters were used for these spectra as were used for the SAC and VPT synthesized samples, the VPSU spectra required more scans in order to get a comparable signal-to-noise ratio. This, along with the lack of any reagent silicon sites being apparent in the ^{29}Si NMR, are solid NMR evidence that there is less silicon inside the VPSU samples, regardless of how well the present silicon is incorporated.

3.4 Comparisons Between DGC Methods

Mechanistically, the three synthesis methods follow noticeably different pathways. Using the SAC method, the dry-gel is amorphous, containing silicon in a dense, silica-like state and appreciable amounts of aluminum and phosphorus in both amorphous and co-ordinated states, respectively, indicating some very early action of the SDA on the gel. The sieves become crystallographically evident after 2.75 hours and

quickly grow into hexagonal crystals. These crystals contain aluminum, silicon and phosphorous in framework positions, in addition to some silica-like silicon, and have incorporated a relatively high amount of silicon in the SM3 fashion. In contrast, the VPT dry-gel seems to possess a short-lived semi-crystalline phase in the XRD at early reaction times. This dry-gel contains silica, as did the SAC dry-gel, but shows no evidence of co-ordination between aluminum and phosphorous until at least 1 hour reaction time. At that point the aluminum and phosphorous are in the tetrahedral and not fully condensed form, respectively. Crystalline sieves begin to show at 4.75 hours reaction time, when framework phosphorous becomes detectable by NMR. Crystalline VPT samples are similar in appearance, diffraction and spectroscopy to SAC samples, except they contain significantly less silicon (also incorporated in the SM3 fashion). It is apparent that the SAC and VPT methods begin in different reaction conditions, but shortly after the introduction of the SDA to the dry-gel in VPT, the two methods converge mechanistically and begin to resemble one another. The VPSU samples stand out, however the dry-gel is highly similar to that of the SAC method in terms of ^{27}Al and ^{31}P NMR. The silicon is detectable in the sample as early as 2 hours, long before crystallinity becomes noticeable at 6.5 hours. Under these reaction conditions a low amount of silicon was incorporated into the sieves, this time following SM2 substitution. No silica phase was observed.

The most significant findings of this study come from the VPSU results. The VPSU method delivers silicon to the developing sieve in an individual manner, and so the silicon that is incorporated preferentially crystallizes in a more dispersed manner than is seen in SAC and VPT. This is important to the catalytic activity of the sieve, as the

incorporation of dispersed silicon centers leads to more acid sites and a stronger acid catalyst.[51, 52] There is markedly less silicon in the VPSU crystals, as determined using EDX. These results show that the concentration and type of silicon center (i.e. acid site) inside AFI frameworks can be directly controlled as a result of synthesis conditions, and that a tailored molecular sieve catalyst is a realistic aspiration.

3.5 Analogous Study of SAPO-11

An analogous study of the similarly structured SAPO-11 molecular sieve was attempted alongside the SAPO-5 study. The SAPO-11 sieve, with AEL topology, has a smaller, ovular pore opening and, like SAPO-5, a one-dimensional network of channels.[5] SAPO-11 has proven to be useful in a number of catalytic applications, and has been studied well when synthesized via HTS and DGC in terms of its catalytic activity as well as molecular dynamic studies focussing on the SDA (commonly dipropylamine, DPA) residing within the channel network.[53-58] For these reasons, and for its structural similarity to SAPO-5, SAPO-11 was chosen as a target system to provide insight into any differences in the crystallizations of these two materials. The SAPO-11 project was significantly less successful than the SAPO-5 project, but any useful progress made is detailed within this section. The target molar ratio of the product, the reagents used and the methods of synthesis and characterization are all identical to those detailed for SAPO-5 (*vide supra*) except for the SDA, where DPA (+99%, Sigma) replaces TEA. The synthesis of SAPO-11 as well as any diffraction or NMR assignments were based on previously published literature.[59, 60]

An optimization of the amount of added water for the SAC synthesis of SAPO-11 resulted in crystalline samples for added amounts between 0.25 and 2.00 g of water per

gram of dry-gel as evidenced by XRD. The dry-gel itself displayed some broad low angle reflections in the XRD, similar to those noted in the early stages of the SAPO-5 VPT crystallization. When examined through ^{29}Si solid state NMR these samples all displayed broad peaks spread around the entire Q^n range of silicon nuclear environments. The bulk of the intensity of these peaks, however, was centred around ca. -110 ppm, indicating that the silicon was not incorporating in a homogeneous manner, if indeed it was incorporating into the sieve at all. Other accounts of SAPO-11 synthesis show well incorporated silicon centers signified by a sharp peak at ca. -90 ppm. This makes it safe to assume that efficient silicon incorporation had failed under these conditions, and that the vast majority of silicon was in its precursor silicate form.

The VPT method of synthesis was less successful than the SAC method. After optimising the amount of added water/DPA mixture, the concentration of DPA in the mix was varied for optimization. Lack of reproducibility was the main source of experimental failure for this run of experiments. A successful batch of samples which showed a steady progression from amorphous precursor to crystalline product was not synthesized. Often, the dry-gel would possess crystalline structure, and an as-yet unidentified structure would dominate the product patterns. Re-optimization of the synthesis parameters and development of a reliable synthesis would be necessary before this line of experimentation could move forward.

The VPSU method of synthesis was modestly successful. Crystalline samples were achieved from amorphous precursors. Figure 3.14 shows the XRD and ^{29}Si NMR
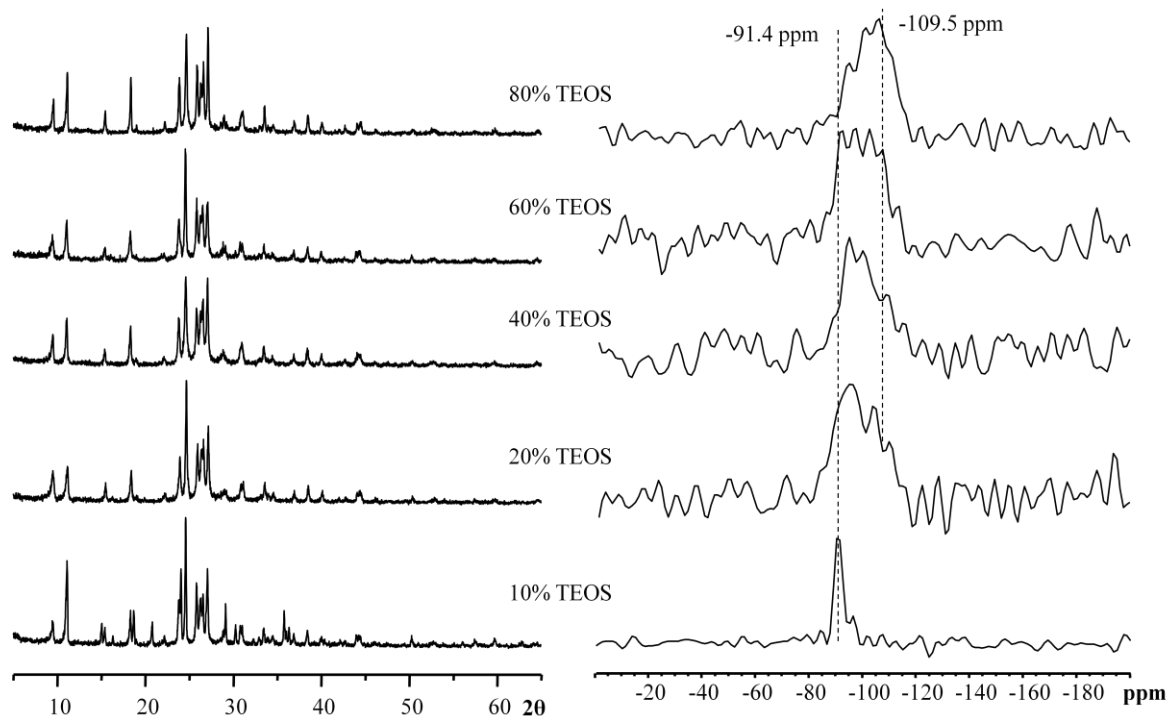
Figure 3.14: XRD and ^{29}Si NMR for products in the optimization of TEOS concentration in the VPSU synthesis of SAPO-11.

results of the optimization of TEOS/water mixture concentration. The incorporation of silicon into the sieve was effective when the concentration of TEOS was low as evidenced by the sharp peak at -91.4 ppm. The XRD for this sample does seem to show some co-crystalline AFI material as well, however. The other concentrations appear to produce more crystalline products, however a broader array of silicon environments are present. This indicates a less homogenous method of silicon incorporation is occurring within this sample when synthesized with a higher concentration of TEOS. Higher concentrations of TEOS mixture push the intensity of the broad peak toward the -110 ppm Q^4 nuclei area, showing that at high concentrations the silicon tends to aggregate and form Si-O-Si bridges more readily as TEOS decomposes on the dry-gel, as might be

expected. The low signal-to-noise ratio of these spectra indicates that a relatively low amount of silicon is entering the sieve, despite the increase in TEOS mixture concentration.

Reliable methods of sieve synthesis which are reproducible and incorporate silicon in a homogeneous manner must be developed before any interpretations can be made for the results of studying the incorporation of silicon during the crystallization of the SAPO-11 sieve under DGC conditions.

3.6 Conclusions

We have been able to collect crystallization intermediates for the DGC synthesis of SAPO-5, the silicoaluminophosphate molecular sieve with AFI topology, made three different ways as confirmed using XRD. The VPT synthesis shows a dry-gel that adopts a layered precursor phase before crystallizing into the AFI framework, while the SAC and VPSU methods crystallize to AFI straight from the amorphous precursor. All three methods form highly crystalline AFI sieves after a timescale of hours, with the ordering of relative rate of crystal formation being SAC>VPT>VPSU. The sieves continue to crystallize stably up to at least 3 days reaction time.

The methods of silicon incorporation for the SAC and VPT methods are similar as evidenced by ^{29}Si NMR experiments. After a brief period early in the synthesis where the methods differ significantly, the crystallizations become similar after the SDA is introduced to the dry-gel. The VPSU method does not show the presence of dense silica. Instead, the silicon incorporates into the sieve shortly after being hydrolysed from its TEOS source, with little evidence of permanent or significant condensation into a dense silica-like state. Organosilicon species were detected in the sieve precursors for this

synthesis, indicating that the TEOS source is not completely hydrolyzed and condensed into silica before it begins to interact with aluminum in the developing dry-gel.

These three synthetic methods, despite their similarities, show that control over the physical properties of SAPO-5 catalysts can be achieved through control of synthesis conditions. We have shown the ability to control the concentration and level of substitution of silicon within these sieves by switching DGC methods. This control, when developed, can be used to create tailored acid catalysts for specific purposes. Future work should focus on catalytic performance and fine control of the amount of silicon incorporation in the VPSU method.

3.7 References

1. Dyer, A. *An Introduction to Zeolite Molecular Sieves*. **1988**, Avon, GB: John Wiley & Sons, Ltd.

2. Davis, M.E. *Nature* **2002**, *417*(6891), 813-821.

3. Payra, P.; Dutta, P.K. *Handbook of Zeolite Science and Technology*. **2003**, New York, USA: Marcel Dekker.

4. Szostak, R. *Molecular Sieves: Principles of Synthesis and Identification*. **1998**, Suffolk, GB: Thomson Science.

5. *Images & figures from IZA Database of Zeolite Structures*. [cited 2011 Aug. 6th]; Available from: http://www.iza-structure.org/databases/.

6. Michiels, P., *Molecular Sieve Catalysts*. **1987** , Virginia, USA: Pergamon Infoline Inc.

7. Menon, V.C.; Komarneni, S. *J. Porous Mater.* **1998**, *5*(1), 43-58.

8. Dincă, M.; Dailly, A.; Liu, Y.; Brown, C.M.; Neumann, D.A.; Long, J.R. *J. Am. Chem. Soc.* **2006**, *128*(51), 16876-16883.

9. Hedge, S.G.; Ratnasamy, P.; Kustov, L.M.; Kazansky, V.B. *Zeolites* **1988**, *8*(2), 137-141.

10. Wilson, S.T.; Lok, B.M.; Messina, C.A.; Cannan, T.R.; Flanigen, E.M. *J. Am. Chem. Soc.* **1982**, *104*(4), 1146-1147.

11. Pauling, L. *Proc. N.A.S.* **1930**, *16*(7), 453 - 459.

12. Loewenstein, W. *Am. Mineral.* **1954**, *39*, 92.

13. Lok, B.M.; Messina, C.A.; Patton, R.L.; Gajek, R.T.; Cannan, T.R.; Flanigen, E.M. *J. Am. Chem. Soc.* **1984**, *106*(20), 6092-6093.

14. Cundy, C.S.; Cox, P.A. *Chem. Rev.* **2003**, *103*(3), 663-701.

15. Cundy, C.S.; Cox, P.A. *Micropor. Mesopor. Mater.* **2005**, *82*(1–2), 1-78.

16. Matsukata, M.; Ogura, M.; Osaki, T.; Hari Prasad Rao, P.; Nomura, M.; Kikuchi, E. *Top. Catal.* **1999**, *9*(1), 77-92.

17. Bandyopadhyay, R.; Bandyopadhyay, M.; Kubota, Y.; Sugi, Y. *J. Porous Mater.* **2002**, *9*(2), 83-95.

18. Matsukata, M.; Osaki, T.; Ogura, M.; Kikuchi, E. *Micropor. Mesopor. Mater.* **2002**, *56*(1), 1-10.

19. Kim, M.-H.; Li, H.-X.; Davis, M.E. *Microporous Mater.* **1993**, *1*(3), 191-200.

20. Danilina, N.; Krumeich, F.; van Bokhoven, J.A. *J. Catal.* **2010**, *272*(1), 37-43.

21. Zhao, X.; Wang, H.; Kang, C.; Sun, Z.; Li, G.; Wang, X. *Micropor. Mesopor. Mater.* **2012**, *151*(0), 501-505.

22. Zhou, D.; Luo, X.B.; Zhang, H.L.; Dong, C.; Xia, Q.H.; Liu, Z.M.; Deng, F. *Micropor. Mesopor. Mater.* **2009**, *121*(1–3), 194-199.

23. Hu, E.; Lai, Z.; Wang, K. *J. Chem. Eng. Data* **2010**, *55*(9), 3286-3289.

24. Yang, W.; Zhang, B.; Liu, X. *Micropor. Mesopor. Mater.* **2009**, *117*(1–2), 391-394

25. Mathisen, K.; Nilsen, M.H.; Nordhei, C.; Nicholson, D.G. *J. Phys. Chem. C* **2011**, *116*(1), 171-184.

26. Borade, R.B.; Clearfield, A. *J. Mol. Catal.* **1994**, *88*(2), 249-265.

27. Martin, C.; Tosi-Pellenq, N.; Patarin, J.; Coulomb, J.P. *Langmuir* **1998**, *14*(7), 1774-1778.

28. Xue, M.; Fan, L.; Kang, Z.; Zhang, W.; Li, H.; Qiu, S. *J. Mater. Chem.* **2012**, *22*(34), 17644-17648.

29. Zhang, Q.; Li, C.; Xu, S.; Shan, H.; Yang, C. *J. Porous Mater.* **2012,** DOI: 10.1007/s10934-012-9586-x.

30. Danilina, N.; Castelanelli, S.A.; Troussard, E.; van Bokhoven, J.A. *Catal. Today* **2011**, *168*(1), 80-85.

31. Jhung, S.H.; Chang, J.-S.; Hwang, J.S.; Park, S.-E. *Micropor. Mesopor. Mater.* **2003**, *64*(1–3), 33-39.

32. Sastre, G.; Lewis, D.W.; Catlow, C.R.A. *J. Phys. Chem. B* **1997**, *101*(27), 5249-5262.

33. Zibrowius, B.; Löffler, E.; Hunger, M. *Zeolites* **1992**, *12*(2), 167-174.

34. Li, M.; Zeng, C.; Zhang, L. *Cryst. Eng. Comm.* **2012**, *14*(10), 3787-3792.

35. Pujadó, P.R.; Rabó, J.A.; Antos, G.J.; Gembicki, S.A. *Catal. Today* **1992**, *13*(1), 113-141.

36. Campelo, J.M.; Lafont, F.; Marinas, J.M. *J. Catal.* **1995**, *156*(1), 11-18.

37. Campelo, J.M.; Lafont, F.; Marinas, J.M. *J. Chem. Soc. Faraday T.* **1995**, *91*(10), 1551-1555.

38. Chen, B.; Huang, Y. *Micropor. Mesopor. Mater.* **2009**, *123*(1–3), 71-77.

39. Chen, B.; Kirby, C.W.; Huang, Y. *J. Phys. Chem. C.* **2009**, *113*(36), 15868-15876.

40. Eichele, K.; Wasylishen, R.E. *J. Phys. Chem.* **1994**, *98*(12), 3108-3113.

41. Hayashi, S.; Hayamizu, K. *Bull. Chem. Soc. Jpn.* **1991**, *64*, 685-687.

42. Hu, D.; Xia, Q.H.; Lu, X.H.; Luo, X.B.; Liu, Z.M. *Mat. Res. Bull.* **2008**, *43*(12), 3553-3561.

43. Freude, D.; Ernst, H.; Hunger, M.; Pfeifer, H.; Jahn, E. *Chem. Phys. Lett.* **1988**, *143*(5), 477-481.

44. Seelan, S.; Sinha, A.K. *J. Mol. Catal. A-Chem.* **2004**, *215*(1–2), 149-152.

45. Chen, J.; Thomas, J.M.; Wright, P.A.; Townsend, R.P. *Catal. Lett.* **1994**, *28*(2), 241-248.

46. Sayari, A.; Moudrakovski, I.; Reddy, J.S.; Ratcliffe, C.I.; Ripmeester, J.A.; Preston, K.F. *Chem. Mater.* **1996**, *8*(8), 2080-2088.

47. Bandyopadhyay, M.; Bandyopadhyay, R.; Tawada, S.; Kubota, Y.; Sugi, Y. *Appl. Catal. A-Gen.* **2002**, *225*(1–2), 51-62.

48. Wang, L., Guo, C., Yan, S., Huang, X., and Li, Q. *Micropor. Mesopor. Mater.* **2003**, *64*(1–3), 63-68

49. Babonneau, F.; Thorne, K.; Mackenzie, J.D. *Chem. Mater.* **1989**, *1*(5), 554-558

50. Desu, S.B. *J. Am. Chem. Soc.* **1989**, *72*(9), 1615-1621.

51. Martens, J.A.; Grobet, P.J.; Jacobs, P.A. *J. Catal.* **1990**, *126*(1), 299-305.

52. Barthomeuf, D. *J. Phys. Chem.* **1993**, *97*(39), 10092-10096.

53. Gharibeh, M., Tompsett, G.A., Conner, W.C., and Yngvesson, K.S. *Chem. Phys. Chem.* **2008**, *9*(17), 2580-2591.

54. Yang, X.; Ma, H.; Xu, Z.; Xu, Y.; Tian, Z.; Lin, L. *Catal. Commun.* **2007**, *8*(8), 1232-1238.

55. Liu, Y.; Liu, C.; Liu, C.; Tian, Z.; Lin, L. *Energ. Fuel* **2004**, *18*(5), 1266-1271.

56. Liu, P.; Ren, J.; Sun, Y. *Micropor.Mesopor. Mater.* **2008**, *114*, 365-372.

57.   Wei, Y.; Wang, G.; Liu, Z.; Xie, P.; He, Y.; Xu, L. *Catal. Lett.* **2003**, *91*(1), 35-40.

58.   Han, B.; Shin, C.-H.; Cox, P.A.; Hong, S.B. *J. Phys. Chem. B* **2006**, *110*(16), 8188-8193.

59.   Bandyopadhyay, R.; Bandyopadhyay, M.; Kubota, Y.; Sugi, Y. *J. Porous Mater.* **2002**, *9*, 83-95.

60.   Chen, B.; Huang, Y. *J. Phys. Chem. C* **2007**, *111*(42), 15236-15243.

CHAPTER FOUR

The Crystallization of Transition-Metal Substituted AlPO$_4$-5 Molecular Sieves Under Hydrothermal Synthesis Conditions

4.1 Introduction

Porous materials have been used to catalyze reactions for a large part of history. Especially in the last several decades, porous aluminosilicates, called zeolites, have been particularly useful, not just to those interested in their catalytic activity but also in the fields of molecular storage and ion exchange.[1-7] The similar family of framework aluminophosphates (AlPO$_4$s) have attracted significant attention over the past few decades.[8] Both these systems are repeating frameworks of tetrahedrally coordinated p-block elements bridged by oxygen. These materials feature large cavities, pores and channels as a repeating motif in their crystal structure. Their popularity came partly as a result of their inherent catalytic inactivity as neutrally charged frameworks. Though unable to perform any catalysis themselves, they serve as excellent supports for catalytic sites. In the past, precious metal catalysts have been adsorbed onto and absorbed into AlPO$_4$s to take catalytic advantage of their shape selectivity.[9-11] Substitution of catalytic framework elements into the AlPO$_4$ framework itself is another way AlPO$_4$ sieves can become catalysts. Incorporation of silicon tetrahedra into an AlPO$_4$, for instance, leads to the solid acid catalyst SAPO-n family.[12-14] The focus of this work is the substitution of first row transition metals into the AlPO$_4$ framework, leading to solid redox catalysts belonging to the MAPO-n family.[15-17]

The majority of publications regarding MAPO systems are concerned with the function of finished sieves. MAPO catalytic activity is constantly being probed and

tested, and so a large number of publications concern optimization or study of specific reactions.[18-22] For instance, MnAPO-5 has shown promising results in the catalysis of several reactions, e.g. the oxidation of cyclohexane, the oxydehydrogenation of ethane and the isopropylation of ethylbenzene.[23-25] Efforts have been made in an attempt to synthesize and study MAPOs in novel ways, for instance using microwave heating to speed up the reaction, or attempting to get information from electron pair resonance.[26, 27] Sensor applications have also been tested, and FeAPO-5 has proven itself to be a useful humidity sensor.[28, 29] This wide array of research is not surprising given the versatility and robustness of the MAPO family. An important feature of these systems is that the metal centers can cycle between oxidations states (in the case of Mn and Fe, between the 2+ and 3+) during redox catalysis within the framework[23, 30, 31] without disrupting the overall crystal structure of the sieve.

The $AlPO_4$-5 sieve with AFI topology is well-studied and can be easily synthesized by a variety of methods, most popularly by HTS. It has a high thermal stability and (like all crystalline molecular sieves) extremely narrow pore size distribution,[3, 4, 32] In addition to these desirable qualities, it has proven to be highly amenable to framework substitution by a large number of heteroatoms. Many publications detail substitution of silicon, light alkaline earth metals and first row transition metals, in addition to some more exotic elements.[33-38] Incorporation of heteroatoms gives these materials the ability to perform in catalytic applications of various kinds, and the fact that several heteroatoms can be incorporated means that a wide array of different materials can be made to cater to numerous applications. For this reason, study of the substitution of first row transition metals into the $AlPO_4$-5 sieve was

seen as a desirable research goal. Despite a great deal of effort being put into the study of the functional activity of transition metals in molecular sieves, relatively few publications are available which detail the crystallization of these sieves and the metal substitution which occurs therein. Solid state NMR has been useful in analyzing these reaction features, but the introduction of potentially paramagnetic transition metals makes collection and interpretation of NMR data complicated. Nevertheless, there is a wealth of information that can be had when studying reaction intermediates in the crystallization, and this study aims to produce some of that information. In this work, the hydrothermal method of molecular sieve synthesis was used to study the crystallization of transition metal substituted AFI-type aluminophosphate molecular sieves. Crystallization intermediates were collected during the synthesis of MnAPO-5 and FeAPO-5, two well-studied and industrially relevant systems. The intermediates were characterized using solid state NMR, supported by XRD and SEM/EDX, in an attempt to develop a picture of the crystallization and substitution that occurred while these complex molecular superstructures formed.

4.2 Experimental
4.2.1 Synthesis and Preparation

The synthesis of MAPO sieves (MnAPO-5 and FeAPO-5) were carried out according to a literature procedure.[37] The structure directing agent used was triethylamine (TEA). The desired molar ratio was set at 0.94 Al : 1.00 P : 0.06 Me : 0.75 TEA : 20 H_2O, where Me represents the transition metal and TEA was the organic structure directing agent. First, the 3.00 g of the aluminum source (CATAPAL B pseudoboehmite, 72% Al_2O_3, Sasol) was added to 6.48 g of deionised water and stirred for thirty minutes. A

solution of either 0.60 g of the manganese source or 0.99 g of the iron source in 6.48 g of deionised water ($Mn(CH_3COO)_2 \cdot 4H_2O$, 99%   and $Fe(NO_3)_3 \cdot 9H_2O$, 99%, Sigma-Aldrich) was then added slowly and allowed to homogenize for one hour. 4.59 g of phosphoric acid (H_3PO_4, 85%, Caledon) was added drop wise as the source of phosphorus, and the developing gel was stirred for two hours. Lastly, 3.09 g of triethylamine (99.5%, EMD) was added and the gel was stirred for an additional two hours.

After stirring, the gel was transferred to TEFLON lined stainless steel autoclaves. The autoclaves were sealed and placed in the oven at temperatures ranging from 160 to 180°C for times ranging from thirty minutes to three days. On removal from the ovens, the autoclaves were quenched in cold water to decrease the temperature and then opened (as soon as it was safe to do so) to decrease the pressure. These were done in an attempt to halt the reaction as reliably as possible with the aim of collecting crystallization intermediates. After removal from the autoclave, the samples were washed liberally with deionised water, isolated and dried in air at 80°C overnight. The samples were then ground into a fine powder for analysis.

4.2.2 Characterization

Product identification and determination of relative crystallinity was done using XRD. The instrument used was a Rigaku diffractometer using Co Kα radiation (λ = 1.7902 Å). NMR experiments investigating ^{27}Al and ^{31}P nuclei were performed using a Varian/Chemagnetics Infinityplus 400 WB NMR spectrometer operating at 9.4 T. The Larmor frequencies of ^{27}Al and ^{31}P nuclei were set at 104.1 and 161.7 MHz, respectively. The spectra taken were standardized against 1M $Al(NO_3)_3$ solution (0 ppm) and

ammonium dihydrogen phosphate (0.81 ppm from 85% H_3PO_4) for ^{27}Al and ^{31}P, respectively.[39] In addition to one-pulse MAS experiments, inversion recovery and saturation recovery pulse sequences were used to determine the spin-lattice relaxation times, T_1, using the normal exponential and stretched exponential modelling functions.[40-44] SEM and EDX measurements were done using a Hitachi S-4500 field emission scanning electron microscope equipped for EDX with an EDAXTM system. Crystallized samples were calcined in air, increasing the temperature by 100°C per hour up to 550°C and then maintaining that temperature for 24 hours. Any colour change in the sample was noted by visual inspection and the samples were re-analyzed using XRD in order to confirm the structures had not collapsed during calcination.

4.3 Results and Discussion

4.3.1 XRD: Synthesis and Calcination

Figure 4.1 shows the X-ray diffractograms for selected intermediates in the hydrothermal synthesis of MnAPO-5 synthesized at 170˚C. The zero hour sample shows a small reflection around the 8˚ 2θ region which is an unidentified impurity. The reflection lines up with the lowest angle reflection seen for the desired AFI framework, but the pattern for the starting material is otherwise featureless; the pattern describes (mainly) an amorphous solid with no apparent layering or periodicity of any kind. As the reaction progresses, reflections indicative of the AFI framework become apparent at the two hour reaction time mark[45]. As the reaction proceeds, these reflections become more intense, indicating reaction progress and crystal growth. The intermediates at two and

three hours reaction time show semi-crystalline samples, while any samples collected

after that time show highly crystalline AFI sieves. These sieves are stable up to the three
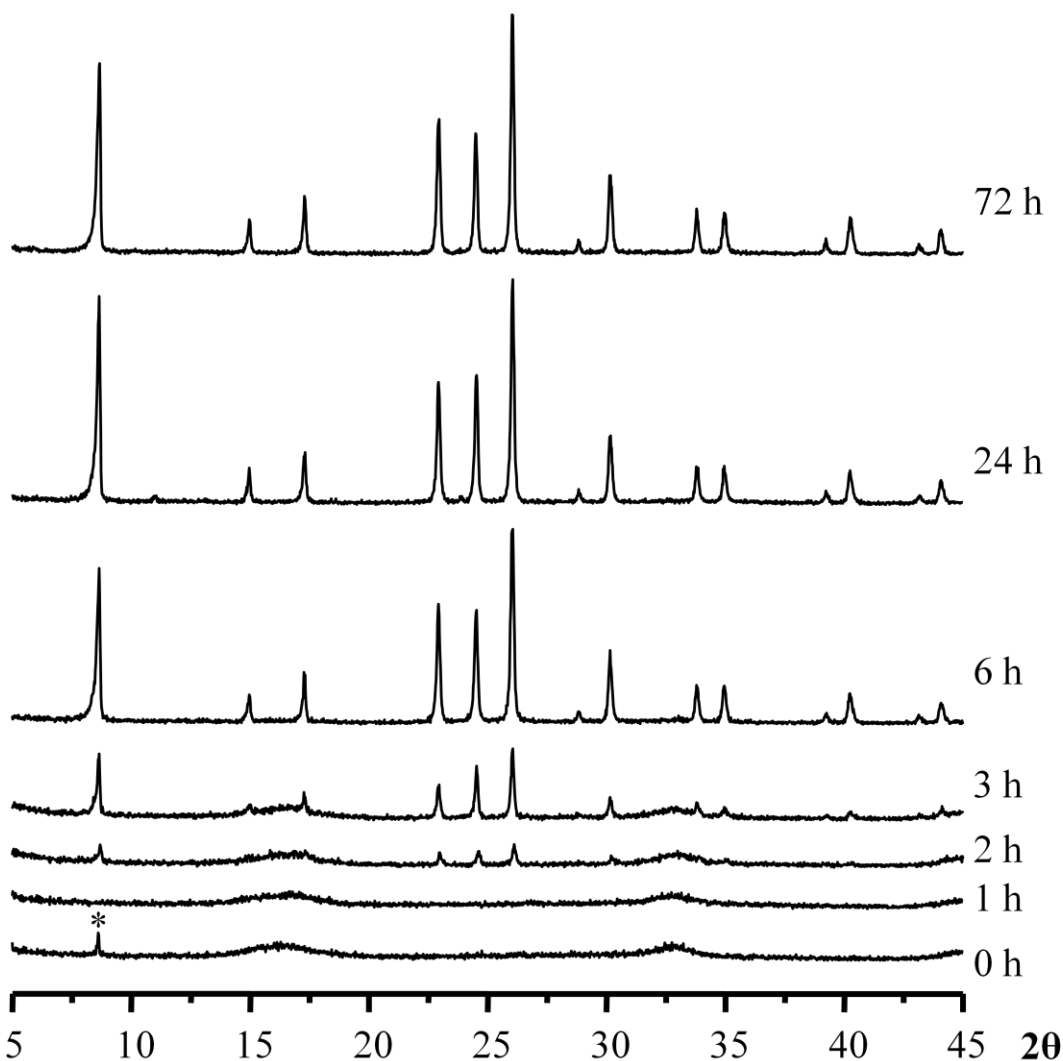
Figure 4.1: X-ray diffractograms for the crystallization of MnAPO-5 under HTS conditions. Impurity peaks are marked with an asterisk.

day reaction time, showing no degradation or any co-crystalline phase. This indicates

that, even in the presence of manganese and acetate ions, the AFI sieve is able to form

efficiently under the structure direction of triethylamine, and that the introduction of the

new species did not alter the gel environment enough to stop vital framework constituents

from becoming active and reacting.

A similar series of diffractograms can be found in Figure 4.2 representing the hydrothermal synthesis of FeAPO-5 at 180˚C. This higher reaction temperature has accelerated the reaction. Samples collected up to 1.5 hours show a purely amorphous
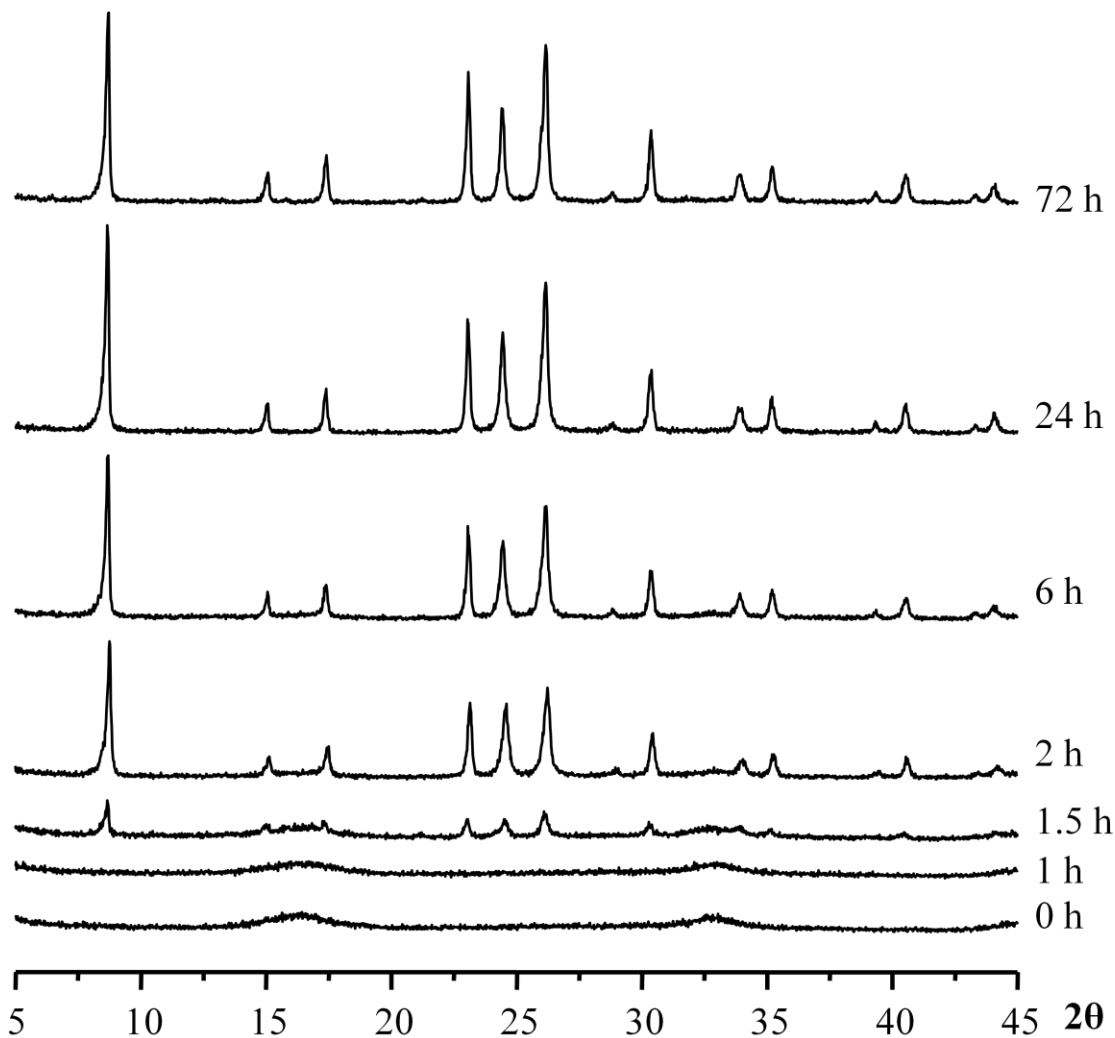
Figure 4.2: X-ray diffractograms for the crystallization of FeAPO-5 under HTS conditions.

material. A semi-crystalline intermediate that begins to show the AFI framework reflections was collected at 1.5 hours. At two hours, highly crystalline AFI is present, and these reflections remain, becoming slightly more intense, over the next three days of reaction time. As was seen in the MnAPO-5 crystallization run, no co-crystalline phase can be detected by XRD from the outset of the reaction up to the longest reacted sample

at three days. No significant degradation in the crystallinity is detectable from six hours up to three days.

Figure 4.3 shows the results of the calcination of the three day reaction time sample of MnAPO-5 and FeAPO-5. A small portion of the sample was slowly heated to 550°C and held at that temperature for three days. As the XRD patterns show, no significant degradation occurred over this time. The sieves are stable at this temperature. The first evidence for transition metal framework incorporation came as a result of the calcination experiments as well. After calcination, a colour change was readily apparent in the materials. The MnAPO-5 sample changed in colour from white to deep purple, and the FeAPO-5 samples changed from a light grey colour to a light yellow colour, seen in Figure 4.4. These changes are consistent with oxidation occurring between the 2+ and 3+ states of tetrahedrally coordinated Mn and Fe centers, possibly within the framework.[23, 30, 31] On long-term exposure to air, the intensity of the colour of the samples fades noticeably. Introduction of a reductant (e.g. $H_2(g)$) to the system would likely speed up this process. These results provide evidence that metal species exist within these samples that can be used for cyclic catalytic redox chemistry. Confirmation of these results, clarification of the actual state of the metal centers (framework or extra-framework) and the determining the role of the metal centers in sieve crystallization would be the next goal of these works.
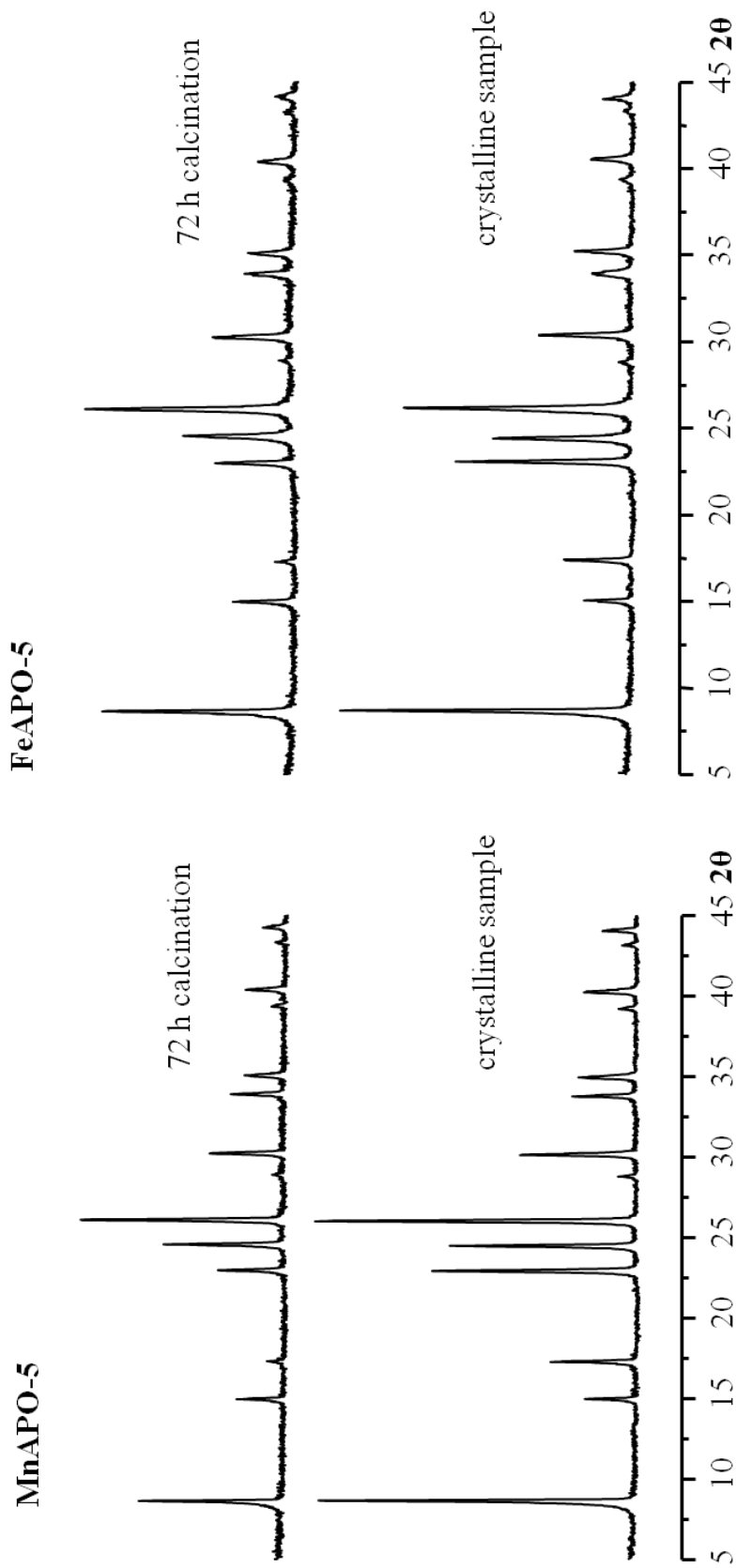
MnAPO-5

FeAPO-5

Figure 4.3: X-ray diffractograms of crystalline samples of MnAPO-5 and FeAPO-5 before and after calcination at 550°C.
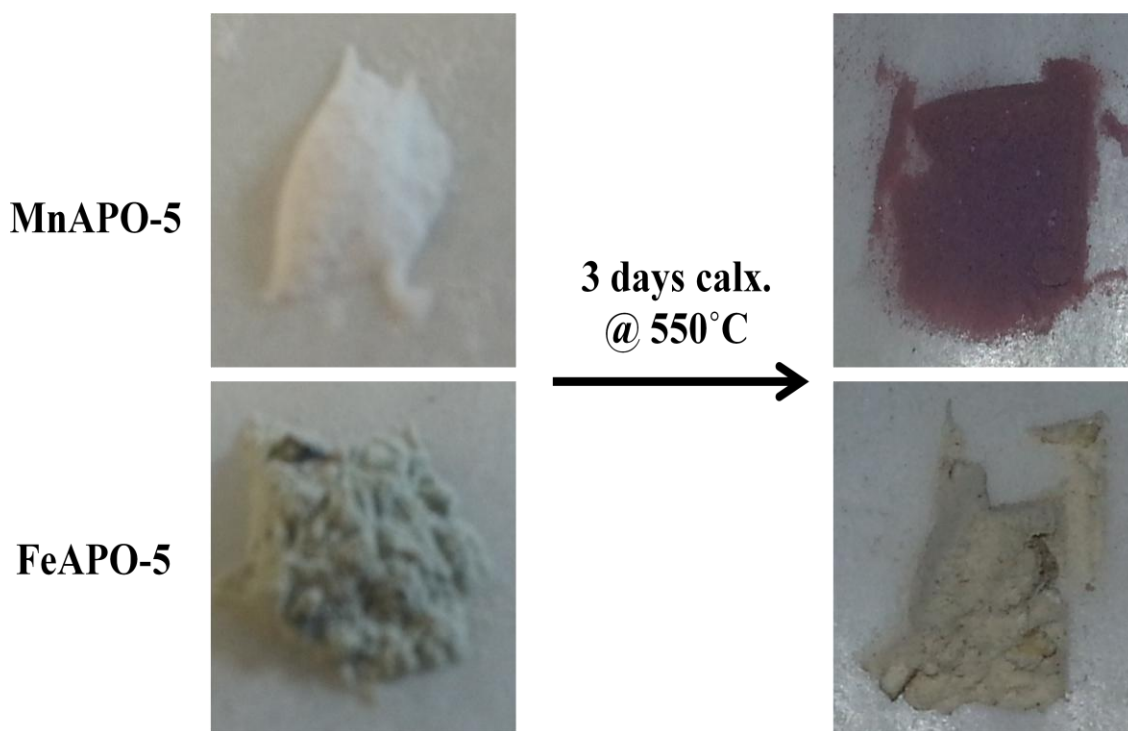
Figure 4.4: Effect of calcination on the colour of MAPO samples synthesized via HTS. MnAPO-5 changes from white to dark purple, while the FeAPO-5 changes from pale grey to pale brown-yellow. No change to crystal structure is observable using XRD. The colours slowly revert over long time scales exposed to air.

4.3.2 SEM/EDX Results

SEM/EDX results investigating the crystal morphology and elemental composition of crystalline three-day samples of MnAPO-5 and FeAPO-5 are shown in Figure 4.5. The SEM images show highly crystalline aggregates of crystals, box-like or barrel-like in appearance, with ~10 μm to a side. Little to no amorphous material could be seen in the sample. Flat crystal surfaces on the "walls" as well as the "lids" of the barrels were used as targets for EDX analysis. The Al/P ratios of MnAPO-5 and FeAPO-5 were calculated at 0.91 and 0.90, respectively. The (Al+M)/P ratios, where M represents Mn or Fe, were calculated as 1.0 and 0.96, respectively. This result offers further proof that transition metal substitution had occurred to an appreciable degree. An Al/P
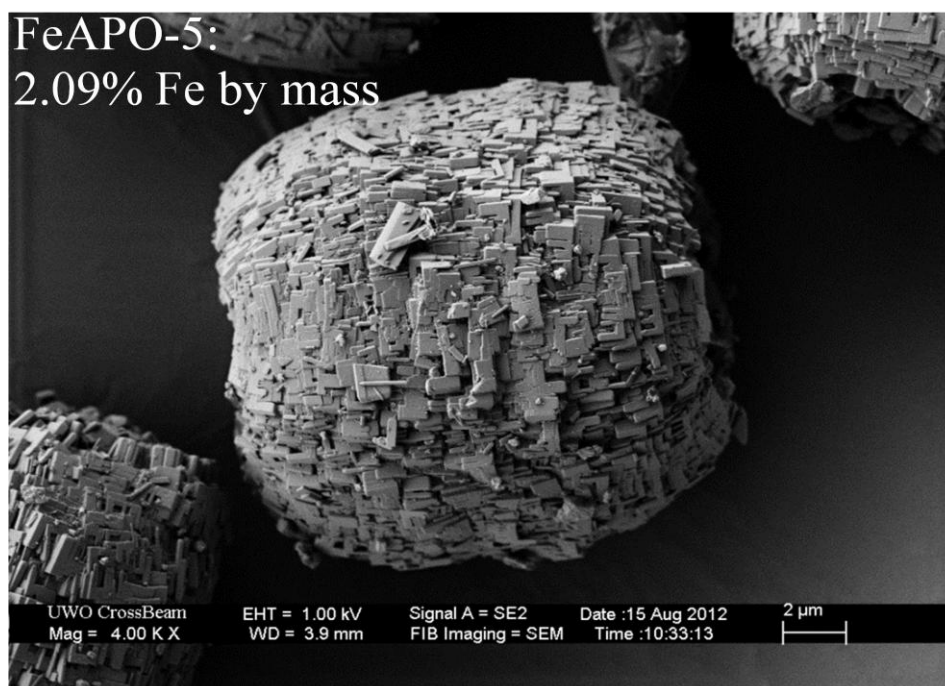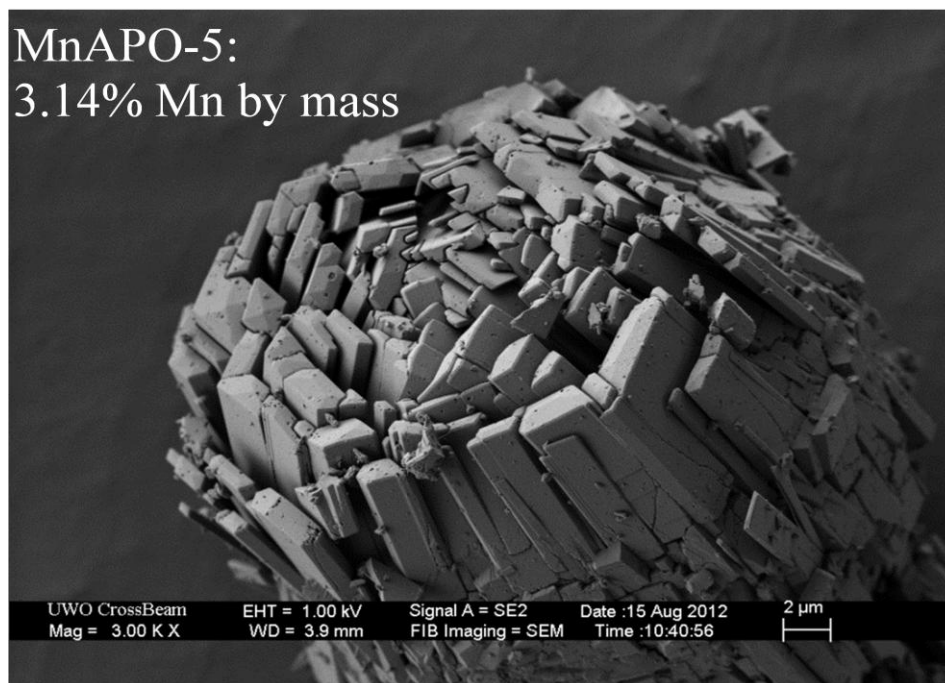
Figure 4.5: SEM images of MnAPO-5 and FeAPO-5 crystals. Mass % determined by EDX.

ratio lower than one indicates that the metals preferentially replace Al^{3+} in a method similar to the SM1 substitution seen in SAPO-5.[46] As noted in Figure 4.5, the metal content of the MnAPO-5 and FeAPO-5 sieves were 3.14% and 2.09% by mass,

respectively. Similar metal loadings into AFI sieves have been reported via EDX in previously referenced literature.[37, 47, 48]

4.3.3 Solid-State NMR results
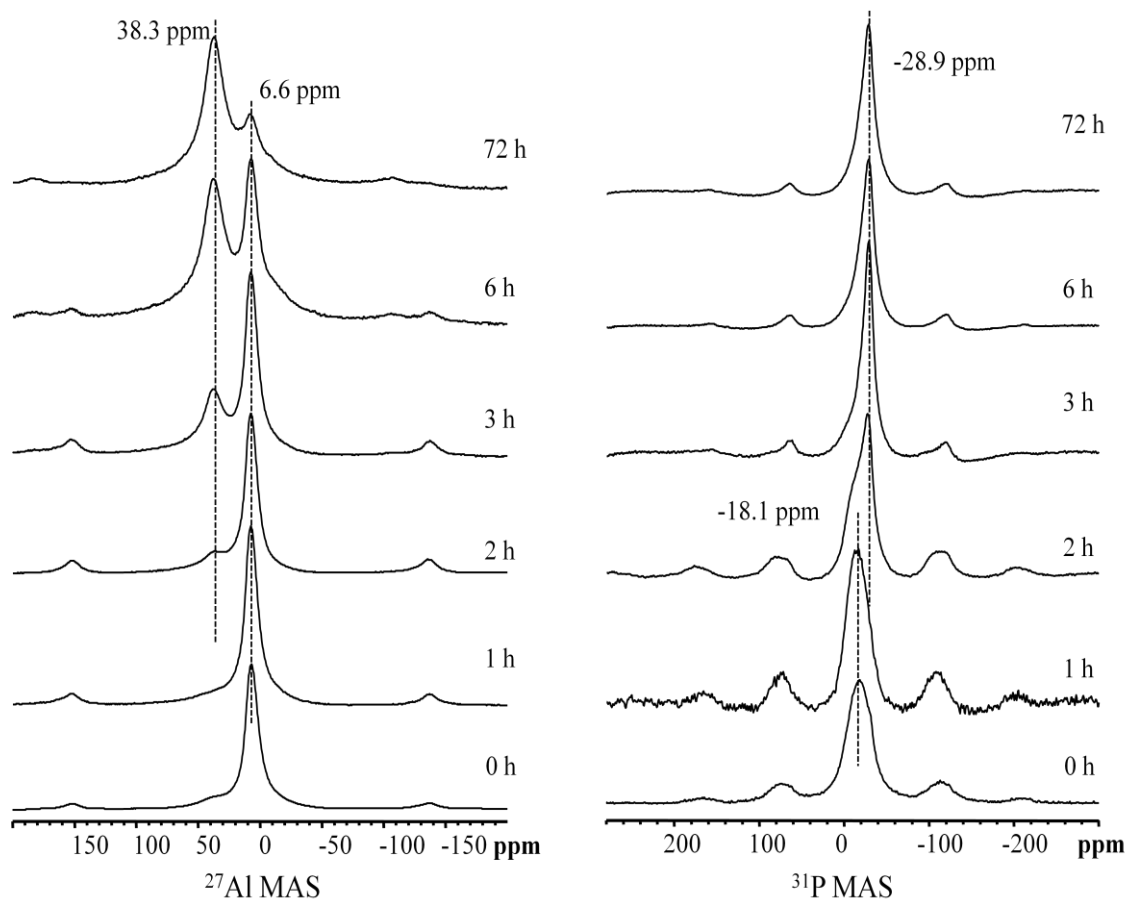
Figure 4.6: ^{27}Al and ^{31}P MAS NMR spectra of crystallization intermediates in the hydrothermal synthesis of MnAPO-5. Note the enlarged spinning sidebands.

^{27}Al and ^{31}P MAS NMR spectra of selected crystallization intermediates in the hydrothermal synthesis of MnAPO-5 are shown in Figure 4.6. All resonances for both nuclei can been assigned in terms of previously published work, and no anomalous resonances were detected.[49, 50] At the outset of the reaction, the aluminum spectrum is dominated by a sharp, symmetric peak centralized around 6.6 ppm. This peak has been attributed to octahedrally coordinated aluminum, i.e. $Al(-OAl)_6$. This signal remains as

the dominant spectral contributor until a small resonance becomes detectable at the two hours reaction time mark. This resonance is centralized at 38.3 ppm and represents tetrahedrally coordinated, framework aluminum, i.e. $Al(-OP)_4$. From two to six hours, this new signal becomes more intense until it nearly matches the intensity of the reagent peak at the six hour mark. From six hours until a maximum reaction time of three days, the product peak becomes the new dominant resonance in the spectrum, although some reagent alumina is still apparent. This extra aluminum is likely present due to unreacted, extraframework alumina. This would technically lead to an over-representation of aluminum in the final, bulk crystalline sample, but this was not apparent in the EDX results (vide supra), confirming that the aluminum resonance at 6.6 ppm was either removed during the washing procedure or was otherwise excluded from the crystalline framework. No resonances were detected in any intermediates other than those for amorphous alumina and framework aluminum centers, providing evidence that there is a direct transition between these two forms of aluminum without an intermediate phase during the crystallization of MnAPO-5.

The ^{31}P NMR spectra in Figure 4.6 show the development of the phosphorous environments. The spectrum collected for the zero time sample shows a broad resonance centered at -17.4 ppm. This resonance has been assigned to bulk, amorphous phosphorous oxide species at varying degrees of condensation. Resonances in this spectral region can be assigned to phosphorous atoms connected to tetrahedrally or octahedrally coordinated aluminum or hydroxyl groups, or which are coordinated to cationic SDA species, but they do not represent framework phosphorous.[51] This resonance is the dominant signal from the outset of the reaction until roughly the one

hour and thirty minutes mark. As will be explained below, the peaks centered at 80 ppm and -120 ppm are spinning side bands which have been amplified by the presence of paramagnetic material within the sample. Within a reaction time of thirty minutes, a new signal develops and overtakes the broad precursor phosphorous signal, centered around -28.9 ppm. This broad, asymmetric signal has been attributed to tetrahedrally co-ordinated framework phosphorous. After only two hours, this signal is the dominant contributor to the ^{31}P spectrum. As the reaction proceeds, the signal remains mainly unchanged. No other phosphorous environment was detected in any reaction intermediate, indicating another direct transition from dense, amorphous starting material to framework phosphorous. The framework phosphorous signal appears earlier in the reaction than does the framework aluminum signal. This indicates that phosphorous becomes reactive earlier in the hydrothermal synthesis of these AFI sieves than aluminum. At the end of the three day crystallization time, the only notable peak in the ^{31}P spectrum is that of the tetrahedrally coordinated framework phosphorus. The NMR spectra show that framework environments for ^{27}Al and ^{31}P do not appear until the 1.5-2 hour mark in reaction time, which coincides with the appearance of AFI reflections in the XRD developing from the amorphous precursor occurring at roughly two hours as well.

Figure 4.7 shows complimentary one pulse ^{27}Al and ^{31}P NMR results for the hydrothermal synthesis of FeAPO-5. The results shown here match those for the MnAPO-5 sieves closely, and so it is likely that a similar reaction mechanism is followed for these two materials. Small but important differences can, however, be detected. The ^{27}Al spectra of the zero hour mark sample shows a sharp peak at 6.4 ppm. Once again,

this peak can be assigned to octahedrally coordinated alumina-phase aluminum. The amorphous aluminum remains as the major signal contributor until one hour and thirty minutes reaction time, at which point a small resonance is detected at 37.6 ppm. This signal can be assigned to tetrahedrally coordinated, framework aluminum. In as little as thirty minutes from that point, the product peak nearly matches the reagent peak, and after six hours it has become the dominant signal in the spectrum. Over the next three days of reaction, the product peak grows even more, and at this point the reagent peak has nearly vanished. A resonance is present at 6.4 ppm in the final spectrum, signifying the presence of octahedral, alumina-phase aluminum in the final product. The diminishment of this signal with respect to the analogous MnAPO-5 [27]Al crystalline spectrum is reflected in the relative amount of metal within the samples as determined by EDX. Nearly twice as much Mn made it into the sieve as did Fe, and this result is echoed in the reduced presence of alumina in the FeAPO-5 crystalline product.

The ^{31}P spectra in Figure 4.7 show the very rapid transformation of amorphous phosphorous into framework phosphorous. The zero time sample shows only the amorphous peak, as does the one hour sample, centered at -17.4 ppm. Within thirty minutes from that time, the amorphous peak has all but disappeared, replaced in near-entirety by a sharp, symmetric peak centered at -29.4 ppm. As was the case with MnAPO-5, this peak represents tetrahedral framework phosphorous. A small residual peak representing amorphous starting material can be detected in the one hour and thirty minutes sample spectrum. After two hours, no amorphous material can be detected, and the product phosphorous peak grows in intensity and sharpness from that point up to three days reaction time. No intermediate spectrum showed the presence of other

phosphorous environments, and so another direct transformation is suspected. The presence of framework environments as early as one hour and thirty minutes reaction time matches nicely with the appearance of AFI reflections in the XRD progression at the same time.
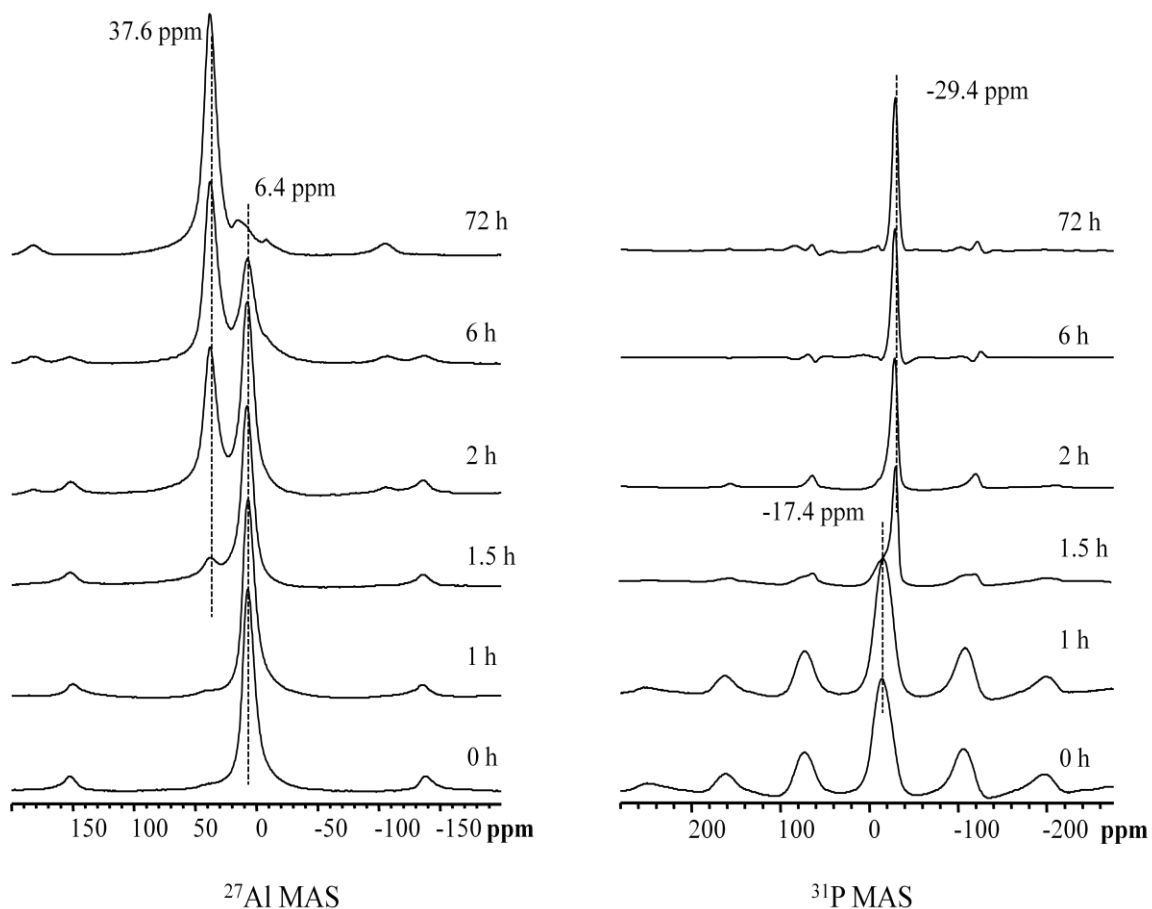
Figure 4.7: ^{27}Al and ^{31}P MAS NMR spectra of crystallization intermediates in the hydrothermal synthesis of FeAPO-5.

4.4 Data Analysis

4.4.1 T_1 Relaxation

Direct observation of the metal environments in intermediates by NMR would provide useful information about structure and substitution. NMR-active isotopes of both Mn and Fe exist, however collection of ^{55}Mn and ^{57}Fe solid-state NMR spectra is not

trivial in the case of these molecular sieves.[39] This is due partly to the poor NMR receptivity of ^{57}Fe but is mainly due to the fact that the metals are paramagnetic. The magnetic moments of a nucleus and an unpaired electron in a strong external magnetic field are able to interact with one another, and the introduction of this "paramagnetic moment" allows nuclei to relax much more efficiently.[41, 42] Too efficiently, in many cases, to allow direct observation of a nucleus with a paramagnetic electron configuration. The effect of this phenomenon is that spectra for paramagnetic nuclei are difficult to acquire; the signals are severely broadened and can potentially be shifted from their "diamagnetic" values determined by the CSA interaction. This does not, however, mean that NMR is not useful in the study of paramagnetic materials.

The effect of an available paramagnetic relaxation pathway from one nucleus on another neighbouring nucleus is a source of valuable information. In this case, the paramagnetic Mn or Fe centers can cause relaxation enhancement in ^{31}P nuclei. In the case of a system with poor spin diffusion, this enhancement is a through-space interaction that depends on $r_{(I-S)}^{-6}$, where I and S are the target nucleus and the paramagnetic electron (i.e. the paramagnetic nucleus) respectively.[52] Any evidence for paramagnetic relaxation enhancement in ^{31}P nuclei would therefore mean that paramagnetic centers are physically close to P sites, i.e. within the framework (if the framework is present). This distance dependence would mean that the majority of the P sites in the MAPO solids would not be close enough to a paramagnetic center to feel the effects of this paramagnetic relaxation (the number of Al being replaced by transition metals is less than 5%), and the NMR spectra would be dominated by a signal representing this majority which behaved as though it were in a purely diamagnetic solid. A much smaller paramagnetic signal which

would be broadened, have enhanced spinning sidebands and may experience a paramagnetic shift would also appear, representing those P sites directly linked to a metal center. These P sites could potentially have paramagnetic shifts severe enough to make it difficult to detect them (so-called "NMR invisible" phosphorous).[53-55]

There are cases, however, where the effects of paramagnetic relaxation can propagate throughout a solid; for instance, if the system possesses efficient spin diffusion, or where the other nuclear relaxation mechanisms are not strong enough to dominate over paramagnetic relaxation, even at considerable distances (the strength of paramagnetic coupling is orders of magnitude higher than most internuclear interactions). In general, paramagnetic effects are known to travel well throughout solids and in some solutions.[42, 56-58] With this information in mind, ^{31}P data was collected in an effort to provide further proof of paramagnetic metal framework incorporation and to determine if any important information could be obtained from reaction intermediates.

Table 4.1: T_1 relaxation times for reaction intermediates of SAPO-5, MnAPO-5 and FeAPO-5 measured using ^{31}P saturation or inversion recovery pulse sequences.

Sample	Reaction Progress	T_1 (s)
SAPO-5	Amorphous	25.7
	Semi-crystalline	44.2
	Crystalline	36.6
MnAPO-5	Amorphous	0.0462
	Semi-crystalline	0.0135
	Crystalline	0.0088
FeAPO-5	Amorphous	0.0610
	Semi-crystalline	0.0111
	Crystalline	0.0119

Table 4.1 lists the T_1 spin-lattice relaxation times for amorphous, semi-crystalline and crystalline samples of MnAPO-5 and FeAPO-5 synthesized hydrothermally and determined by the ^{31}P inversion recovery experiment. For comparison, T_1 relaxation times for crystallographically similar samples of diamagnetic SAPO-5 were also examined via saturation recovery. There is a stark contrast between the T_1s of the paramagnetic and diamagnetic materials. The diamagnetic sample data was fit to and optimized with the standard exponential saturation recovery equation in order to extract the relaxation time, while the more suitable stretched exponential equation was used in the case of the paramagnetic samples when studied using the inversion recovery sequence. These two pulse sequences are described in detail in the experimental section, but it is worth mentioning that while the inversion recovery sequence provides more accurate relaxation data, it also requires that efficient relaxation occurs between scans, and so is only experimentally feasible for samples with short T_1s. The saturation recovery sequence provides adequately reliable relaxation data and the delay between scans is independent of the sample relaxation efficiency, and so this sequence is useful for samples with longer T_1s. Figure 4.8 shows the fitting of a representative set of data for a paramagnetic sample. The curve is fit to the stretched exponential equation postulated by Bain et al., and agrees with it adequately with an acceptable β value (the "stretching" exponent, $0 \leq \beta \leq 1$) of 0.44. The stretched exponential equation is detailed below:

$$M_\tau = b - a(\exp\left[-\left(\frac{\tau}{T_1}\right)^\beta\right])$$

$M_{(\tau)}$ represents the signal intensity of a certain peak after delay time τ, b and a are optimized values representing the hypothetical intensity of signals $M_{(\infty)}$ and $M_{(0)}$, respectively, T_1 is the calculated spin-lattice relaxation time and β is the stretching

exponent (the value of b is set at 100 due to the fact that intensity data was scaled for this experiment). The equation for a diamagnetic relaxation system is identical except for the presence of the stretching exponent β. This bi-exponentiality has been found to better represent a system with uniformly-spaced paramagnetic centers in solids, which closely resembles the MAPO-5 samples under study here.[40] The tables at the bottom of Figure 4.8 show the details of the fit, listing the fit equation used, R^2 values approaching unity, and optimized values of a, b, β and T_1 along with standard errors.

The difference between the relaxation times of the materials spans four orders of magnitude in the largest cases, but in general, diamagnetic samples have T_1s in the tens of seconds range, while paramagnetic samples have T_1s in the tens of milliseconds range. This effect is noted throughout the crystallization, indicating that paramagnetic metal centers affecting the relaxation of P sites throughout the entire synthesis. This indicates that the precursor is highly homogeneous, making it amenable to efficient metal incorporation. The T_1s for the amorphous paramagnetic materials are notably longer than those of semi-crystalline or crystalline samples. The metals inside the precursor gel could be in a mixture of oxidation states, and so the relaxation pathways available to these two samples would not be identical. The lack of amorphous material in the samples evidenced by XRD and the molar ratios noted by EDX indicate that the paramagnetic Mn and Fe are incorporated into the sieve network and are not in the form of extraframework metal oxides. The relaxation data for a comparable diamagnetic sample of SAPO-5 are also detailed in Figure 4.8. It shows that, using the standard exponential fitting equation, a T_1 relaxation time of 44.4 s fits the data very accurately. This T_1 is significantly longer than

Model	StretchedExp		
Equation	100-a*exp(-(x/T)^)		
R²	0.99837		
		Value	Std.Err
Optimized values	a	232.05567	10.35364
	β	0.43922	0.02024
	T_1	0.00885	0.00107

Model	T1SatRec		
Equation	b-a*exp(-(x/T))		
R²	0.99837		
		Value	Std.Err
Optimized values	a	97.18066	1.04989
	b	101.12043	0.73831
	T_1	30.00159	0.77341
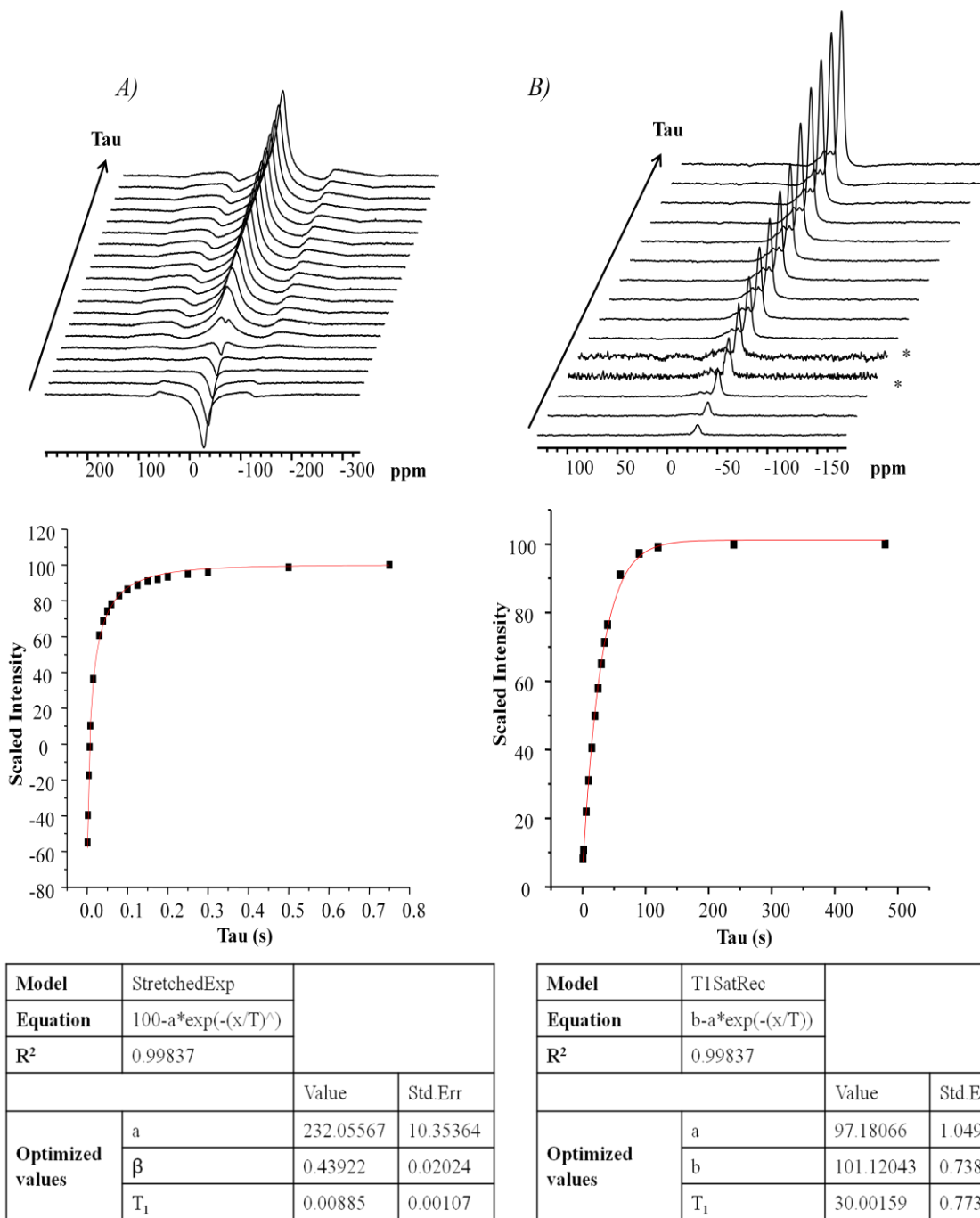
Figure 4.8: A) Representative ^{31}P inversion recovery spectra for a sample of MnAPO-5 with scaled intensity vs. τ for the same data set in the graph below. τ increases along the z-axis. The data fit is detailed in the table below. B) A similar set of representative saturation recovery spectra for a sample of SAPO-5. Spectra marked with an asterisk have a lower signal-to-noise ratio due to a temporary drop in ^{1}H decoupling efficiency.

that found for the paramagnetic sample, and is more typical for a phosphorous nucleus in a diamagnetic environment, providing further evidence that paramagnetic coupling is a major contributor to the relaxation of P site spins within the MAPO samples.

4.4.2 Spinning Side-Band Enhancement
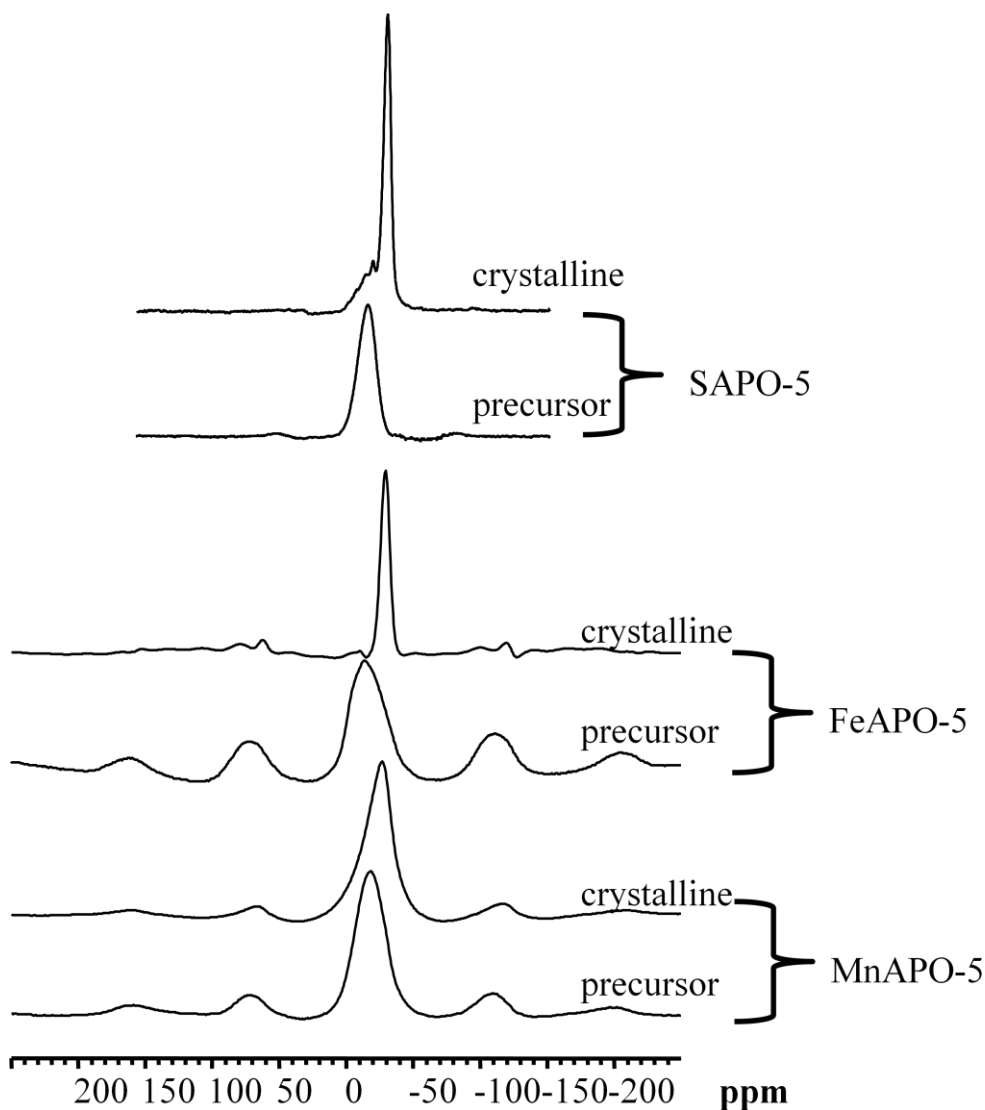
Figure 4.9: Comparison of the ^{31}P NMR spectra of crystalline and precursor gel samples of diamagnetic SAPO-5 with paramagneticFeAPO-5 and MnAPO-5.

Dipolar coupling between ^{31}P nuclei and a paramagnetic electron (the pseudo-contact effect) is very strong. As a result of this, MAS is less effective in averaging an

anisotropic powder pattern into an isotropic peak, and so at the same spinning speed a paramagnetic sample will produce a spectrum with more intense spinning sidebands than a diamagnetic sample.[42, 59-61] Figure 4.9 shows ^{31}P MAS spectra for precursor and crystalline samples of MnAPO-5 and FeAPO-5 synthesized hydrothermally, as well as crystallographically similar SAPO-5 samples synthesized via dry-gel conversion. The difference between the diamagnetic and paramagnetic spectra are obvious on sight, and are caused by the effect of paramagnetic transition metals on ^{31}P sites. First, the spinning side band enhancement effect described above is readily apparent. The paramagnetic samples show enhanced spinning sidebands in both the amorphous precursor and the crystalline product, while the diamagnetic SAPO-5 spectra show flat baseline where the spinning sidebands would be. The resonances for the paramagnetic samples are notably broader than corresponding diamagnetic SAPO-5 samples; an effect commonly noted in NMR studies of paramagnetic materials.[62-67] This effect is most apparent for the MnAPO-5 samples as a possible result of the higher weight % of Mn in the samples which was earlier noted by EDX. The chemical shifts for amorphous phosphorus and framework phosphorous are similar between sample types. This could either mean that no paramagnetic shift had occurred and the signal represents the entire P population, or that a severe paramagnetic shift had occurred, and the signal at the diamagnetic value represents only the diamagnetic P sites. The recycle delay used for these acquisitions was 0.5 s, which is not enough time for a P site in a diamagnetic sample to relax efficiently between scans. After the first few pulses the P population would become saturated and no new information would be obtained by subsequent scans. The data obtained indicate that the T_1 for diamagnetic SAPO-5 samples is on the order of 20-40 seconds, meaning that

an effective time to wait between scans would be on the order of 1-3 minutes. On repeating these acquisitions under identical conditions (except for the pulse delay which was set to 60 s) the spectra produced are similar to those for the initial acquisition. These results, coupled with the previously mentioned T_1 data, show that paramagnetic relaxation pathways are available to P sites homogeneously over the entire course of the crystallization and that efficient spin diffusion is present in both the systems studied by this work.

Previous work done within this group noted similar NMR results when working with paramagnetic metal substitution. Chen et al. noted enhanced spinning sidebands and a broadening of signal in ^{31}P NMR inside cobalt-substituted $AlPO_4$-5 sieves without any paramagnetic shift.[68] Labouriau et al. noted a similar effect when studying the same system[54], going on to note that the intensity of the unshifted peak increased upon sample calcination. They interpret this result by stating that extraframework paramagnetic cobalt (in the oxide form) would exit the pore network on calcination, and so a larger population of phosphorous would become NMR "visible" as they gained distance from paramagnetic centers. The shifted NMR invisible phosphorous signal would, presumably, decrease in intensity at the same rate, however they note that the enhanced spinning side bands and signal broadening are applied to the diamagnetic phosphorous signal, as is the case in this work. ^{31}P signal broadening and enhanced spinning sidebands are noted in other $AlPO_4$ framework when studying Mn and Fe substitution. Sinha et al. noted the effects in MnAPO-41 and MnAPO-11, and used EPR to classify the metal centers more directly, eventually identifying at least 4 distinct Mn^{2+} sites in their samples.[69] These examples, alongside the work presented here, indicate that the effects of paramagnetic relaxation

inside $AlPO_4$ molecular sieves seem to act on these systems in a bulk fashion, rather than a more localized manner noted in some other systems.

The crystallization and substitution which occurs during the hydrothermal synthesis of the AFI framework sieves MnAPO-5 and FeAPO-5 has become clearer through the use of solid state NMR spectroscopy, complimented by XRD and SEM/EDX data. These processes are similar between the two metals studied by this work. Based on these results, it appears that the ageing period before reaction in the autoclave helps to efficiently homogenize the eventual framework constituents. The aluminum in the precursor is still octahedral and the phosphorous is amorphous, but due to the efficient paramagnetic relaxation enhancement noted in the ^{31}P NMR analysis, it would appear that paramagnetic metals are in close proximity to the phosphorous source, if not already bridged to phosphorous through oxygen. The latter hypothesis is supported by the fact that framework P sites are evident in the spectrum shortly before framework Al sites, and also before significant presence of the framework in X-ray diffractograms. As the reaction proceeds the crystal structure becomes more apparent via XRD as octahedral Al is attached to P-O-M complexes under the structure direction of TEA. The precursor ^{27}Al and ^{31}P signals shrink as the product signals grow, and eventually the crystalline sieve is finished with well-incorporated metal centers. The higher weight % of Mn in the sieve can be explained by the fact that the ionic radius of Mn^{3+} is closer to that of Al^{3+} than Fe^{3+}, and so Mn^{3+} is a better fit within the sieve than is Fe^{3+}.[70] In addition, it has been noted that in this synthesis both Fe^{2+} and Fe^{3+} [71] would be present, and a difference in the difficulty of these two ions in terms of framework incorporation can also be used to explain the slight difference in weight % between the two metals studied here.

4.5 Conclusions

The hydrothermal method of molecular sieve synthesis was used to produce transition metal substituted variants of the AFI-framework aluminophosphate $AlPO_4$-5. Manganese and iron were chosen as model systems due to their past use in sieve synthesis as well as the potential application of MnAPO-5 and FeAPO-5 in heterogeneous redox catalysis of industrially important processes. Through the use of XRD, solid state NMR and SEM/EDX, important aspects of the crystallization process, which was quite similar between metals, were determined. The precursor material is amorphous, however paramagnetic relaxation enhancement of ^{31}P nuclei indicates that the metals are in close proximity or even oxygen-bridged to phosphorous at the start of the reaction, where no sieve crystals are apparent and all aluminum is in the octahedral alumina phase. This is evidence of metal incorporation at a very early stage in the reaction. Framework phosphorous sites are evident earlier than crystalline sieves or indeed framework aluminum, providing evidence for preferential metal bridge building and the presence of P-O-M complexes. As crystallization progresses, the aluminum is incorporated into a tetrahedral position in the framework directly from its precursor octahedral state through reaction with P-O-M complexes, and the crystal is formed in as little time as two hours. Over as many as three days, the crystals grow into large, barrel-like aggregations. More manganese can be incorporated into the AFI sieve than iron, explained by the larger ionic radius and ambiguous oxidation state of iron in the precursor. Efficient spin diffusion is present in both samples, and the effects of paramagnetic relaxation pathways can been seen in the NMR spectra for amorphous precursors as well as crystalline samples.

In the future, an even clearer picture of the reaction and incorporation mechanism for these materials and many like them could be painted using increasingly complex NMR experiments. Studying interatomic distances and connectivity in crystallization intermediates would provide increasingly precise information about the movement of reagents and development of the framework. Further NMR studies of organic nuclei (^{13}C, $^{14\text{-}15}$N, etc.) within the SDA or other reagents could also provide useful information. Once again, solid state NMR has proven to be invaluable in the study of the crystallization process of molecular sieve systems.

4.6 References

1.   Davis, M.E. *Nature* **2002**, *417*(6891), 813-821.

2.   Dyer, A. *An Introduction to Zeolite Molecular Sieves*. **1988**, Avon, GB: John Wiley & Sons, Ltd.

3.   Szostak, R. *Molecular Sieves: Principles of Synthesis and Identification*. **1998**, Suffolk, GB: Thomson Science.

4.   Michiels, P. *Molecular Sieve Catalysts*. **1987**, Virginia, USA:Pergamon Infoline Inc.

5.   Menon, V.C.; Komarneni, S. *J. Porous Mater.* **1998**, *5*(1), 43-58.

6.   Dincă, M.; Dailly, A.; Liu, Y.; Brown, C.M.; Neumann, D.A.; Long, J.R. *J. Am. Chem. Soc.* **2006**, *128*(51), 16876-16883.

7.   Hedge, S.G.; Ratnasamy, P.; Kustov, L.M.; Kazansky, V.B. *Zeolites* **1988**, *8*(2), 137-141.

8.   Wilson, S.T.; Lok, B.M.; Messina, C.A.; Cannan, T.R.; Flanigen, E.M. *J. Am. Chem. Soc.* **1982**, *104*(4), 1146-1147.

9.   Fujii, R.; Seki, M.; Shinoda, J.; Okazaki, N.; Tada, A. *Chem. Lett.* **2003**, *32*(8), 764-765.

10.   Aramendia, M.; Borau, V.; Jiménez, C.; Marinas, J.; Rodero, F. *React. Kinet. Catal, L.* **1988**, *37*(2), 331-335.

11.   Vieira, A.; Tovar, M.A.; Pfaff, C.; Méndez, B.; López, C.M.; Machado, F.J.; Goldwasser, J.; de Agudelo, M.M.R. *J. Catal.* **1998**, *177*(1), 60-71.

12.   Lok, B.M.; Messina, C.A.; Patton, R.L.; Gajek, R.T.; Cannan, T.R.; Flanigen, E.M. *J. Am. Chem. Soc.* **1984**, *106*(20), 6092-6093.

13.   Danilina, N.; Krumeich, F.; van Bokhoven, J.A. *J. Catal.* **2010**, *272*(1), 37-43.

14.   Sastre, G.; Lewis, D.W.; Catlow, C.R.A. *J. Phys. Chem. B* **1997**, *101*(27), 5249-5262.

15.   Lü, J.-M.; Ranjit, K.T.; Rungrojchaipan, P.; Kevan, L. *J. Phys. Chem. B* **2005**, *109*(19), 9284-9293.

16.   Xu, Y.; Maddox, P.J.; Thomas, J.M. *Polyhedron* **1989**, *8*(6), 819-826.

17.   Nur, H.; Hamdan, H. *Mater. Res. Bull.* **2001**, *36*(1–2), 315-322.

18. Luna, F.J.; Ukawa, S.E.; Wallau, M.; Schuchardt, U. *J. Mol. Catal. A-Chem.* **1997**, *117*(1–3), 405-411.

19. Machado, M.d.S.; Pérez-Pariente, J.; Sastre, E.; Cardoso, D.; Giotto, M.V.; García-Fierro, J.L.; Fornés, V. *J. Catal.* **2002**, *205*(2), 299-308.

20. Akolekar, D.B. *J. Catal.* **1993**, *143*(1), 227-238.

21. Akolekar, D.B. *J. Mol. Catal. A-Chem.* **1995**, *104*(1), 95-102.

22. Venuto, P.B. *Microporous Mater.* **1994**, *2*(5), 297-411.

23. Raja, R.; Sankar, G.; Thomas, J.M. *J. Am. Chem. Soc.* **1999**, *121*(50), 11926-11927.

24. Raj, K.J.A.; Vijayaraghavan, V.R. *Catal. Lett.* **2004**, *96*(1), 67-70.

25. Wan, B.-Z.; Huang, K. *Appl. Catal.* **1991**, *73*(1), 113-124.

26. Bruckner, A.; Lohse, U.; Mehner, H. *Micropor. Mesopor. Mater.* **1998**, *20*(1–3), 207-215.

27. Lohse, U.; Brückner, A.; Schreier, E.; Bertram, R.; Jänchen, J.; Fricke, R. *Microporous Mater.* **1996**, *7*(2–3), 139-149.

28. Muñoz, T.; Balkus, K.J. *Chem. Mater.* **1998**, *10*(12), 4114-4122.

29. Balkus, K.J.; Ball, L.J.; Gnade, B.E.; Anthony, J.M. *Chem. of Mater.* **1997**, *9*(1), 380-386.

30. Dugal, M.; Sankar, G.; Raja, R.; Thomas, J.M. *Angew. Chem. Int. Ed.* **2000**, *39*(13), 2310-2313.

31. Chao, K.J.; Wei, A.C.; Wu, H.C.; Lee, J.F. *Catal. Today* **1999**, *49*(1–3), 277-284.

32. Davis, M.E. *Acc. Chem. Res.* **1993**, *26*(3), 111-115.

33. Dai, P.-S.E.; Petty, R.H.; Ingram, C.W.; Szostak, R. *Appl. Catal. A-Gen.* **1996**, *143*(1), 101-110.

34. Rakoczy, R.A.; Ernst, S.; Hartmann, M.; Traa, Y.; Weitkamp, J. *Catal. Today* **1999**, *49*(1–3), 261-266.

35. Prakash, A.M.; Kevan, L. *J. Am. Chem. Soc.* **1998**, *120*(50), 13148-13155.

36. Lischke, G.; Parlitz, B.; Lohse, U.; Schreier, E.; Fricke, R. *Appl. Catal. A-Gen.* **1998**, *166*(2), 351-361.

37. Zhou, L.; Xu, J.; Chen, C.; Wang, F.; Li, X. *J. Porous Mater.* **2008**, *15*(1), 7-12.

38. Zhou, L.; Lu, T.; Xu, J.; Chen, M.; Zhang, C.; Chen, C.; Yang, X.; Xu, J. *Micropor. Mesopor. Mater.* **2012**, *161*(0), 76-83.

39. Eichele, K.; Wasylishen, R.E. *J. Phys. Chem.* **1994**, *98*(12), 3108-3113.

40. Narayanan, A.; Hartman, J.S.; Bain, A.D. *J. Magn. Reson. Ser. A* **1995**, *112*(1), 58-65.

41. Bakhmutov, V. *Practical NMR Relaxation for Chemists*. **2004**, West Sussex, G.B.: John Wiley and Sons, Ltd.

42. Duer, M.J. *Introduction to Solid-State NMR Spectroscopy*. **2004**, Oxford, GB: Blackwell Science.

43. Vold, R.L.; Waugh, J.S.; Klein, M.P.; Phelps, D.E. *J. Chem. Phys.* **1968**, *48*, 3831-3832.

44. Anderson, J.E.; Ullman, R. *J. Phys. Chem.* **1967**, *71*(12), 4133-4134.

45. Bandyopadhyay, R.; Bandyopadhyay, M.; Kubota, Y.; Sugi, Y. *J. Porous Mater.* **2002**, *9*(2), 83-95.

46. Flanigen, E.M.; Lok, B.M.; Patton, R.L.; Wilson, S.T., in *Studies in Surface Science and Catalysis*, A.I. Y. Murakami and J.W. Ward, Editors. **1986**, Elsevier. 103-112.

47. Chen, J.; Sankar, G.; Thomas, J.M.; Xu, R.; Greaves, G.N.; Waller, D. *Chem. Mater.* **1992**, *4*(6), 1373-1380.

48. Modén, B.; Oliviero, L.; Dakka, J.; Santiesteban, J.G.; Iglesia, E. *J. Phys. Chem. B* **2004**, *108*(18), 5552-5563.

49. Chen, B.; Kirby, C.W.; Huang, Y. *J. Phys. Chem. C.* **2009**, *113*(36), 15868-15876.

50. Sayari, A.; Moudrakovski, I.; Reddy, J.S.; Ratcliffe, C.I.; Ripmeester, J.A.; Preston, K.F. *Chem. Mater.* **1996**, *8*(8), 2080-2088.

51. Huang, Y.; Richer, R.; Kirby, C.W. *J. Phys. Chem. B* **2003**, *107*(6), 1326-1337 (and references therein).

52. Alaimo, M.H.; Roberts, I.E. *Solid State Nucl. Mag.* **1997**, *8*(4), 241-250.

53. Canesson, L.; Boudeville, Y.; Tuel, A. *J. Am. Chem. Soc.* **1997**, *119*(44), 10754-10762.

54. Labouriau, A.; Neugebauer-Crawford, S.; Ott, K.; Earl, W.L.. *Probing the Structure of Metal-Substituted Molecular Sieves by Solid-State NMR*, presented at *the 12th International Zeolite Conference*. Baltimore, MD, **1998**.

55.   Canesson, L.; Tuel, A. *Chem. Comm.* **1997**(2), 241-242.

56.   Kalverda, A.P.; Salgado, J.; Dennison, C.; Canters, G.W. *Biochemistry-US* **1996**, *35*(9), 3085-3092.

57.   VanderHart, D.L.; Asano, A.; Gilman, J.W. *Chem. Mater.* **2001**, *13*(10), 3796-3809.

58.   Liu, K.; Ryan, D.; Nakanishi, K.; McDermott, A. *J. Am. Chem. Soc.* **1995**, *117*(26), 6897-6906.

59.   Vassallo, A.M.; Wilson, M.A.; Collin, P.J.; Oades, J.M.; Waters, A.G.; Malcolm, R.L. *Anal. Chem.* **1987**, *59*(4), 558-562.

60.   Brough, A.R.; Grey, C.P.; Dobson, C.M. *J. Am. Chem. Soc.* **1993**, *115*(16), 7318-7327.

61.   Huang, W.; Schopfer, M.; Zhang, C.; Howell, R.C.; Todaro, L.; Gee, B.A.; Francesconi, L.C.; Polenova, T. *J. Am. Chem. Soc.* **2007**, *130*(2), 481-490.

62.   Tuel, A.; Canesson, L.; Volta, J.C. *Colloid Surface A* **1999**, *158*(1–2), 97-106.

63.   Resing H, A.; Murday J, S. *NMR Relaxation and Molecular Motion in Zeolites*, in *Molecular Sieves*. **1973**, New York US: American Chemical Society. 414-429.

64.   Kubo, A.; Spaniol, T.P.; Terao, T. *J. Magn. Res.* **1998**, *133*(2), 330-340.

65.   Bertini, I.; Luchinat, C.; Parigi, G.; Pierattelli, R. *Chem. Bio. Chem.* **2005**, *6*(9), 1536-1549.

66.   Wickramasinghe, N.P.; Shaibat, M.; Ishii, Y. *J. Am. Chem. Soc.* **2005**, *127*(16), 5796-5797.

67.   Pintacuda, G.; Giraud, N.; Pierattelli, R.; Böckmann, A.; Bertini, I.; Emsley, L. *Angew. Chem. Int. Ed.* **2007**, *46*(7), 1079-1082.

68.   Chen, B.; Huang, Y. *Micropor. Mesopor. Mater.* **2009**, *123*(1–3), 71-77.

69.   Sinha, A.K.; Satyanarayana, C.V.V.; Srinivas, D.; Sivasanker, S.; Ratnasamy, P. *Micropor. Mesopor. Mater.* **2000**, *35–36*(0), 471-481.

70.   Shannon, R.D.; Prewitt, C.T. *Acta Crystallogr. B* **1969**, *25*(5), 925-946.

71.   Weckhuysen, B.M.; Rao, R.R.A.: Martens, J.; Schoonheydt, R.A. *Eur. J. Inorg. Chem.* **1999**, *1999*(4), 565-577.

CHAPTER FIVE

Summary and Suggestions for Future Work

5.1 Thesis Summary

Microporous materials, being of considerable industrial utility and research interest, have been under serious chemical investigation since their first synthesis the mid-20th century.[1-8] In that short time, molecular sieves have evolved into a diverse family of materials with industrially relevant applications. This work attempted to characterize the processes by which these remarkable materials crystallize, paying particular attention to heteroatomic substitution; the process by which interesting new catalytic properties can be introduced into otherwise non-catalytically active frameworks.

With that background, this work sought to study the crystallization of molecular sieve systems where heteroatomic framework substitution took place, building on previous work from within this group. Successful projects studying the substitution of multiple heteroatoms into the $AlPO_4$-5 molecular sieve (AFI topology) have been detailed. Hydrothermal and dry-gel conversion syntheses of these systems were performed and optimized based on previously published literature. Reaction intermediates were collected for study and analyzed using XRD, NMR and SEM/EDX.

Chapter three details the study of the silicon substituted aluminophosphate system with AFI topology known as SAPO-5.[8-11] This material has significant potential as, among other things, a heterogenous acid catalyst. The number and the type of acid sites found within this material are dependent on the substitution of silicon into the aluminophosphate framework during crystallization, and so its study will hopefully lead to a heightened ability to tailor these useful acid catalysts. The process was monitored

using three different modifications of the dry-gel conversion method, SAC, VPT and VPSU.

Through solid state NMR, it was determined that the SAC and VPT methods are very closely related. At the outset of the reaction, the two dry-gels are significantly different, both by XRD and NMR, as a result of the absence of triethylamine structure directing agent in the VPT dry-gel. After a very brief time under VPT conditions, however, the two crystallization methods converge. The incorporation of silicon also appears to occur in a similar fashion as well. In the dry-gel, the silicon exists as a dense silica-like phase, which through hydrolysis becomes activated and available for incorporation into the developing sieve under the influence of structure direction. In both the SAC and VPT cases, there exists a remnant of that dense phase in the crystalline sieve, either as framework silica islands or extra-framework starting material. The SM3 method of substitution was found to dominate in these syntheses. The VPSU method uses a volatile organosilicon species as a source of framework silicon, and was found to follow a similar crystallization pathway as the SAC method. The silicon incorporation was, however, much more dispersed, with only well-incorporated silicon centers found in the final product. Organically linked silicon were present in the precursor prior to sieve crystallization, but were absent from the finished sieve. The SM2 method of substitution was the dominant form in this synthesis.

Chapter four details the substitution of manganese and iron atoms into the $AlPO_4$-5 sieve, creating MnAPO-5 and FeAPO-5, respectively, under hydrothermal synthesis conditions.[12-14] Metal-substituted aluminophosphates (MAPOs) are highly sought after materials due to their redox catalytic activity, although relatively few publications detail

their crystallization or substitution. The introduction of paramagnetism means that direct observation of the metal centers in these materials using NMR would be non-trivial, but indirect observation would provide useful information. In the case of both metals, the crystallization from precursor to sieve occurred directly from amorphous to crystalline materials with no intermediate phase. The crystallites formed were uniformly large, barrel-like aggregates of thick plate-like crystals. Metal loadings were less in the iron case than with manganese: likely a result of the similarity in ionic radius of Mn^{3+} to Al^{3+}. EDX-determined molar ratios agree with the popular assertion that metals preferentially substitute for Al^{3+} in the sieve framework. Calcination of these materials resulted in a dramatic colour change as a result of the redox activity of the MAPO sieves. Long-term exposure to air resulted in a reversal of this colour change.

Paramagnetic effects on ^{31}P MNR spectra were evident early in the synthesis, and remain evident for the entirety of the crystallization. The paramagnetic effects of even a relatively small number of metal centers are felt by the majority of the ^{31}P spin population. Signal broadening and enhanced spinning sidebands are evident from the ^{31}P spectra, but no paramagnetic shift seems to have occurred and the signal is found at the "diamagnetic" chemical shift. This indicates that in both cases that efficient spin diffusion is present, and the signal coming from the relatively small number of phosphorous directly bridged to paramagnetic metal centers is not readily apparent. These "NMR invisible phosphorous" may be represented as a part of the main signal, or they may be shifted further than the boundaries of the frequency range of interest. Direct observation of the paramagnetic metal centers by NMR would be non-trivial, but the

effect of these paramagnetic centers on neighbouring ^{31}P nuclei provides useful information.

The results of these studies likely apply to systems other than those mentioned here. This thesis represents a possible standard method of study for the crystallization of all molecular sieves, resulting in faster publication of crystallization data and a heightened awareness of occurrences during molecular sieve synthesis. This awareness will become more important as new synthesis methods and new types of molecular sieves become more prevalent.

5.2 Future Work

It is recommended that the following steps be taken in order to complete or expand upon the studies mentioned in this thesis. They serve the purpose of expanding the amount of available data on molecular sieve crystallization in order to discover significant patterns and draw meaningful conclusions.

1) Expand on the number of microporous systems under study, exploring other $AlPO_4$ frameworks, as well as analogous sieves of different construction (true zeolites, $GaPO_4$s, MOFs, etc.).

2) Attempt to incorporate different elements, both novel and well-studied (Mg, Cr, V, Co, Zn, Cu etc.) into well-studied frameworks and study their incorporation and substitution patterns looking for contrasts.

3) Attempt to synthesize well-characterized systems using novel methods (i.e. solvothermal, ionothermal) in an attempt to correlate solvent type to incorporation and/or substitution.

4) Use more complicated solid state NMR techniques (REDOR, HETCOR, 3QMAS, etc.) and/or vibrational spectroscopy to study intermediates and obtain clearer information about the crystallization process.

5) Perform catalytic testing on fully crystallized, pure sieves, in an attempt to correlate synthesis or incorporation parameters to catalytic activity.

5.3 References

1.   Davis, M.E.; Lobo, R.F. *Chem. Mater.* **1992**, *4*(4), 756-768.

2.   Davis, M.E. *Acc. Chem. Res.* **1993**, *26*(3), 111-115.

3.   Davis, M.E. *Ind. Eng. Chem. Res.* **1991**, *30*(8), 1675-1683.

4.   Barrer, R.M. *Proc. Roy. Soc. A.* **1938**, *167*, 392-406.

5.   Barrer, R.M. *Zeolites* **1981**, *1*(3), 130-140.

6.   Wilson, S.T.; Lok, B.M.; Messina, C.A.; Cannan, T.R.; Flanigen, E.M. *J. Am. Chem. Soc.* **1982**, *104*(4), 1146-1147.

7.   Flanigen, E.M.; Lok, B.M.; Patton, R.L.; Wilson, S.T. in *Studies in Surface Science and Catalysis*, A.I. Y. Murakami and J.W. Ward, Editors. **1986**, Elsevier, 103-112.

8.   Lok, B.M.; Messina, C.A.; Patton, R.L.; Gajek, R.T.; Cannan, T.R.; Flanigen, E.M. *J. Am. Chem. Soc.* **1984**, *106*(20), 6092-6093.

9.   Chen, B.; Huang, Y. *Micropor. Mesopor. Mater.* **2009**, *123*(1–3), 71-77.

10.   Bandyopadhyay, R.; Bandyopadhyay, M.; Kubota, Y.; and Sugi, Y. *J. Porous Mater.* **2002**, *9*(2), 83-95.

11.   Bandyopadhyay, M.; Bandyopadhyay, R.; Tawada, S.; Kubota, Y.; Sugi, Y. *Appl. Catal. A- Gen.* **2002**, *225*(1–2), 51-62.

12.   Zhou, L.; Xu, J.; Chen, C.; Wang, F.; Li, X. *J. Porous Mater.* **2008**, *15*(1), 7-12.

13.   Zhou, L.; Lu, T.; Xu, J.; Chen, M.; Zhang, C.; Chen, C.; Yang, X.; Xu, J. *Micropor. Mesopor. Mater.* **2012**, *161*(0), 76-83.

14.   Prakash, A.M.; Hartmann, M.; Zhu, Z.; Kevan, L. *J. Phys. Chem. B* **2000**, *104*(7), 1610-1616.

CURRICULUM VITAE

Name: Adam Robert MacIntosh

Date of Birth   03-09-1987

Post-secondary   The University of Western Ontario
Education/ Degree: London, Ontario, Canada
        2005-2010 B.Sc.

Honours / Awards: WGRS: fall term 2010 and summer, fall terms 2011

Work Experience: Graduate Teaching Assistant, Chemistry 1100, 1200 (lab/help
        desk)
         The University of Western Ontario
         London, Ontario, Canada
         2010-2012

        Synthetic Chemist
         Chemtura Canada Co./Cie.
         Guelph, Ontario, Canada
         2008-2009

Presentations/publications:

1. (Oral Presentation) **A.R. MacIntosh**, <u>Y. Huang</u>. "*Studies on AlPO$_4$-5 Molecular Sieve Crystallization and Heteroatomic Framework Substitution*". 2nd meeting of the Center for Advanced Material and Biomaterial Research (CAMBR), November 13th, **2012.** The University of Western Ontario, London, Ontario, Canada.

2. (Oral Presentation of Distinction) **A.R. MacIntosh**, <u>Y. Huang</u>. *'Studying Atomic Incorporation into the Frameworks of SAPO-n Molecular Sieves*". 43rd Inorganic Discussion Weekend (IDW), August 19-21, **2011**. Niagara Falls, Ontario, Canada.

3. (Poster Presentation) **A.R. MacIntosh**, <u>Y. Huang</u>. "*Investigations into the Dry-Gel Conversion Crystallization Mechanisms of SAPO-11 and GaPO$_4$ (LTA) Molecular Sieves*". 1st meeting of the Center for Advanced Material and Biomaterial Research (CAMBR), June 23, **2011.** The University of Western Ontario, London, Ontario, Canada.

4. (Oral Presentation) **A.R. MacIntosh**, <u>R.H. Lipson</u>. "*Tuneable Photonic Crystals*". 38th Southern Ontario Undergraduate Student Chemistry Conference (SOUSCC), March 20, **2010.** The University of Western Ontario, London, Ontario, Canada.